



Biomimetic Strategies for Motion Camouflage

Nicole E Carey

A thesis submitted for the degree of
Doctor of Philosophy of the
The Australian National University

March, 2007



Biomimetic Strategies for Motion Compensation

Nick E. Cory

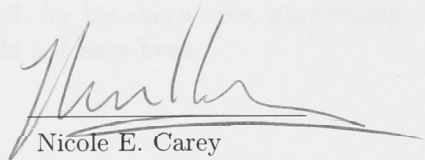
A thesis submitted for the degree of
Doctor of Philosophy of the
The Australian National University

March, 2007

Declaration

This thesis is an account of research undertaken between 2003 and 2007 at the Research School of Biological Sciences, The Australian National University, Canberra, Australia.

Except where acknowledged in the customary manner, the material presented in this thesis is, to the best of my knowledge, original and has not been submitted in whole or part for a degree in any university.



Nicole E. Carey

March, 2007

Oct.



Declaration

I declare that the content of research undertaken between 2005 and 2007 at the Research School of Biological Sciences, The Australian National University, Canberra, Australia, is original work undertaken in the ordinary manner of the research process in this field, to the best of my knowledge, original and has not been submitted in whole or part for a degree in any university.


 Mark J. Cain
 School of Biological Sciences
 The Australian National University
 Canberra, ACT 2601, Australia

Acknowledgements

I thank my family, particularly my mother Cristene whose time and effort did not go unappreciated. To Kasey, who never failed in knowing just when a phone call was needed. To Byron, whose support, confidence and humour kept me going. To all my friends, especially the other VS post-grads, both past and present. To Srimi, for your kind words and unfailing accuracy in finding my errors. To David and Colin, for periodically dragging me kicking and screaming outside of the university.

But most especially I must thank Jochen Zeil, for his sharp eyes, unrelenting rigor, and precise mind, without whom this thesis would not have been.

Acknowledgements

I thank my family, particularly my mother, Christine, for her love and effort that are so
unappreciated. To Kasey, who never failed to know just what I needed and who was always
there to support, encourage and motivate me. To all my friends,
especially the other US post-grads, both past and present. To find for your kind words
and reliable accuracy in taking on a project. To David and Collin for persistently dragging
me kicking and screaming on side of the university.
But most especially I must thank Robert Ford for his sharp eye, his helpful ideas
and precise mind, without whom this thesis would not have been.

“Abstract

The thesis studies the the inter-related control strategies in both the theoretical and experimental aspects of several innovative insect behavioral strategies. The theory of motion planning is explored, and an optimal-energy strategy for motion-manipulated paths is developed using Lagrangian mechanics. To determine the key dynamic variables used by insects to fly in a complex world, flight interactions between dragonflies are analyzed and compared to similar fly-flight interactions, with specific attention paid to aspects of natural world complexity.

To the motion planning of a given world or heading strategy, higher-level control algorithms are required. Three new motion-control methods for generating coordinated trajectories are explored in the thesis. Firstly, a class of linear quadratic techniques is developed, including optimal forward control as well as three-dimensional and sub-optimal forward-time control using genetic control methods. Secondly, it is shown that dynamic gain proportional navigation can be used to obtain coordinated flight trajectories and hence a dynamic gain-based guidance algorithm is developed using proportional navigation. Finally, a method for implementing force-based path-following control and flight wing control systems is discussed.

It's an empty journey to triumph
if you don't plant the seeds of catastrophe along the way.
J. Allison, 2005

Abstract

This thesis investigates the principles behind motion camouflage, in both the theoretical sense and as a subset of general interactive insect behavioural strategies. The theory of motion camouflage is explored, and an optimal-energy formula for motion camouflaged paths is developed using lagrangian mechanics. To determine the key dynamic variables used by insects to respond to one another while in flight, interactions between dragonflies are analyzed and compared to satellite fly/wasp interactions, with special attention paid to instances of natural motion camouflage.

To use motion camouflage as a robotic stealth or tracking strategy, higher-level control algorithms are required. Hence two main control methods for generating camouflaged trajectories are explored in the thesis. Firstly, a class of linear quadratic techniques is developed, including optimal cost-based control in two and three dimensions, and sub-optimal forward-time control using greedy control methods. Secondly, it is shown that dynamic gain proportional navigation can be used to mimic recorded insect trajectories, and hence a biomimetic camouflage guidance algorithm is theorized using proportional navigation. Finally, a method for implementing force-based camouflage control into fixed wing aerial robots is discussed.

Abstract

This thesis investigates the principles behind motion camouflage, in both the theoretical sense and in a subset of general interactive insect behavioural strategies. The theory of motion camouflage is explored, and an optimal-energy formula for motion camouflage is developed using Lagrangian mechanics. To determine the key dynamic variables used by insects to respond to one another while in flight, interactions between dragonflies are analysed and compared to satellite fly/wasp interactions, with spatial attention paid to instances of natural motion camouflage.

To use motion camouflage as a robotic stealth or tracking strategy, higher-level control algorithms are required. Hence two main control methods for generating camouflaged trajectories are explored in the thesis. Firstly, a class of linear quadratic techniques is developed, including optimal cost-based control in two and three dimensions, and sub-optimal forward-time control using greedy control methods. Secondly, it is shown that dynamic gain proportional navigation can be used to mimic recorded insect trajectories, and hence a heuristic camouflage guidance algorithm is developed using proportional navigation. Finally, a method for implementing force-based camouflage control into fixed-wing aerial robots is discussed.

Contents

| | |
|------------------------------------------------------------------------|------------|
| Declaration | iii |
| 1 Introduction | 1 |
| 1.1 Background | 1 |
| 1.1.1 An overview of insect vision | 1 |
| 1.1.2 Visually guided behaviour in free-flying insects | 3 |
| 1.2 Motion Camouflage | 8 |
| 1.2.1 A Neural Network Model | 9 |
| 1.2.2 Mathematical laws defining camouflage geometry | 11 |
| 1.2.3 Further biological inspiration | 11 |
| 1.2.4 Analysis of a differential game formulation of motion camouflage | 12 |
| 1.3 Contribution of this thesis | 12 |
| 1.3.1 Thesis Structure | 13 |
| 2 An Exploration of Motion Camouflage | 15 |
| 2.1 Introduction | 15 |
| 2.2 Defining a motion camouflage interaction | 16 |
| 2.2.1 Two-dimensional camouflage geometry | 16 |
| 2.2.2 Three-dimensional camouflage geometry | 18 |
| 2.3 Optimal Motion Camouflage Paths | 22 |
| 2.3.1 Introduction to Lagrangian Mechanics | 22 |
| 2.3.2 Procedure | 23 |
| 2.3.3 Discussion | 29 |
| 3 Control for Camouflage | 31 |
| 3.1 Introduction to LQR control | 31 |
| 3.2 Two-Dimensional Linear Quadratic Regulator for Motion Camouflage | 32 |
| 3.2.1 Dynamics of Motion | 33 |
| 3.2.2 Motion Camouflage Constraints | 34 |
| 3.2.3 Problem Formulation and Solution | 35 |
| 3.2.4 Optimal Motion Camouflage Guidance | 37 |
| 3.2.5 Infinite point camouflage | 37 |
| 3.3 Results | 38 |
| 3.3.1 General Example: Pursuit | 38 |
| 3.3.2 Mimicking Dragonfly Encounters: Realistic Constraints | 39 |
| 3.3.3 Infinite Point Camouflage | 41 |
| 3.4 LQR: Extension to 3 Dimensions | 42 |
| 3.4.1 Dynamics of motion | 42 |
| 3.5 Problem formulation | 42 |
| 3.5.1 Performance Index | 42 |
| 3.5.2 Augmented dynamics | 44 |

| | | |
|----------|------------------------------------------------------------------------|------------|
| 3.5.3 | Results | 44 |
| 3.5.4 | Spherical co-ordinate transformation | 44 |
| 3.6 | Greedy Optimal Control | 45 |
| 3.6.1 | Problems with LQR | 45 |
| 3.6.2 | Problem formulation | 46 |
| 3.6.3 | Results | 48 |
| 3.6.4 | Analysis | 48 |
| 3.7 | Implementing Force-based Control in Flexible Aerial Vehicles | 49 |
| 3.7.1 | Attitude from Wind-Axis Forces | 51 |
| 3.7.2 | Attitude from Inertial Acceleration | 55 |
| 3.8 | Discussion | 62 |
| 4 | Characteristics of Dragonfly and Satellite Fly Pursuit | 65 |
| 4.1 | Introduction | 65 |
| 4.2 | Variable definition | 66 |
| 4.3 | Method | 66 |
| 4.3.1 | Monoscopic filming in the horizontal plane | 67 |
| 4.3.2 | Monoscopic filming in the vertical plane | 67 |
| 4.3.3 | Stereo footage, filmed from the horizontal plane | 68 |
| 4.3.4 | 3D reconstruction from stereo cameras | 68 |
| 4.3.5 | Data processing | 69 |
| 4.3.6 | Error sources | 71 |
| 4.4 | Results from Dragonfly Interactions | 71 |
| 4.4.1 | Results from monoscopic data | 71 |
| 4.4.2 | Pursuit characteristics in three dimensions | 91 |
| 4.5 | Results from Satellite Flies | 103 |
| 4.6 | Motion Camouflage in Dragonflies | 103 |
| 4.6.1 | Method for determining camouflaged sequences | 105 |
| 4.6.2 | Results | 107 |
| 4.7 | Motion Camouflage in Satellite Flies | 111 |
| 4.7.1 | Results | 111 |
| 4.8 | Discussion | 111 |
| 5 | Proportional Navigation and Insect Flight | 121 |
| 5.1 | Variable definition | 121 |
| 5.2 | Introduction | 121 |
| 5.3 | Decoupling the Control Systems | 122 |
| 5.3.1 | Forward Speed Control | 123 |
| 5.3.2 | Directional Control | 123 |
| 5.3.3 | Implementing a Decoupled Control System | 124 |
| 5.4 | Acceleration-based Control and PN guidance | 129 |
| 5.4.1 | Explanation of PN guidance | 130 |
| 5.5 | Extrapolation into Three Dimensions | 131 |
| 5.6 | PN Guidance and Motion Camouflage | 133 |
| 5.6.1 | Background | 133 |
| 5.6.2 | 2D Problem Definition | 133 |
| 5.6.3 | Required acceleration for a non-maneuvering target | 135 |
| 5.6.4 | Solution for a maneuvering target | 138 |

| | | |
|----------|-----------------------------------------------------------|------------|
| 5.6.5 | PN guidance for motion camouflage | 140 |
| 5.6.6 | Stability | 140 |
| 5.7 | Discussion | 142 |
| 5.7.1 | Limitations of the biomimetic decoupled control | 142 |
| 5.7.2 | Proportional Navigation and biomimetic control | 143 |
| 6 | Discussion | 145 |
| 6.1 | Thesis summary | 145 |
| 6.2 | Future Work | 148 |
| A | Lagrangian Optimization and Lagrange Multipliers | 151 |
| A.1 | Virtual Velocity | 151 |
| A.2 | Multipliers and constrained systems | 151 |
| B | Attitude Representation | 155 |
| B.1 | Rotation matrices | 155 |
| B.1.1 | Co-ordinate transformations | 155 |
| B.1.2 | Co-ordinate rotations | 156 |
| B.1.3 | Rotation matrix multiplication | 156 |
| B.2 | Euler Angles | 156 |
| B.2.1 | Euler angle rates | 157 |
| B.2.2 | Valid rotation sequences | 157 |
| B.2.3 | Singularities | 158 |
| B.3 | Quaternions | 158 |
| B.3.1 | Conversions | 159 |
| | Bibliography | 161 |

| | | |
|-----|-------------------------------------------------------|-----|
| 180 | 2.5.5. IV subcase for motion constraints | 180 |
| 180 | 2.5.6. Stability | 180 |
| 182 | 2.7. Discussion | 182 |
| 183 | 2.7.1. Limitations of the kinematic decoupled control | 183 |
| 183 | 2.7.2. Proportional Navigation and nonlinear control | 183 |
| 184 | Discussion | 184 |
| 184 | 2.7.3. Three angular | 184 |
| 185 | 2.7.4. Future Work | 185 |
| 185 | 2.8. Lagrangian Optimization and Lagrange Multipliers | 185 |
| 185 | 2.8.1. Virtual Velocity | 185 |
| 187 | 2.8.2. Multipliers and associated | 187 |
| 178 | 2.9. Attitude Representation | 178 |
| 178 | 2.9.1. Rotation matrix | 178 |
| 180 | 2.9.2. Quaternion representation | 180 |
| 180 | 2.9.3. Rotation matrix properties | 180 |
| 180 | 2.9.4. Euler angles | 180 |
| 187 | 2.9.5. Euler axis-angle | 187 |
| 187 | 2.9.6. Quaternion operations | 187 |
| 188 | 2.9.7. Euler angles | 188 |
| 188 | 2.9.8. Conversion | 188 |
| 188 | 2.9.9. Conversion | 188 |
| 188 | 2.9.10. Conversion | 188 |
| 188 | 2.9.11. Conversion | 188 |
| 188 | 2.9.12. Conversion | 188 |
| 188 | 2.9.13. Conversion | 188 |
| 188 | 2.9.14. Conversion | 188 |
| 188 | 2.9.15. Conversion | 188 |
| 188 | 2.9.16. Conversion | 188 |
| 188 | 2.9.17. Conversion | 188 |
| 188 | 2.9.18. Conversion | 188 |
| 188 | 2.9.19. Conversion | 188 |
| 188 | 2.9.20. Conversion | 188 |
| 188 | 2.9.21. Conversion | 188 |
| 188 | 2.9.22. Conversion | 188 |
| 188 | 2.9.23. Conversion | 188 |
| 188 | 2.9.24. Conversion | 188 |
| 188 | 2.9.25. Conversion | 188 |
| 188 | 2.9.26. Conversion | 188 |
| 188 | 2.9.27. Conversion | 188 |
| 188 | 2.9.28. Conversion | 188 |
| 188 | 2.9.29. Conversion | 188 |
| 188 | 2.9.30. Conversion | 188 |
| 188 | 2.9.31. Conversion | 188 |
| 188 | 2.9.32. Conversion | 188 |
| 188 | 2.9.33. Conversion | 188 |
| 188 | 2.9.34. Conversion | 188 |
| 188 | 2.9.35. Conversion | 188 |
| 188 | 2.9.36. Conversion | 188 |
| 188 | 2.9.37. Conversion | 188 |
| 188 | 2.9.38. Conversion | 188 |
| 188 | 2.9.39. Conversion | 188 |
| 188 | 2.9.40. Conversion | 188 |
| 188 | 2.9.41. Conversion | 188 |
| 188 | 2.9.42. Conversion | 188 |
| 188 | 2.9.43. Conversion | 188 |
| 188 | 2.9.44. Conversion | 188 |
| 188 | 2.9.45. Conversion | 188 |
| 188 | 2.9.46. Conversion | 188 |
| 188 | 2.9.47. Conversion | 188 |
| 188 | 2.9.48. Conversion | 188 |
| 188 | 2.9.49. Conversion | 188 |
| 188 | 2.9.50. Conversion | 188 |
| 188 | 2.9.51. Conversion | 188 |
| 188 | 2.9.52. Conversion | 188 |
| 188 | 2.9.53. Conversion | 188 |
| 188 | 2.9.54. Conversion | 188 |
| 188 | 2.9.55. Conversion | 188 |
| 188 | 2.9.56. Conversion | 188 |
| 188 | 2.9.57. Conversion | 188 |
| 188 | 2.9.58. Conversion | 188 |
| 188 | 2.9.59. Conversion | 188 |
| 188 | 2.9.60. Conversion | 188 |
| 188 | 2.9.61. Conversion | 188 |
| 188 | 2.9.62. Conversion | 188 |
| 188 | 2.9.63. Conversion | 188 |
| 188 | 2.9.64. Conversion | 188 |
| 188 | 2.9.65. Conversion | 188 |
| 188 | 2.9.66. Conversion | 188 |
| 188 | 2.9.67. Conversion | 188 |
| 188 | 2.9.68. Conversion | 188 |
| 188 | 2.9.69. Conversion | 188 |
| 188 | 2.9.70. Conversion | 188 |
| 188 | 2.9.71. Conversion | 188 |
| 188 | 2.9.72. Conversion | 188 |
| 188 | 2.9.73. Conversion | 188 |
| 188 | 2.9.74. Conversion | 188 |
| 188 | 2.9.75. Conversion | 188 |
| 188 | 2.9.76. Conversion | 188 |
| 188 | 2.9.77. Conversion | 188 |
| 188 | 2.9.78. Conversion | 188 |
| 188 | 2.9.79. Conversion | 188 |
| 188 | 2.9.80. Conversion | 188 |
| 188 | 2.9.81. Conversion | 188 |
| 188 | 2.9.82. Conversion | 188 |
| 188 | 2.9.83. Conversion | 188 |
| 188 | 2.9.84. Conversion | 188 |
| 188 | 2.9.85. Conversion | 188 |
| 188 | 2.9.86. Conversion | 188 |
| 188 | 2.9.87. Conversion | 188 |
| 188 | 2.9.88. Conversion | 188 |
| 188 | 2.9.89. Conversion | 188 |
| 188 | 2.9.90. Conversion | 188 |
| 188 | 2.9.91. Conversion | 188 |
| 188 | 2.9.92. Conversion | 188 |
| 188 | 2.9.93. Conversion | 188 |
| 188 | 2.9.94. Conversion | 188 |
| 188 | 2.9.95. Conversion | 188 |
| 188 | 2.9.96. Conversion | 188 |
| 188 | 2.9.97. Conversion | 188 |
| 188 | 2.9.98. Conversion | 188 |
| 188 | 2.9.99. Conversion | 188 |
| 188 | 2.9.100. Conversion | 188 |

List of Figures

| | | |
|------|--------------------------------------------------------------------------------------------------------------|----|
| 1.1 | Diagram of the compound eye | 2 |
| 1.2 | The phenomenon of motion camouflage | 9 |
| 1.3 | Neural network control system architecture | 10 |
| 2.1 | Depiction of the two primary types of motion camouflage | 15 |
| 2.2 | Static point motion camouflage geometry | 17 |
| 2.3 | Infinite point camouflage geometry | 18 |
| 2.4 | Non-collinear pursuer and target | 19 |
| 2.5 | Vector diagram of required velocity conditions | 20 |
| 2.6 | Constant LOS direction | 20 |
| 2.7 | 3D non-collinear geometry | 21 |
| 2.8 | Optimal solutions to linear trajectories | 26 |
| 2.9 | Comparison between a straight interception trajectory and an energy optimal trajectory | 27 |
| 2.10 | Energy-efficient capture trajectory | 28 |
| 2.11 | Tracking at a constant distance | 29 |
| 3.1 | Reference frames | 36 |
| 3.2 | Examples of static point motion camouflage using a two-dimensional linear quadratic solution | 38 |
| 3.3 | Error and control acceleration curves | 39 |
| 3.4 | Example of a nonlinear target trajectory. | 39 |
| 3.5 | Trajectory with a systematic range estimation error | 40 |
| 3.6 | Shadowing and capture | 41 |
| 3.7 | Examples of static point motion camouflage using a three-dimensional linear quadratic solution | 45 |
| 3.8 | LQR against a manoeuvring target | 46 |
| 3.9 | Greedy optimal control performance | 49 |
| 3.10 | Comparison of trajectories and velocity control inputs required for greedy and LQR trajectories | 50 |
| 3.11 | Angle comparison between greedy and LQR control | 51 |
| 3.12 | Various methods of losing altitude by changing the inertial orientation of the aircraft | 52 |
| 3.13 | Attitude: output/setpoints derived from inertial inputs | 56 |
| 3.14 | Angular rates and inertial accelerations for direct attitude control using an F16 flight simulator | 57 |
| 3.15 | Screenshots from flight simulator | 57 |
| 3.16 | Force-based autopilot following an LQR trajectory | 58 |
| 3.17 | Parameterization of the waypoint paths | 60 |
| 3.18 | Waypoint-following trajectory | 62 |
| 3.19 | Control accelerations and resultant accelerations | 63 |

| | | |
|------|------------------------------------------------------------------------------------------------------------------------------|-----|
| 4.1 | Inertial, or world axes | 67 |
| 4.2 | Two-dimensional camera arrangements | 68 |
| 4.3 | Reconstruction of depth from images generated by two parallel cameras | 69 |
| 4.4 | Lateral movement of <i>Hemicordulia tau</i> | 72 |
| 4.5 | Actual retinal angular position and position if the body were aligned with the flight direction | 73 |
| 4.6 | Retinal position, in degrees | 74 |
| 4.7 | Dragonfly fixation | 76 |
| 4.8 | An example of pursuer and target swapping roles partway through a pursuit | 77 |
| 4.9 | Example 1: Error angle and body orientation | 78 |
| 4.10 | Example 2: Error angle and body orientation | 79 |
| 4.11 | Example 3: Error angle and body orientation | 80 |
| 4.12 | Example 4: Error angle and body orientation | 81 |
| 4.13 | Example 5: Error angle and body orientation | 82 |
| 4.14 | Example 6: Error angle and body orientation | 83 |
| 4.15 | Cross-correlation between error angle and yaw velocity | 84 |
| 4.16 | Error angle rate influencing yaw velocity | 85 |
| 4.17 | Scatter diagrams showing LOS velocity and body axis angular velocity | 86 |
| 4.18 | Example 1: Error angle and flight direction | 87 |
| 4.19 | Example 2: Error angle and flight direction | 88 |
| 4.20 | Example 3: Error angle and flight direction | 89 |
| 4.21 | Example 4: Error angle and flight direction | 90 |
| 4.22 | Example of significant lag between a change in LOS angular velocity and a corresponding change in flight direction | 92 |
| 4.23 | Cross-correlation between error angle velocity and flight angle velocity. | 93 |
| 4.24 | Inverted turning response | 93 |
| 4.25 | Example 1: Range, speed and change in flight direction | 94 |
| 4.26 | Example 2: Range, speed and change in flight direction | 95 |
| 4.27 | Example 3: Range, speed and change in flight direction | 96 |
| 4.28 | Example 4: Range, speed and change in flight direction | 97 |
| 4.29 | Example 5: Range, speed and change in flight direction | 98 |
| 4.30 | Example 1: Speed profiles | 99 |
| 4.31 | Example 2: Speed profiles | 100 |
| 4.32 | Example 3: Speed profiles | 101 |
| 4.33 | Relative speed between the participants | 102 |
| 4.34 | Satellite fly fixation | 104 |
| 4.35 | Determining a motion camouflage interaction | 106 |
| 4.36 | Typical camouflage sequences in dragonfly flight | 108 |
| 4.37 | Example 1: Motion camouflage in dragonflies | 109 |
| 4.38 | Example 2: Motion camouflage in dragonflies | 109 |
| 4.39 | Example 3: Motion camouflage in dragonflies | 110 |
| 4.40 | Trivial motion camouflage in dragonflies | 110 |
| 4.41 | Example 1: Motion camouflage in satellite flies | 112 |
| 4.42 | Example 2: Motion camouflage in satellite flies | 112 |
| 4.43 | Example 3: Motion camouflage in satellite flies | 113 |
| 4.44 | Example 4: Motion camouflage in satellite flies | 113 |
| 4.45 | Satellite flies: Cross-correlation between changes in flight direction and changes in LOS angular position | 116 |

| | | |
|------|------------------------------------------------------------------------------------------------------------------|-----|
| 4.46 | Dragonflies: Cross-correlation between changes in flight direction and changes in LOS angular position | 117 |
| 4.47 | Motion camouflage: Cars on a highway | 118 |
| 4.48 | Time-asymmetric trajectory | 119 |
| 5.1 | Example 1: Flight direction and line of sight angle | 125 |
| 5.2 | Example 2: Flight direction and line of sight angle | 125 |
| 5.3 | Example 3: Flight direction and line of sight angle | 126 |
| 5.4 | Example: Trajectory matching | 127 |
| 5.5 | Further examples of trajectory matching | 128 |
| 5.6 | System geometry and dynamics | 129 |
| 5.7 | System geometry and dynamics: 3D | 131 |
| 5.8 | Dynamics in the horizontal and vertical plane | 131 |
| 5.9 | Spherical reference frame: unit vectors | 132 |
| 5.10 | Motion camouflage dynamics in a spherical inertial reference frame | 134 |
| 5.11 | Motion camouflage path for a non-maneuvering target using PN-derived acceleration commands | 137 |
| 5.12 | Control commands for a linear quadratic regulator solution | 137 |
| 5.13 | MCPN path for tracking an oblivious biomimetic target | 138 |
| 5.14 | MCPN path against an active target using GTPN guidance | 139 |

Introduction

Over millions of years of evolution, biological systems have developed robust strategies of achieving complex navigational behaviors. Insects, having small brains and comparatively simple nervous systems, yet with an adeptness of performance that far outstrips most purpose-built robots, are of especial interest. They are remarkably swift and accomplish feats of astonishing agility and accuracy.

Insects, therefore, have for many years intrigued roboticists, biologists and anyone seeking methods of matching sensory input to action. In terms of guidance, flying insects are particularly interesting, since they are often quite tiny yet fully capable of movement in all three dimensions with six degrees of freedom.

Most highly adept arthropod fliers rely heavily on vision to navigate through their environment. For roboticists and engineers, accurately interpreting and reacting to objects and changes in the visual field is a complex task, often requiring much processing power and many layers of information filtering. For insects, it is a process which occurs with enviable speed. Hence it is likely that much can be learned from insects on how best to link vision to action.

1.1 Background

1.1.1 An overview of insect vision

Insect eyes are markedly different from those of mammals or birds. Insects have compound eyes consisting of many individual visual units called ommatidia, each equipped with a separate lens that focusses light onto a photoreceptor unit that functions like an individual 'pixel', unlike mammalian eyes where a single lens will focus light onto a retina comprised of several million photoreceptors. The number of ommatidia varies between insects, and their precise structure and spacing can differ even within a single eye. For instance, the

inter-ommatidial angle and the size of the facet lenses, which together determine resolution, vary across the eyes of many insects. The acuity of a given portion of an eye is inversely related to the interommatidial angles in that region. These regions of high acuity, where resolution is considerably better than in other areas, are called acute zones, the location of which depend on the species [Lan89].

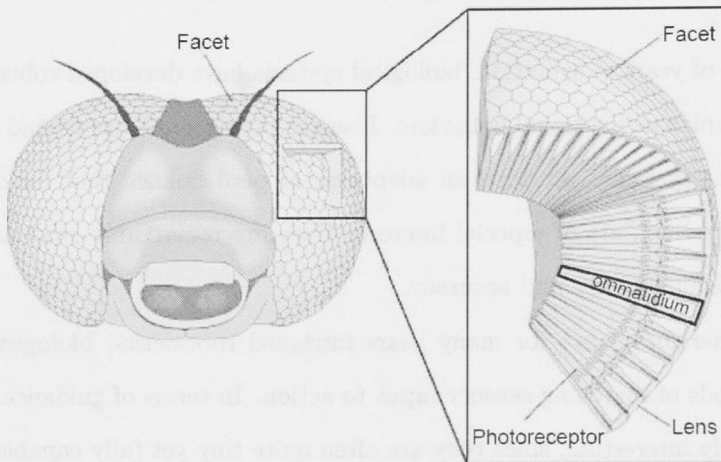


Figure 1.1: Compound eyes are made up of repeating units, the ommatidia, each of which functions as a separate visual receptor. Each ommatidium consists of a lens (the front surface of which makes up a single facet), a transparent crystalline cone, light-sensitive visual cells arranged in a radial pattern, and pigment cells which optically separate the ommatidium from its neighbours. Figure adapted from <http://soma.npa.uiuc.edu>.

Predatory insects such as wasps and dragonflies tend to have much smaller interommatidial angles than non-predatory insects, at least in the forward pointing region of the eye (the region generally used for tracking prey). But foveal location and the degree of resolution therein can vary even within species; for example, many insects from the order *Diptera* display a sexual dimorphism in the location or even existence of acute zones in their eyes [Str80].

The consequence of this eye design is a fixed-focus, low-resolution, panoramic field of view, with regions of greater or lesser sensitivity and resolution. Because compound eyes cannot be focussed, are not mobile within the head and in most cases are very close together, most insects cannot assess range and spatial arrangements in the same way mammals do. Instead, they make heavy use of optic flow cues when navigating through

their environment using alternative visual strategies. Indeed, most responsive behaviour observed in flying insects can be described as reactions to detectible features of motion in the visual field, in other words features of the optic flow experienced by the insect. Optic flow is the term for the visual field motion experienced by a moving body. It comprises both the relative motion induced by the parameters of the body's own movements and that caused by the three-dimensional layout and relative velocities of the environment. As described by Eckert and Zeil [EZ01]:

An actively moving or passively displaced observer experiences a distinct optic flow structure superimposed on the environmental motion field which depends on eye or body rotation, on the direction of translation, on the spatial layout of objects, and on contrast in the environment.

A great deal of the optic flow structure is determined by the observer's own behaviour, and so navigation and vision are for insects tightly coupled, with each feeding back on the other [SZ04].

1.1.2 Visually guided behaviour in free-flying insects

During flight, the retinal image flow can be used to regulate speed and orientation, and provide information about the location and movement of objects in the environment. Such optic flow has been demonstrated to assist insects in tracking [BKE03], hovering [CL75], patrolling [Zei86], foraging [HJZB03] and in migratory flight [BSR92]. The picture of insect navigation that has been built up is one where the interaction of a few simple guidance rules underlies complex behavioral responses.

Orientation and attitude control:

Attitude stabilization can be accomplished by compensating for the rotary component of optic flow. This compensation can be readily observed in the well-studied optomotor response, where an insect responds to a (horizontally) rotating environment by generating a counteractive yaw torque, thus bringing the insect back on course [Rei69]. Similar mechanisms are thought to exist to stabilize attitude around the other body axes. For example, compensatory head movements to stabilize perceived changes in roll and pitch have been observed [Hen93] in flies.

Insects are thought to accomplish course stabilization by the possession of motion-sensitive neurons with large visual fields [BSO⁺06], each responding preferentially to motion in a specific direction [HE89], [Kra00]. These neurons each typically cover particular sections of the visual field, and a straight course can be achieved by balancing the responses of two neurons on either side of the head, sensitive to front-to-back motion in one eye. This works well in a symmetrical environment, but in an asymmetric world a slightly different mechanism is required. In this case, steering a straight course necessitates compensating for image motion in only a small patch of the visual field, facing the direction in which the insect wishes to fly [SZ04]. Hoverflies have been shown to use just such a mechanism [Col80b].

Roll and pitch stabilization are assisted by the ocelli (three single-lens eyes situated on the top of the insect's head). Each ocelli has a large visual field, and stabilizes orientation by reference to the horizon [SH79]. The two laterally directed ocelli stabilize roll, the median ocelli stabilizes pitch [SH79], [Wil78].

Obstacle avoidance and landing:

Flying insects use expansion and contraction of the image of an object to avoid collisions and to land on surfaces. When the image expansion exceeds a certain threshold, the insect turns away from whichever eye experiences greater image expansion [TD02]. Similarly, when approaching a surface for landing, an insect needs to monitor the rate of expansion very precisely. Translatory optic flow plays a large part in the latter. For example, when accomplishing grazing landings, bees have been shown to keep the velocity of the horizontal surface image approximately constant as they reduce height. In this way, the bee's speed is progressively decreased as it approaches the landing surface [SZC⁺00]. The same principle can be used to control head-on landing, where it is the rate of image expansion that is held constant. For example, in female houseflies deceleration prior to landing is triggered when the ratio of image expansion of a target on the retina to the actual image size exceeds a certain threshold [Wag82].

Control of flight speed and height:

The above mechanism for controlling landing can also give us insight into that used for monitoring speed during cruising flights [SZ04]. Fruit flies hold the angular velocity of

the environment constant and can be tricked into stationary hovering within a tunnel by adjusting the apparent speed of the tunnel's walls [Dav82]. Bees appear to use a similar method of measuring flight speed [SZLC96]. Both insects have been shown to compensate for headwind, and interestingly, measurement of the angular velocity of the image appears to be independent of the spatial structure [SLKZ91], [DOL01], [Ibb01]. The movement-detecting subsystem mediating this response seems quite different from that governing the optomotor response [Sri93].

Since the optic flow rate of the ground decreases as height increases, it is possible that insects can use this to monitor their altitude, provided they know their own speed, although this speculation is as yet unsubstantiated. Apparent optic flow of the ground at a known speed has certainly been used extensively to measure altitude in autonomous vehicles [BCS03], [NB02], [STS06].

Odometry:

Insects are not simply opportunistic navigators responding only to immediate circumstance. They also are capable of navigating great distances in search of food sources and returning precisely to their nests [Col96], [ZKV96], or communicating to nest mates the location of the food source [SZLC96]. It is increasingly apparent that visual information plays a vital role in how insects negotiate and calculate the distance traveled. For example, wasps can home accurately when transported away from their nests in transparent containers, but not opaque ones [Ugo87]. Bees have been shown to estimate distance flown by integrating over time the image motion of the environment [SZB97]. The advantages of using visual cues to monitor distance traveled, rather than energy-based cues, for example, are several fold. For one, a visually-driven odometer is not affected by wind or the load carried. Moreover, it is independent of the speed of the insect, although highly dependent on visual texture [TZS⁺04]. However, there is a disadvantage in communicating location in this way, namely that a visual odometer works only if the insect receiving the information follows the same route previously traversed (or, if the method is being used to return to the nest, the insect must follow the same path on both outbound and inbound journeys) [SZ04].

Tracking moving targets:

Insects must not only move through an often complex but essentially stationary environment, they also need to interact with other living creatures in order to survive. This interaction may take the form of avoiding predators, catching prey, chasing potential mates, or warding off intruders into their territory. In all these behaviors, vision is of vital importance.

Pursuit, whether of prey or conspecifics, can be observed in a large variety of insects. Male houseflies engage in territorial chases with other males [LC74], [Zei86]. Blowflies chase and catch females for mating purposes [BKE03]. Satellite flies visually track the position of digger wasps in order to lay their eggs on the wasps prey prior to it entering the nest [Wci84]. Dragonflies pursue both prey and each other in fast, acrobatic chases [OWV00], [FO95]. Hoverflies pursue and intercept females in mating flights [CL78]. In fact, tracking and pursuit behaviour is perhaps one of the more interesting attributes of insect flight.

Tracking is defined as the process of keeping an image of a target on a particular region on the retina, whereby the target may be stationary or it may itself be in motion. In tracking, the primary purpose is usually to keep the target image in frontal acute zone, as observed in praying mantises, for example [Ros80]. When tracking is combined with motion towards the target, the activity is termed 'pursuit' [M.F92]. Pursuit may encompass shadowing of the target at a certain distance, capture of the target, or some combination of both.

The common feature of all the visual tracking systems noted in mammals and insects is a control system which attempts to minimize the angular deviation between the retinal position of a target and some region of the eye, often but not always the central or forward part of the retina.

In the simplest control of this type, a target position error thus registered will output a corrective movement by the pursuer. However, many permutations on this basic tactic exist. The methods humans use to track targets visually are classified into two branches, saccadic tracking and smooth pursuit, which serve two different but complementary purposes [CT84]:

Smooth pursuit and saccades subserve two different functions. The effect of

smooth pursuit eye movements is to reduce the slip velocity of the image on the fovea and thereby limit the accumulation of retinal position error. This stabilization is not perfect. Therefore saccades frequently interrupt the smooth eye movements to correct the eye position. Saccades during pursuit are indeed corrective; they bring the image of the target closer to the centre of the fovea. In general, a subject makes a saccade during pursuit if the retinal error rises above a certain unacceptably high level. The saccade which is generated brings the target closer to the fovea and the remaining position error is smaller than the average retinal error during pursuit. The level of retinal position error is not constant, but varies in time and depends on stimulus conditions. The corrective saccades are not perfect and they alleviate the imprecision of pursuit only for short periods of time.

H. Collewijn, E. P. Tamminga, 1984, [CT84]

Mantids turn their heads in response to a change in target retinal position using two different strategies, the choice of which depends on both background features and target velocity [Ros80]. Certain species of hoverfly combine the optomotor response additively with a tracking response, causing a pursuing fly to track with a small position offset [Col80a]. Houseflies manifest both smooth and saccadic tracking [Wag86] using a single continuous control system, where if the target is displaced sufficiently rapidly on the pursuers retina it generates saccadic changes of body orientation [BKE03]. In flies, the apparent size of the target and the deviation of the angular location of the image from the frontal region of the eye drive a simple servomechanism that controls the direction and forward speed of a pursuer [BE05]. Dragonflies, too, target and chase potential prey by responding to size and angular velocity across the retina [OWV00]. It is known that male flies possess 'chasing' neurons which respond selectively to small, rapid targets [GS91], these being distinct from the large-field optomotor neurons [FO95], and similar to small-target selective neurons that have recently been described in female hoverflies [NO96].

The precise tracking system in use depends on the nature of the tasks it is involved in, and the way motion is processed by the visual system of the insect in question. Hoverflies have one of the most interesting tracking mechanisms so far observed, because rather than

heading directly towards a target as do houseflies, they seem to somehow calculate an interception or collision course from their target's apparent speed [CL78]. This chasing mechanism is primarily used by males in attempting to catch females, and they appear to make an assumption about the size of their target to determine an interception point from the angular position and velocity of said target.

Some hoverfly tracking sequences recorded by Collett and Land [CL78] were observed by Srinivasan and Davey [SD95] to contain an interesting geometric property. They named this feature 'motion camouflage', and it is the intriguing nature of motion camouflage which gave rise to this thesis.

1.2 Motion Camouflage

Most insects are adept at distinguishing between stationary and moving objects even when they themselves are in motion [Leh97]. Motion camouflage provides a mechanism by which a pursuer may track a target without revealing itself to be moving at all [SD95]. Srinivasan and Davey identified several types of camouflage, all of which fall into one of two categories: static point camouflage (illustrated in 1.2(a),(b),(d)), or camouflage at infinity (1.2(c)). When lines drawn between the two moving animals at successive time intervals intersect at a single point in space, motion camouflage is said to have occurred. The point thus defined is called the static, or fixed, point of the engagement, and the lines joining the target position and this static point are termed camouflage constraint lines (CCLs), because the motion of the shadower is constrained to these lines if camouflage is to be maintained.

After the presence of this tracking strategy was noted in hoverflies, short sequences of camouflaged motion were subsequently observed in the dragonfly *Hemianax papuensis* by Mizutani et al [MCS03]. An implication of this research is that motion camouflage, whether a deliberate strategy or simply the byproduct of some other guidance system, might be a common phenomenon. By studying those cases where it does occur, we can draw insight into not only the nature of motion camouflage, but into the underlying control systems.

Since these initial observations were made, the possibilities for human use of a camouflage strategy have been seized on by the control and guidance community. Several

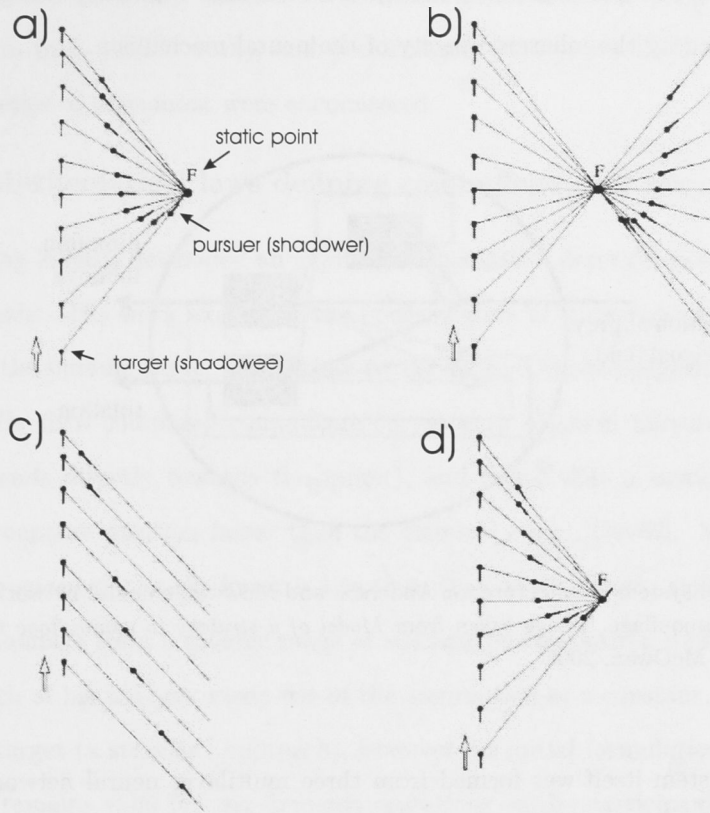


Figure 1.2: The basic phenomenon of motion camouflage. Shadower and shadowee positions are shown at equal time intervals, assuming the shadowee to be on a linear path with constant velocity. The shadower can camouflage its motion by emulating a stationary object at location F (the static point), which can lie behind the shadower (a); between the shadowee and shadower (b); at infinity (c); or at the shadowee's initial position (d). Image taken from *Strategies for active camouflage of motion*, M.V. Srinivasan and M. Davey, 1995

approaches to defining the geometry of camouflage and the control conditions required to produce it have been undertaken.

1.2.1 A Neural Network Model

Anderson and McOwen [AM03] designed a control system for camouflage which was constructed using trained neural networks. They assumed the only information about the target available to the shadower was its position in the shadower's visual field, and that the shadower was aware of the location of the fixed point relative to itself. In addition, the speed of the shadower was held constant. It was thought that the combination of the latter two input variables would enable the shadower to estimate its distance to the fixed

point by path integration, if required, although whether that capability was ever utilized is a matter obscured by the inherent opacity of the neural mechanism.

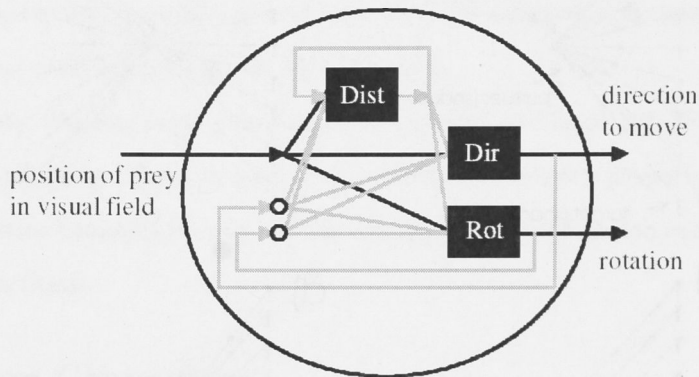


Figure 1.3: Control system architecture for Anderson and McOwan’s neural network-based controller for motion camouflage. Image taken from *Model of a strategy to camouflage motion*, A.J. Anderson and P.W. McOwan, 2003

The control system itself was formed from three multilayer neural networks (Figure 1.3). The first (DIST) is trained to estimate the distance to the fixed point, the second (DIR) the direction to move in, and the third (ROT) the appropriate rotation of the shadower body required to keep the target in the centre of the visual field. Note that this is a meaningless variable when considering a point mass, but may be significant when considering real guidance situations. The pursuing body does not, mathematically, have to point towards the target in order to maintain camouflage, but directional sensitivity issues in the visual sensory mechanism may make this a preferred strategy.

The authors postulated that the above control system is able to estimate the approximate range to the target, most likely from a combination of the existence of an outer bound on the starting conditions, and the errors in yaw created by the control itself - the same lateral movement will produce a greater retinal error when the target is close by than when it is at a distance (a motion parallax effect). However, without the explicit incorporation of range estimation into the model, it is not clear how important this dimensional information is to the solution offered. In addition, the study suffered from the usual limitations of neural network solutions. An exploration of the entire state-space was necessary prior to training the networks. In addition, the resulting controller was tailored

to the trajectories it was trained on (a combination of linear trajectories and hoverfly paths taken from earlier work), and performance quality was likely to deteriorate when other varieties of movement were encountered.

1.2.2 Mathematical laws defining camouflage geometry

Glendinning [Gle04] developed an explicit mathematical description of ideal motion camouflage paths. His work examined the consequences of a motion camouflage constraint acting on the pursuit curve, rather than trying to use a control algorithm to achieve camouflage. He then compared camouflage curves with classical pursuit curves (where the pursuer heads directly towards the target), and found that a motion camouflage path reaches a capture position faster than the classical curve [Dav62]. Moreover he showed that if the speed of the shadower is less than that of the target, capture is still possible using camouflage from a greater range of starting positions than if classical pursuit were used. Much of his analysis made use of the assumption of a constant speed for both pursuer and target (a standard approach), however his initial formulation of the camouflage geometry remains valid for any dynamic conditions on the participants.

1.2.3 Further biological inspiration

Justh and Krishnaprasad [JK06], inspired by insect-capture behaviour in echo-locating bats, used these equations of motion camouflaged paths to explore models in both two [JK06] and three [RJK06] dimensions, restricting the case to camouflage at infinity (although the principle can be extended to the static point case). The three-dimensional extension was accomplished by describing the particle trajectories using natural Frenet frames¹. They modeled the shadower and shadowee as points subject to curvature control, with a cost function representing the ratio of the change in radial distance to the target (along the line of sight vector) to the total rate of change of the vector over all. Notably, they observed that their formulation of the problem belonged to a subset of missile guidance laws known as pure proportional navigation, albeit with a range-dependent variable gain, of which more will be discussed later. Their contribution used a biologically plausible sensor data and feedback law, and was key in deriving an infinitesimal

¹Frenet frames are a useful vehicle for analysing invariant Euclidean curves [Bis75]. For more information, see [JK06], [JK05], [Bis75].

characterization of the dynamics of the motion camouflage problem.

1.2.4 Analysis of a differential game formulation of motion camouflage

Finally, Matchyn and Chikrii [MC06] strengthened the already established ties between motion camouflage and the field of missile guidance by considering the problem as a form of differential pursuit game. Using the method of resolving functions [Chi97], they established that given a linear dynamical system where the controls of shadower and shadowee are both chosen from defined compact sets, motion camouflage can be achieved and the shadower can capture the shadowee in a finite boundary time T for any shadowee motion, provided the integral inclusion condition [MC06] holds.

1.3 Contribution of this thesis

Although most of the methods described above consider the problem in terms of target angular position and velocity, and thus use information that is at least qualitatively available to insects attempting to perform motion camouflage, little work has been done in examining the dynamic behaviour surrounding those instances of camouflage actually observed in nature.

Geometry

Although the criteria for determining a motion camouflaged path have been well-established, it provides a dauntingly broad solution space. The task of selecting an appropriate path has heretofore been left to the controller, depending ultimately on assumptions and constraints on the dynamics. Therefore, as a preliminary step, I establish for any interaction, with no constraints other than the initial conditions and the movement of the target, a unique motion camouflaged path which minimizes the energy required by the controller (in a local sense).

Control

In a previous paper [CFC04], Jason Ford and I created a linear quadratic method of controlling for camouflage in two dimensions. Although this procedure built upon long-established traditions in missile guidance, ensuring a stable, robust feedback controller, it was in certain respects highly limited. The procedure and its limitations are detailed

within this thesis, and the theory is extended into three dimensions. An additional result which attempts to address and rectify some of the problems inherent in the traditional controller is also presented.

Camouflage in nature

Little research has been done into the biological examples of motion camouflage, even though it was the animal kingdom which first provided inspiration for the technique. Examining the flights of insects known to exhibit camouflaged behaviour, I extrapolate certain features of the guidance system in use in order to develop a controller which utilizes similar inputs and guidance techniques to those of insects.

1.3.1 Thesis Structure

Chapter 2

I first define the common terms used in discussing motion camouflage and write down the overall geometric law that describes a motion camouflage path. From this, I derive a simple condition that must be satisfied for a path to be classified as non-trivial motion camouflage. Then, using Glendinning's formula for ideal motion camouflage, I develop an equation which for any initial condition will describe a unique extremal motion camouflaged pathway, using Lagrangian optimization.

Chapter 3

I derive a linear-quadratic regulator for achieving camouflage in first two, then three dimensions. Using a greedy cost method, an infinite horizon method of linear dynamic control is shown to be successful in creating camouflaged paths. As a demonstration of how such force-based control might be later implemented in aerial robotic systems, a force-based autopilot is developed and several simple navigation tasks are simulated, including an LQR-based motion camouflage controller.

Chapter 4

Investigating interactive behaviour in two species of insect (dragonflies and satellite flies), I seek to establish which visual cues are responsible for guiding the paths and orientation of the pursuing or shadowing insect, first during all interactive flights, then specifically those sequences of interaction which may be described as being camouflaged.

Chapter 5

Using the information found in Chapter 4, I develop a preliminary decoupled control law which governs the forward speed and turning rate of a simulated insect in a manner similar to that observed in dragonflies. I then show that the coupled version of this control law fits into the general class of proportional navigation guidance laws, and use this to develop a biomimetic camouflage control law which uses information about the perceived location and speed of a target to generate a motion camouflaged path.

Chapter 6

A discussion of the results, their limitations and implications, and some suggestions for future work.

An Exploration of Motion Camouflage

2.1 Introduction

It is simple to write down equations that describe two bodies in a camouflaged trajectory. In this preliminary chapter, I introduce a strict mathematical definition for both varieties of camouflage as defined in the introduction, and proceed to establish some universally applicable dynamic rules which govern the motion of camouflaged bodies. I then derive a set of solutions for the motion camouflage problem which can be used to achieve energy-optimal trajectories.

Let \mathbf{r}^P be the position vector of an arbitrary static point in Cartesian space, and let $\mathbf{r}^D(t)$ and $\mathbf{r}^T(t)$ be the vectors representing the time-varying paths of the two participants in the dynamic engagement.

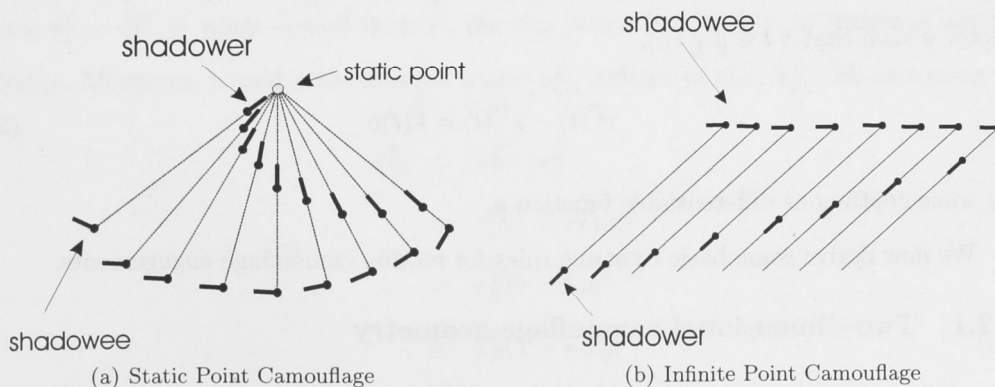


Figure 2.1: Depiction of the two primary types of motion camouflage

2.2 Defining a motion camouflage interaction

Variable Definition: In the following section, subscript text is used to indicate the frame of reference. Where no subscript is present, a stationary inertial frame located at the origin is assumed.

We define the following terms:

Definition We say that a static point camouflage between times t_A and t_B occurs if \exists a point \mathbf{r}^P such that $\forall t \in [t_A, t_B]$,

$$\mathbf{r}^P - \mathbf{r}^D(t) = k(t)(\mathbf{r}^P(t) - \mathbf{r}^T) \quad (2.1)$$

for some continuously differentiable function $k(t)$. If such an \mathbf{r}^P exists, we term it the static point of the engagement.

- If $k(t) < 0 \quad \forall t \in [t_A, t_B]$, the engagement is said to be *camouflaged between* for the period $[t_A, t_B]$.
- If $k(t) > 0 \quad \forall t \in [t_A, t_B]$, the engagement is said to be *camouflaged behind* for the period $[t_A, t_B]$.

These cases are often viewed as separate types of interaction [SD95], but in truth their geometry shares many salient features and there is no reason that k cannot change sign during an engagement. If this occurs, we say the engagement is *mixed*.

Definition We say that infinite point camouflage between times t_A and t_B occurs if \exists a vector \mathbf{e} such that $\forall t \in [t_A, t_B]$,

$$\mathbf{r}^T(t) - \mathbf{r}^D(t) = k(t)\mathbf{e} \quad (2.2)$$

for some continuous differentiable function k .

We now derive some basic dynamic rules for motion camouflage engagements.

2.2.1 Two-dimensional camouflage geometry

Consider a two-dimensional static point situation, as depicted in Figure 2.2. Without loss of generality, we transform the engagement into a polar reference frame with origin at \mathbf{r}^P . So the unit vectors along the polar co-ordinate axes for each point \mathbf{r}_P^D and \mathbf{r}_P^T are

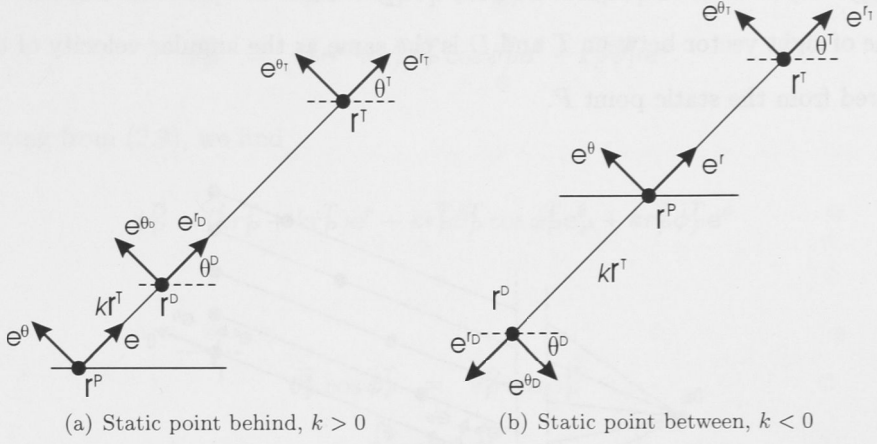


Figure 2.2: Static point motion camouflage geometry

$(e_P^{rD}, e_P^{\theta D})$ and $(e_P^{rT}, e_P^{\theta T})$. Since r_P^D and r_P^T lie on the same line, $e_P^{rD} = e_P^{rT} = e^r$ and $e_P^{\theta D} = e_P^{\theta T} = e^\theta$. Then

$$\begin{aligned} r_P^D &= r_P^D e^r \\ \dot{r}_P^D &= \dot{r}_P^D e^r + r_P^D \dot{\theta}_P^D e^\theta \end{aligned} \quad (2.3)$$

and similarly for r_P^T . Then since r^P is now the origin,

$$\begin{aligned} r_P^D &= k r_P^T \\ \dot{r}_P^D &= \dot{k} r_P^T + k \dot{r}_P^T \\ &= (\dot{k} r_P^T + k \dot{r}_P^T) e^r + k r_P^T \dot{\theta}_P^T e^\theta \end{aligned} \quad (2.4)$$

hence $\dot{\theta}_P^T = \dot{\theta}_P^D$, ie when viewed from P , the two points T and D have the same angular velocity. Moreover, consider the relative vector r_D^T , defined as $r_P^T - r_P^D$. We can write

$$\begin{aligned} r_D^T &= r_P^T - r_P^D \\ &= r_P^T e^r - k r_P^T e^r \\ &= r_P^T (1 - k) e^r \\ &= r_P^T (1 - k) e_P^{rT} \end{aligned} \quad (2.5)$$

hence, differentiating the last equation, we find

$$\dot{r}_D^T = \left(\dot{r}_P^T (1 - k) - k \dot{r}_P^T \right) + \dot{\theta}_P^T r_P^T (1 - k) e_P^{\theta T}. \quad (2.6)$$

Since $r_D^T = r_P^T(1 - k)$, the angular velocity of \mathbf{r}_D^T is equal to $\dot{\theta}_P^T$, ie the angular velocity of the line of sight vector between T and D is the same as the angular velocity of the target measured from the static point P .

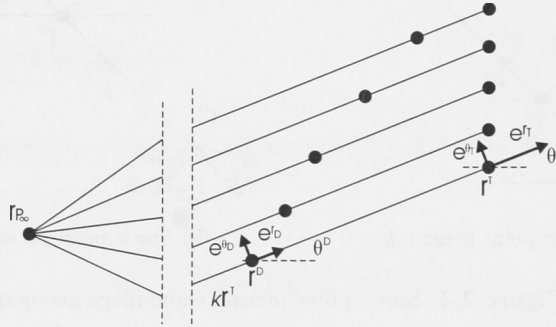


Figure 2.3: Infinite point camouflage geometry

For the two-dimensional infinite camouflage scenario (Figure 2.3), we observe that the set of lines $\{\mathbf{r}^{T_i} - \mathbf{r}^{D_i} \mid \mathbf{r}^{T_i} = \mathbf{r}^T(t_i), \mathbf{r}^{D_i} = \mathbf{r}^D(t_i); t_0 \leq t_i \leq t_f\}$ form a pencil with a meeting point at infinity, P_∞ . Therefore in the projective Euclidean plane encompassing this pencil and point, we can use a similar derivation to that above to show

$$\dot{\theta}_{P_\infty}^T = \dot{\theta}_{P_\infty}^D. \quad (2.7)$$

2.2.2 Three-dimensional camouflage geometry

In three dimensions, the method is similar. First, translate the origin to the static point \mathbf{r}^P and consider the engagement in a spherical co-ordinate system.

$$\begin{aligned} \mathbf{e}_P^{rT} &= \mathbf{e}_P^{rD} = \mathbf{e}^r \\ \mathbf{e}_P^{\theta T} &= \mathbf{e}_P^{\theta D} = \mathbf{e}^\theta \\ \mathbf{e}_P^{\phi T} &= \mathbf{e}_P^{\phi D} = \mathbf{e}^\phi. \end{aligned} \quad (2.8)$$

Proceeding as before:

$$\begin{aligned} \mathbf{r}_P^D &= r_P^D \mathbf{e}^r \\ &= kr_P^T \\ &= kr_P^T \mathbf{e}^r \end{aligned} \quad (2.9)$$

$$\begin{aligned}\dot{\mathbf{r}}_P^D &= \dot{r}_P^D \mathbf{e}^r + r_P^D \dot{\theta}_P^D \cos \phi_P^D \mathbf{e}^\theta + \mathbf{r}_P^D \dot{\phi}_P^D \mathbf{e}^\phi \\ \dot{\mathbf{r}}_P^T &= \dot{r}_P^T \mathbf{e}^r + r_P^T \dot{\theta}_P^T \cos \phi_P^T \mathbf{e}^\theta + \mathbf{r}_P^T \dot{\phi}_P^T \mathbf{e}^\phi.\end{aligned}\quad (2.10)$$

Substituting from (2.9), we find

$$\dot{\mathbf{r}}_P^D = (\dot{k}r_P^T + kr_P^T) \mathbf{e}^r + kr_P^T \dot{\theta}_P^T \cos \phi_P^T \mathbf{e}^\theta + kr_P^T \dot{\phi}_P^T \mathbf{e}^\phi \quad (2.11)$$

hence

$$\dot{\theta}_P^T \cos \phi_P^T = \dot{\theta}_P^D \cos \phi_P^D \quad (2.12)$$

$$\dot{\phi}_P^T = \dot{\phi}_P^D. \quad (2.13)$$

Similarly, let $\mathbf{r}_D^T = r_P^T(1-k)\mathbf{e}^r$. Then, as in section 2.2.1, we find

$$\dot{\mathbf{r}}_D^T = (\dot{r}_P^T(1-k) - \dot{k}r_P^T) \mathbf{e}^r + r_P^T(1-k) \dot{\theta}_P^T \cos \phi_P^T \mathbf{e}^\theta + r_P^T(1-k) \dot{\phi}_P^T \mathbf{e}^\phi. \quad (2.14)$$

So the LOS vector \mathbf{r}_D^T has the same angular velocity components as \mathbf{r}_P^T . (For the infinite case, $\dot{\theta}_{P_\infty}^T = \dot{\theta}_{P_\infty}^D$, $\dot{\phi}_{P_\infty}^T = \dot{\phi}_{P_\infty}^D$). Therefore we submit the following theorem:

Theorem: A two-body trajectory described by \mathbf{r}_D , \mathbf{r}_T is motion camouflaged if \exists a point P such that

$$\Omega_P^D = \Omega_P^T = \Omega_P^T, \quad (2.15)$$

where Ω is the angular velocity vector.

Proof: We have shown in the derivation that equation 2.15 is a necessary component of motion camouflage. To show sufficiency requires a little more work. Consider first the two-dimensional case.

It is immediately clear that the simplest scenario which satisfies 2.15 is that where P , D and T are collinear. In this case, \mathbf{r}_P^D may be said to be some scalar multiple of \mathbf{r}_P^T , and hence the system is camouflaged, QED. Suppose, however, that the points P , D and T are not collinear, as in figure 2.4. Here, \mathbf{r} is the line-of-sight (LOS) vector between T and D . The angle of \mathbf{r} is denoted by ϵ , the length of \mathbf{r} is denoted r , and the relative velocity between T and D is denoted \mathbf{v}^R . Hence the angular velocity of the LOS vector is given by

$$\dot{\epsilon} = \frac{v^{R\epsilon}}{r}$$

where

$$v^{r\epsilon} = v^T \sin(\epsilon - \sigma^T) - v^D \sin(\epsilon - \sigma^D) \quad (2.16)$$

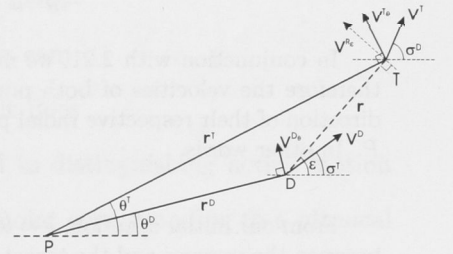


Figure 2.4: Non-collinear pursuer and target

Now, let the direction of the relative velocity vector be denoted σ^R , so $\sigma^R = \sigma^T - \sigma^D$. Similarly, let $\theta^R = \theta^T - \theta^D$. Then by equation 2.15, $\dot{\epsilon} = \dot{\theta}^T$. So

$$\frac{v^R}{r} \sin(\epsilon - \sigma^R) = \frac{v^T}{r^T} \sin(\sigma^T - \theta^T). \tag{2.17}$$

By the cosine rule, we can write the following:

$$\begin{aligned} (v^R)^2 &= (v^T)^2 + (v^D)^2 - 2v^D v^T \cos \sigma^R \\ r^2 &= (r^T)^2 + (r^D)^2 - 2r^T r^D \cos \theta^R. \end{aligned}$$

Again from 2.15, we know $\dot{\theta}^D = \dot{\theta}^T$, so

$$\frac{v^D}{r^D} \sin(\sigma^D - \theta^D) = \frac{v^T}{r^T} \sin(\sigma^T - \theta^T)$$

and hence

$$r^D = r^T \frac{v^D \sin(\sigma^D - \theta^D)}{v^T \sin(\sigma^T - \theta^T)}. \tag{2.18}$$

Substituting this value for r^D into our equations for v^R and r , and then into 2.17, we find

$$\begin{aligned} &(v^T)^2 [\sin^2(\epsilon - \sigma^R) - \sin^2(\sigma^T - \theta^T)] + \\ &(v^D)^2 [\sin^2(\epsilon - \sigma^R) - \sin^2(\sigma^D - \theta^D)] - \\ &2v^T v^D [\sin^2(\epsilon - \sigma^R) \cos \sigma^R - \\ &\sin(\sigma^T - \theta^T) \sin(\sigma^D - \theta^D) \cos \theta^R] = 0. \end{aligned} \tag{2.19}$$

Expanding and simplifying, this reduces easily to

$$(v^{\epsilon R})^2 - (v^{\theta R})^2 = 0$$

hence we can write

$$v^{\epsilon R} = v^T \sin(\sigma^T - \theta^T) - v^D \sin(\sigma^D - \theta^D). \tag{2.20}$$

The angular conditions under which equations 2.16 and 2.20 hold can be easily represented graphically, as shown in the vector diagram 2.5. Examination of triangle BCD (or ACH , for that matter) reveals that

$$\sigma^T - \sigma^D = \theta^T - \theta^D \tag{2.21}$$

Furthermore, triangle ABE demonstrates that the LOS angle ϵ is equal to $(\epsilon - \theta^T) + \sigma^T$, and hence

$$\theta^T = \sigma^T. \tag{2.22}$$

In conjunction with 2.21, we may now state that $\sigma^D = \theta^D$, and therefore the velocities of both pursuer and target are solely in the direction of their respective radial position vectors, as measured from P . In other words,

$$\dot{\theta}^D = \dot{\theta}^T = 0. \tag{2.23}$$

From our initial criterion, $\dot{\epsilon} = \dot{\theta}^T = 0$, which is only possible if the direction of the LOS vector between the pursuer and the target remains constant. This scenario is shown in figure 2.6, and fits the definition of motion camouflage with a static point at infinity. Hence, if equation 2.15 is true and P, D, T are not collinear, the pursuer D is camouflaged at infinity with respect to the target T . Obviously, if P, D, T are collinear, the camouflage equation is already fulfilled, as stated earlier.

In a similar manner, we can extend the above proof to three dimensions. We must first break down the three dimensional geometry into a vertical and horizontal plane, corresponding with the azimuth (θ) and elevation (ϕ) of the bodies in question. Figure 2.7 shows the three dimensional

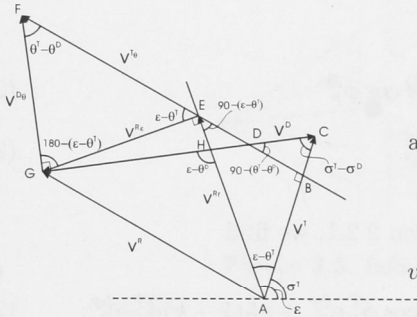


Figure 2.5: Vector diagram of required velocity conditions

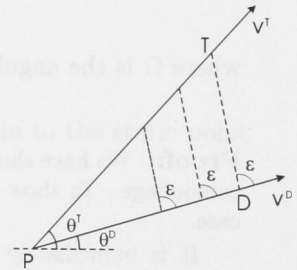


Figure 2.6: Constant LOS direction

case. In the horizontal plane, we observe that

$$v^{R_\eta} = v^T \cos \phi^T \sin(\eta - \sigma^T) - v^D \cos \phi^D \sin(\eta - \sigma^D).$$

Applying equation 2.15, we find also that

$$v^{R_\eta} = v^T \cos \phi^T \sin(\sigma^T - \theta^T) - v^D \cos \phi^D \sin(\eta - \sigma^D).$$

In other words,

$$v^{R_\eta} = v^{T_\eta} - v^{D_\eta} \quad (2.24)$$

$$= v^{T_\theta} - v^{D_\theta} \quad (2.25)$$

and hence we find $\sigma^T = \theta^T$, $\sigma^D = \theta^D$. We can acquire two similar equations in the vertical plane.

$$v^{R_\epsilon} = v^{T_\epsilon} - v^{D_\epsilon} \quad (2.26)$$

$$= v^{T_\phi} - v^{D_\phi} \quad (2.27)$$

hence $\epsilon^T = \phi^T$, $\epsilon^D = \phi^D$. Therefore the angular velocity of T and D , as measured from the origin P , is equal to zero, and the conditions for camouflage at infinity are met.

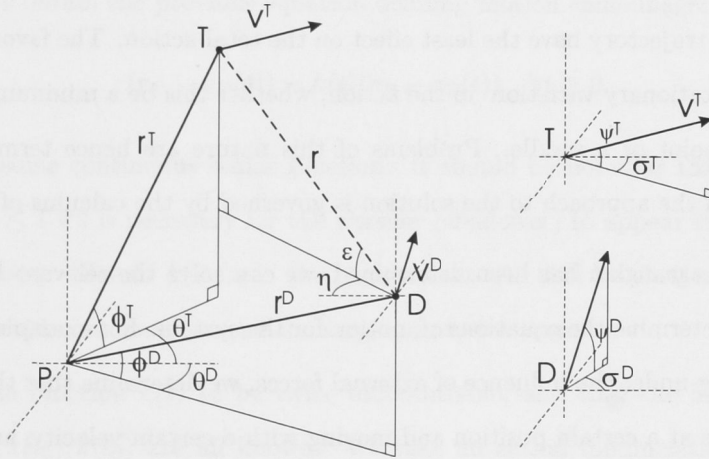


Figure 2.7: 3D non-collinear geometry

The theorem above therefore describes not merely a necessary but indeed a sufficient condition for active motion camouflage to be deemed to have occurred. Significantly, it does not hold for the trivial case of $k = 0$, which is helpful in distinguishing active motion camouflage from passive. Hypothetically, given a static point corresponding to a physical object, a pursuer may remain camouflaged by matching the apparent angular velocities of the static point and the target, keeping them at 180° to each other in the visual field. This corresponds with Srinivasan and Davey's intuited statements as to how camouflage may be accomplished by an insect [SPK99].

2.3 Optimal Motion Camouflage Paths

2.3.1 Introduction to Lagrangian Mechanics

In classical and quantum mechanics, equations of motion are derived from what is termed the principle of least action. ‘Action’ is a quantity which has dimensions of energy integrated over time. The energy in question is expressed by the Lagrangian, and is generally taken as being equal to the kinetic energy of the system minus its potential energy. This is to ensure that the trajectory derived from the variational problem is a second-order differential equation, and thus corresponds with Newton’s laws of motion.

The term ‘least’ in the expression ‘principle of least action’ is somewhat misleading. We don’t actually look for the trajectory of least energy, we look for the one where slight changes in the trajectory have the least effect on the total action. The favoured trajectory is the one of ‘stationary variation’ in the action, whether this be a minimum, a maximum, an inflection point or a saddle. Problems of this nature are hence termed ‘variational problems’, and the approach to the solution is governed by the calculus of variations.

Once the Lagrangian has been determined, we can solve the relevant Euler-Lagrange equations to determine the equations of motion for the system. For example, given a single particle moving under the influence of external forces, we determine that the particle will, at one time, be at a certain position and moving with a certain velocity, and at a second, fixed time will have another position and velocity. Then using the principle of least action, we ask what trajectory, connecting these two points, will minimize the action, and claim that the particle will follow that trajectory, as long as all external forces have been taken into account. In terms of force-based control, we say we are looking for paths which require the least control action to achieve, usually while satisfying some other criterion.

Should the system be more complex, with multiple forces acting on a body, we can incorporate their influence with the use of the theory of Lagrange multipliers and solve for the equations of motion with these additional constraints. Lagrange multipliers are a powerful tool, explained more fully in Appendix A, and they will be returned to in Chapter 3, however in this preliminary result their use is unnecessary. Note that [MO98] and [Ber96] are excellent resources for the theory of Lagrangian optimization.

2.3.2 Procedure

Camouflage with a non-infinite static point

Glendinning [Gle04] characterized motion camouflaged paths mathematically in the following way: in 3-D Cartesian space, let $\mathbf{r}_D(t)$ and $\mathbf{r}_T(t)$ be the vectors representing the time-varying paths of the pursuer and the target, respectively, and let \mathbf{r}_P be the vector that represents the position of the fixed point. The camouflage constraint then requires that, at all times,

$$\mathbf{r}_D(t) = \mathbf{r}_D(0) + k(t)(\mathbf{r}_T(t) - \mathbf{r}_P) \quad (2.28)$$

where \mathbf{r}_P is the fixed point of the engagement. Clearly this holds true for any continuous function $k(t)$. Then if we allow \mathbf{r}_P to be the static camouflage point for non-infinite motion camouflage, we obtain the previous equation defining motion camouflage:

$$(\mathbf{r}_P - \mathbf{r}_D(t)) = k(t)(\mathbf{r}_P - \mathbf{r}_T(t)) \quad \forall t \geq 0 \quad (2.29)$$

where $k(t)$ is some continuous scalar function. It should be noted at this time that the condition $k(t) \leq 1 \forall t$ is necessary for the pursuer (shadower) to appear stationary to the target (shadowee). Should $k(t) > 1$, the engagement will still be camouflaged, however the pursuer would now have become the target, and vice versa.

Assume the function $k(t)$ to be twice differentiable, and that the initial conditions $\mathbf{r}_D(t_0), \dot{\mathbf{r}}_D(t_0), k(t_0), \dot{k}(t_0)$ are all known. We take an action minimization approach to finding an optimal path, and we can do this via Lagrangian mechanics. Assume a particle of unit mass, then the Lagrangian for the system can be written as kinetic energy minus potential energy [MO98], that is

$$\mathcal{L} = KE - PE = \frac{1}{2} \dot{\mathbf{r}}_D' \dot{\mathbf{r}}_D \quad (2.30)$$

(note that since we are ignoring any gravitational force, the potential energy term can be neglected). Then the control cost can be written

$$J = \frac{1}{2} \int_{t_0}^{t_f} \dot{\mathbf{r}}_D' \dot{\mathbf{r}}_D dt. \quad (2.31)$$

In physical terms, the derivation can be described as follows: instead of assuming a freely moving body and then attempting to constrain that motion to a camouflaged

path, we instead begin by assuming that the only forces acting on the shadower are those required to hold it to a camouflaged path. By solving the Euler-Lagrange equations for such a system, we can use Hamilton's Principle of Least Action to find the path the particle will take if no other forces are acting on it besides the minimum required to keep the motion camouflaged.

Differentiating equation (2.29) with respect to time, we obtain

$$-\dot{\mathbf{r}}_D(t) = \dot{k}(t)(\mathbf{r}_P - \mathbf{r}_T(t)) - k(t)\dot{\mathbf{r}}_T(t). \quad (2.32)$$

Since $k(t)$ parameterizes the path of the shadower, finding an appropriate stationary value for the energy curve

$$\frac{1}{2} \int_{t_0}^{t_f} \dot{\mathbf{r}}_D(t)' \dot{\mathbf{r}}_D(t) dt \quad (2.33)$$

is equivalent to finding the function $k(t)$ such that

$$\frac{1}{2} \int_{t_0}^{t_f} \left[k(t)\dot{\mathbf{r}}_T(t) - \dot{k}(t)(\mathbf{r}_P - \mathbf{r}_T(t)) \right]' \left[k(t)\dot{\mathbf{r}}_T(t) - \dot{k}(t)(\mathbf{r}_P - \mathbf{r}_T(t)) \right] dt \quad (2.34)$$

is minimised.

With \mathcal{L} as before, the Euler-Lagrange equation for the system is then

$$\frac{\partial \mathcal{L}}{\partial k} - \frac{d}{dt} \frac{\partial \mathcal{L}}{\partial \dot{k}} = 0. \quad (2.35)$$

$$\frac{\partial \mathcal{L}}{\partial k} = k\dot{\mathbf{r}}_T^T \dot{\mathbf{r}}_T - \dot{k}\dot{\mathbf{r}}_T^T(\mathbf{r}_P - \mathbf{r}_T) \quad (2.36)$$

$$\frac{\partial \mathcal{L}}{\partial \dot{k}} = -k\dot{\mathbf{r}}_T^T(\mathbf{r}_P - \mathbf{r}_T) + \dot{k}(\mathbf{r}_P - \mathbf{r}_T)'(\mathbf{r}_P - \mathbf{r}_T) \quad (2.37)$$

$$\begin{aligned} \frac{d}{dt} \frac{\partial \mathcal{L}}{\partial \dot{k}} &= -\dot{k}\dot{\mathbf{r}}_T^T(\mathbf{r}_P - \mathbf{r}_T) - k[\ddot{\mathbf{r}}_T^T(\mathbf{r}_P - \mathbf{r}_T) - \dot{\mathbf{r}}_T^T \dot{\mathbf{r}}_T] + \\ &\quad \ddot{k}(\mathbf{r}_P - \mathbf{r}_T)'(\mathbf{r}_P - \mathbf{r}_T) - 2\dot{k}\dot{\mathbf{r}}_T^T(\mathbf{r}_P - \mathbf{r}_T). \end{aligned} \quad (2.38)$$

Substituting these values into equation (2.35), we get a second-order differential equation in k :

$$\begin{aligned} &\ddot{k} [(\mathbf{r}_P - \mathbf{r}_T)'(\mathbf{r}_P - \mathbf{r}_T)] + \\ &2(-\dot{k} [\dot{\mathbf{r}}_T^T(\mathbf{r}_P - \mathbf{r}_T)]) + k[-\ddot{\mathbf{r}}_T^T(\mathbf{r}_P - \mathbf{r}_T)] = 0. \end{aligned} \quad (2.39)$$

Let $(\mathbf{r}_P - \mathbf{r}_T(t)) = \alpha(t)$, then we can write (2.39) as:

$$\ddot{k}\alpha' + 2\dot{k}\dot{\alpha}' + k\ddot{\alpha}' = 0. \quad (2.40)$$

Hence the vector quantity

$$\ddot{k}\alpha + 2\dot{k}\dot{\alpha} + k\ddot{\alpha}$$

is orthogonal to α . To find a unique solution for k , note that equation (2.40) is equivalent¹ to the second-order differential equation

$$\ddot{k}|\alpha| + 2\dot{k}\frac{d}{dt}(|\alpha|) + k\frac{d^2}{dt^2}(|\alpha|) = 0 \quad (2.41)$$

which has a solution of the form

$$k|\alpha| = c_1t + c_2 \quad (2.42)$$

for some integration constants c_1, c_2 ; therefore

$$k(t) = \frac{c_1t + c_2}{|\mathbf{r}_P - \mathbf{r}_T(t)|}. \quad (2.43)$$

This represents a general formula for extremals of $k(t)$. Clearly it encompasses the trivial solution, $k(t) = 0 \forall t$. Explicit values for the constants depend on the initial conditions, so it is evident that the solution is highly sensitive to the choice of starting position and velocity, as is often the case with variational problems [MO98]. The value of c_2 is found as follows:

$$\begin{aligned} k_0 &= \frac{c_2}{|\mathbf{r}_P - \mathbf{r}_T(0)|} \\ c_2 &= k_0(|\mathbf{r}_P - \mathbf{r}_T(0)|). \end{aligned} \quad (2.44)$$

¹For any column vector α , the following holds true:

$$\begin{aligned} \alpha'\alpha &= |\alpha|^2 \\ \dot{\alpha}'\alpha &= \frac{\dot{\alpha}'\alpha}{|\alpha|}|\alpha| \\ &= \left(\frac{d}{dt}|\alpha|\right)|\alpha| \\ \ddot{\alpha}'\alpha &= \ddot{\alpha}'\alpha + \dot{\alpha}'\dot{\alpha} - \dot{\alpha}'\dot{\alpha} \\ &= \frac{d}{dt}\left(|\alpha|\frac{d}{dt}|\alpha|\right) - \left(\frac{d}{dt}|\alpha|\right)^2 \\ &= |\alpha|\frac{d^2}{dt^2}|\alpha| \end{aligned}$$

For an engagement that ends in an interception, c_1 can be similarly found from the desired terminal conditions, a procedure outlined shortly. However for an open-ended interaction, a suitable value for the constant c_1 can still be established from the first-order initial conditions. Differentiating (2.42) gives us

$$\dot{k} = \frac{c_1}{|\mathbf{r}_P - \mathbf{r}_T|} + k \frac{\dot{\mathbf{r}}'_T(\mathbf{r}_P - \mathbf{r}_T)}{|\mathbf{r}_P - \mathbf{r}_T|^2} \quad (2.45)$$

therefore by defining the initial condition \dot{k}_0 , we obtain

$$c_1 = \dot{k}_0(|\mathbf{r}_P - \mathbf{r}_{T_0}|) - k_0 \frac{\dot{\mathbf{r}}'_T(\mathbf{r}_P - \mathbf{r}_T)}{|\mathbf{r}_P - \mathbf{r}_T|}.$$

A positive value of \dot{k}_0 generates a trajectory with a pursuit characteristic, a negative value gives an escape path. Different engagements are illustrated below. Figure 2.8(a) shows a simple pursuit scenario, chasing a target with constant velocity. Figure 2.8(b) shows the same starting conditions with the shadower escaping from the shadowee.

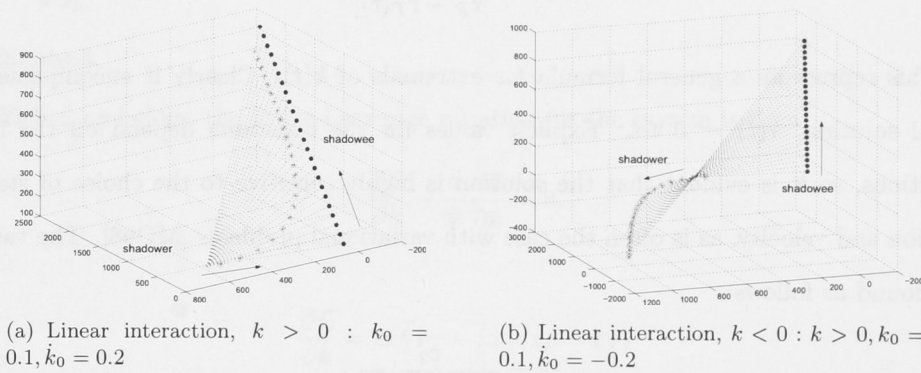


Figure 2.8: Optimal solutions to linear trajectories

To demonstrate the efficacy of these paths, consider two particles with the same starting position and velocity, camouflaging against a shadowee moving along the same straight trajectory, where one is using the extremal path derived above and one is moving in a straight line to the interception point (while still maintaining camouflage). Figure 2.9 demonstrates the paths taken. (For simplicity, we look at only two dimensions in this instance).

Define the following variables: let θ be the angle between the two participants (what is often referred to as the line-of-sight angle in missile guidance), and let σ be the direction

of the pursuers trajectory (relative to the x baseline). To define a straight camouflaged interception line, in simple terms, set a time horizon t_H , and from the initial velocity of the target and this time horizon, determine a suitable direction σ for a straight interception path. (Note that this is an open-loop ballistic control system which assumes no change in velocity or direction of the target. If such a change occurs, interception will not be achieved, since σ is constant). The required lateral velocity of the pursuer is found by the ratio

$$\frac{v_{\theta}^D}{r^D} = \frac{v_{\theta}^T}{r^T}. \quad (2.46)$$

Then the total velocity is straightforward:

$$v^D = \frac{-v_{\theta}^D}{\sin(\sigma - \theta)}. \quad (2.47)$$

In cartesian space, the requisite velocity is

$$v_x^D = v^D \cos \sigma \quad (2.48)$$

$$v_y^D = v^D \sin \sigma. \quad (2.49)$$

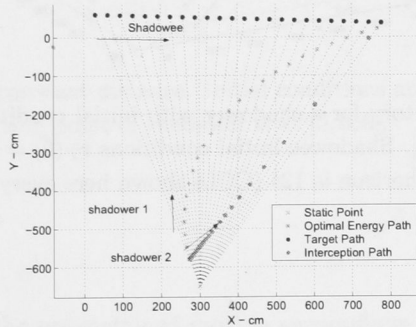


Figure 2.9: Comparison between a straight interception trajectory and an energy optimal trajectory. Initial conditions, in cm, are as follows: $X_T(0) = [30, 60]$, $V_T(0) = [650, -20]$, $X_D(0) = [300, -650]$, $V_D(0) = [9, 11]$

The initial velocity vector of the straight line path was set to point in the approximate direction of the interception point of the optimal trajectory, so that that we can make a meaningful comparison. The forward velocity of both pursuers at the beginning of the interaction is 14 cm/s. The final speed required for the straight trajectory to still be camouflaged at the interception point is 1.14×10^3 cm/s, whereas that required for the

optimal energy path is 187.8 cm/s. Given these initial conditions, then, to pursue a target along a straight line while remaining camouflaged a shadower must input more than 40 times the energy than if an optimal pursuit path were chosen.

As alluded to previously, if it is desired to intercept the shadower within a predetermined time, or indeed if another geometric condition is to be met, then we can determine the necessary constant c_1 from the end boundary conditions. In the case of capture in some finite time t_f , we say $k(t_f) = 1$, so we can write:

$$c_1 = \frac{1}{t_f} [|\mathbf{r}_P - \mathbf{r}_T(t_f)| - k_0 |\mathbf{r}_P - \mathbf{r}_T(0)|]. \quad (2.50)$$

Figure 2.10 demonstrates a finite horizon capture path.

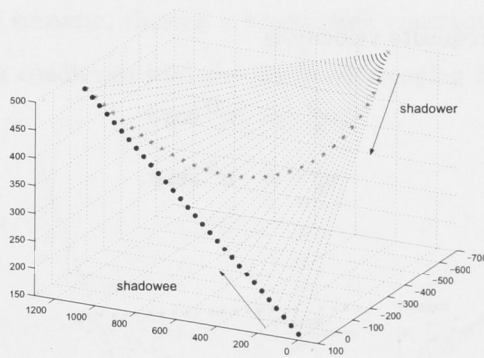


Figure 2.10: Capture trajectory for a shadower with initial conditions $k_0 = 0.1$, $\dot{k}_0 = 0.2$, static point at $\mathbf{r}_P = [200, -650, 500]$. Shadowee initial conditions $\mathbf{r}_T(0) = [30, 60, 150]$, constant velocity $\mathbf{r}'_T = [200, -20, 60]$. Capture horizon is 12s (CCLs shown here every 0.4s).

Camouflage at Infinity

A similar method can be used to generate optimal paths with camouflage at infinity [SD95].

We again use a general formulation given by Glendinning [Gle04]:

$$\mathbf{r}_T - \mathbf{r}_D = k(t)\mathbf{e} \quad (2.51)$$

where \mathbf{e} is a constant vector. For the sake of simplicity, we choose \mathbf{e} to correspond with the initial conditions, so

$$\mathbf{e} = \mathbf{r}_T(t_0) - \mathbf{r}_D(t_0). \quad (2.52)$$

Differentiating and applying the same cost function as before, we obtain the Lagrangian and develop a solution of the form

$$k\mathbf{e}^T\mathbf{e} = \mathbf{r}'_T\mathbf{e} + c_1t + c_2 \quad (2.53)$$

for some constants of integration c_1, c_2 .

We can again find c_1 and c_2 from the initial conditions. For a capture trajectory, we can determine the optimal c_1 for a given final time from the terminal boundary conditions, so

$$c_1 = \frac{1}{t_f} (k(t_f)\mathbf{e}'\mathbf{e} - \mathbf{r}'_T(t_f)\mathbf{e} - c_2). \quad (2.54)$$

For a capture trajectory, $k(t_f) = 0$. For tracking at a constant distance $d = |\mathbf{r}_{T_0} - \mathbf{r}_{D_0}| = |\mathbf{e}|$, we set $k(t_f) = 1$. An example of the latter can be seen in Figure 2.11.

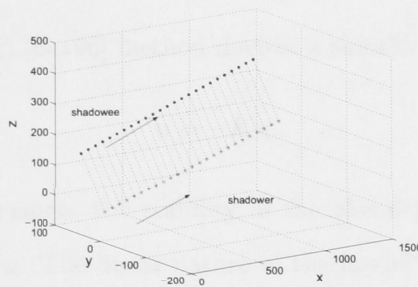


Figure 2.11: Tracking at a constant distance. Initial conditions and velocity of the shadowee are identical to Figure 2.10. Starting point of shadower is at $[0, 0, 0]$.

2.3.3 Discussion

In this chapter, I defined the geometry of motion camouflage and established a necessary and sufficient condition for a two-body pursuit to be considered camouflage. This dynamic condition has the advantage of not relying explicitly on distance information. Subsequently, I derived a formula for a class of ‘natural’ three-dimensional camouflage paths that maximize energy conservation and can be used for emulating a stationary object at a finite distance from the target, or at infinity. The results can be used to examine the energy optimality of experimentally observed trajectories that exhibit motion camouflage, or in the design of optimal closed-loop guidance systems for motion camouflage

Control for Camouflage

3.1 Introduction to LQR control

A linear state-space model of a system takes the form

$$\dot{\mathbf{x}} = A\mathbf{x} + B\mathbf{u}.$$

The Linear Quadratic (LQ) [Ber95] method devises a suitable feedback control law

$$\mathbf{u} = -K\mathbf{x}.$$

The feedback gain K guarantees the stability of the closed loop system, regulating the states of the system to zero. The linear nature of the model means that taking an error signal $\mathbf{e} = \mathbf{x} - \mathbf{x}_r$ and applying the controller gain such that $\mathbf{u} = -K\mathbf{e}$ regulates the error signal to zero, instead of the state. \mathbf{x}_r represents the vector of desired states, and serves as the external input to the closed-loop system

$$\dot{\mathbf{x}} = (A - BK)\mathbf{x} + K\mathbf{x}_r. \quad (3.1)$$

The objective of dynamic programming is to minimize a certain cost, where cost is the term used for a mathematical expression which quantifies an undesirable outcome [Ber95]. Cost may be expressed in terms of an energy function, as a geometric constraint, or a soft dynamic limitation. Broadly speaking, we consider a sequence of dependent decisions, and seek a balance between the desire for low present cost and the possibility that this might create a need for a high future cost. To apply dynamic programming to a guided trajectory, we model the system using discrete-time dynamics. We ensure the system state encompasses the key variables, then examine the evolution of this system state under the influence of decisions made at discrete instances of time.

In discrete form, the evolution of the system is expressed in the equation

$$x_{k+1} = Ax_k + Bu_k$$

where x_k is the state and u_k the control variable (not considered here are noise-dependent influences on the system). Our control objective is to select the control input u_k at each time in such a way as to minimize the long-term average quadratic cost criterion

$$J(u) = \sum_{k=1}^{T-1} \left[(X_k^R)' Q_k X_k^R + u_k' R u_k \right] + (X_T^R)' Q_T X_T^R$$

where Q is a matrix encompassing the cost on the system state and R represents a cost assigned to the control action. In dynamic programming, this cost minimization is accomplished by using the solution to a series of dependent subproblems to find an optimal solution to a larger problem.

For example, suppose we wish to drive a given system from a known state S_1 to a desired state S_4 , and the path space from S_1 to S_4 is defined by two sequential sets of possible states $\{S_2^i\}, \{S_3^j\}$, $i = 1, \dots, M, j = 1, \dots, N$. Then to solve this problem using dynamic programming, we first compute the 'best' (cost-minimizing) solution for the subproblem of driving the system from each sub-state S_2^i to S_4 . We can then find the best method of getting from S_1 to S_4 , constrained by the already-derived optimal solutions from S_2^i .

For a simple problem like the one described above, the dynamic programming method gives only a small computational advantage. However as we increase the number of possible nodes between S_1 and S_n , and thus the solution space of the problem, the savings in computational effort increase enormously. In this way, a dynamic programming solution to, say, a path-finding problem is solved backwards in time to arrive at an optimal path.

More detail can be found in [Ber95], [CK98].

3.2 Two-Dimensional Linear Quadratic Regulator for Motion Camouflage

Using a linear quadratic regulator to govern motion camouflaged trajectories, the aim is to design an optimal control policy for the shadower which ensures certain constraints (motion camouflage requirements) are met, whilst achieving an overall objective (for example,

attack, tracking, or escape). This optimal control approach is not necessarily expected to represent the mechanism used by an insect, but simply provides a useful frame in which to develop strategies that mimic the observed insect behaviour, and perhaps provide some insight into the essential features of the problem.

The key contribution of this chapter is to describe and solve several varieties of motion camouflage behaviors within an LQ framework, and to find optimal strategies for achieving both the motion constraints and the overall engagement requirements. I will also discuss realistic control constraints, measurement and some higher-level control issues.

3.2.1 Dynamics of Motion

We characterize a motion camouflage engagement as two players (shadower and shadowee) undergoing constrained dynamic motion over time. Although the terms shadower and shadowee are inspired by the insect world, the developed framework can equally be applied to other pursuit games including the missile (shadower) and target (shadowee) problem. Initially we will consider simply two dimensions.

The dynamics are described in an Euclidean reference plane. The shadower position and velocity is represented by $\mathbf{r}_D = [x^D, y^D]'$ and $\dot{\mathbf{r}}_D = [\dot{x}^D, \dot{y}^D]'$ respectively, where $'$ is the transpose symbol. Similarly, the shadowee (target) position and velocity is represented by $\mathbf{r}_T = [x^T, y^T]'$ and $\dot{\mathbf{r}}_T = [\dot{x}^T, \dot{y}^T]'$ respectively. We introduce a shadower state vector $X^D = [x^D, y^D, \dot{x}^D, \dot{y}^D]'$, and a shadowee state vector $X^T = [x^T, y^T, \dot{x}^T, \dot{y}^T]'$. The control problem will be examined in terms of a relative state $X^R = X^D - X^T$.

We assume that the motion of both the shadower and shadowee can be represented using linear dynamics. Hence, for $k = 1, 2, \dots$, the following discrete-time state equation representation of the shadowee and shadower dynamics is proposed:

$$X_{k+1}^T = AX_k^T \quad (3.2)$$

$$X_{k+1}^D = AX_k^D + B^D u_k. \quad (3.3)$$

where

$$A = \begin{bmatrix} 1 & 0 & \Delta t & 0 \\ 0 & 1 & 0 & \Delta t \\ 0 & 0 & 1 & 0 \\ 0 & 0 & 0 & 1 \end{bmatrix} \quad B^D = \begin{bmatrix} 0 & 0 \\ 0 & 0 \\ 1 & 0 \\ 0 & 1 \end{bmatrix}$$

Δt is the sampled period, and u_k is the control.

The relative dynamics of the shadower-shadowee engagement can hence be written as:

$$X_{k+1}^R = AX_k^R + B^P u_k \quad (3.4)$$

Remark

1. Unlike a missile guidance problem [BAY98], the shadower is allowed control over both lateral and longitudinal accelerations. That is, control of forward as well as lateral velocity is assumed possible. Effective motion camouflage leading to capture does not seem viable without control of forward velocity.
2. The shadowee dynamics in (3.2) describe the trivial case where the shadowee has a constant heading and velocity. In practical situations, the shadowee may actually maneuver; however, these manoeuvres are typically not known in advance to the shadower. The motion camouflage problem is therefore solved assuming no shadowee manoeuvres, and then the performance of the resulting guidance algorithm when shadowee maneuvers are present is examined.

3.2.2 Motion Camouflage Constraints

Motion camouflage may be expressed as motion in which the apparent angular position of the shadower appears stationary over time from the perspective of the shadowee. This angular camouflage constraint corresponds to constraining the motion of the shadower to particular lines in 2D space that correspond to the camouflage constraint lines (CCLs) [SD95] at discrete time intervals. We define these as the line between the position of the shadowee $\mathbf{r}_k^T = [x_k^T, y_k^T]'$ at each time instant and the chosen stationary focal point of the engagement, $\mathbf{r}_P = [f_x, f_y]'$. The slope of these CCLs provides sufficient information for the shadower to adequately camouflage its motion.

At this point, the precise formulation of the problem diverges depending on the particular type of engagement being modeled. For LQ control, the distinguishing feature between the different algorithms is the ultimate goal of the engagement, whether that be pursuit from a finite static point, pursuit from an infinite starting point, or tracking at a constant distance.

To an observer, it seems more natural to pose the problem using a cartesian reference frame. However dragonflies and other insects are unlikely to operate in this stationary absolute frame; rather they use something akin to a polar reference frame, with themselves as the moving centre [FW02]. For these reasons, the motion camouflage problem will first be solved in cartesian space, then the simulation will be converted to a polar frame and modified to achieve a more biologically realistic situation in Section 3.3.

3.2.3 Problem Formulation and Solution

Performance Index for Motion Camouflage

Recall the chosen static point of the engagement is given by

$$\mathbf{r}_P = [f_x, f_y]'$$

We begin by determining the slopes of the required camouflage constraint lines, as shown in Figure 3.1. For a pursuit where the focal point is not at infinity, the constraint lines at each time interval, g_k , have slopes as follows:

$$g_k = \frac{y_k^T - f_y}{x_k^T - f_x} \text{ for } k \geq 1. \quad (3.5)$$

For a pursuit where the focal point is taken to be at infinity, the constraint lines have constant slope,

$$g_k = \frac{y_1^T - y_1^D}{x_1^T - x_1^D} \text{ for } k \geq 1. \quad (3.6)$$

As can be seen in Figure 3.1, the relative reference frame is simply a translation of the absolute reference frame. Hence in the relative reference frame, the CCL have the same description, and we note that on a perfectly camouflaged path

$$y_k^R = g_k x_k^R \text{ for } k \geq 1. \quad (3.7)$$

Perfect camouflage is not always possible, or at least requires undesirably excessive control actions, so we represent the requirement to remain close to these CCLs through the following soft running constraint term,

$$\sum_{k=1}^T (y_k^R - g_k x_k^R)^2 \quad (3.8)$$

where T is the final time instant.

We also desire that the shadower intercept the shadowee at time T , and that the control action required not be too severe. It is assumed that T is known in advance by the shadower. This assumption may be unrealistic, but is a common one in missile guidance problems [Zar02]. On the other hand, Collett and Land [CL78] showed that hoverflies using a predictive tracking mechanism which first assumed the target had a certain absolute size and specific average flight speed, and then from the apparent size and speed proceeded to calculate a likely interception point. So an assumption of a known time horizon may not be as unlikely as it first appears.

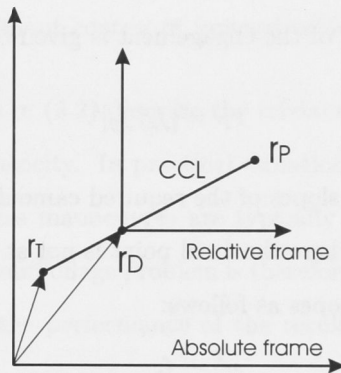


Figure 3.1: Reference frames: shadowee and shadower in absolute and relative reference frames. Also shown is one camouflage constraint line.

These motion camouflage and control energy requirements are used to propose a performance index for the motion camouflage problem. The cost function for the problem can then be written as:

$$J(u) = \sum_{k=1}^{T-1} \left[(X_k^R)' Q_k X_k^R + u_i' R u_i \right] + (X_T^R)' Q_T X_T^R \quad (3.9)$$

where

$$Q_i = \gamma_X \begin{bmatrix} g_i^2 & -g_i & 0 & 0 \\ -g_i & 1 & 0 & 0 \\ 0 & 0 & 0 & 0 \\ 0 & 0 & 0 & 0 \end{bmatrix}, \quad R = \begin{bmatrix} 1 & 0 \\ 0 & 1 \end{bmatrix}$$

and γ_X is a weighting factor used to describe the importance of the camouflage requirement relative to the control energy requirement.

The dynamics (3.4) and performance index (3.9) define a linear quadratic problem to

which standard techniques can be applied [CK98].

3.2.4 Optimal Motion Camouflage Guidance

From [Ber95], the optimal control solution to the linear quadratic problem is

$$u_k = -K_k X_k^R \quad (3.10)$$

where K_k is given by

$$K_k = [(B^P)' P_k B^P + R]^{-1} (B^P)' P_k A \quad (3.11)$$

and P_k is given by the appropriate discrete-form Riccati equation solved backwards in time,

$$\begin{aligned} P_N &= Q_N \\ P_{k-1} &= A' \left(P_k - A' P_k B^P [(B^P)' P_k B^P + R]^{-1} (B^P)' P_k \right) A + Q_{k-1}. \end{aligned} \quad (3.12)$$

3.2.5 Infinite point camouflage

The goal whilst tracking another body in tandem, using camouflage with a static point at infinity, is for the shadower to remain at a fixed distance from the shadowee, and the cost is determined by how far the challenger deviates from this desired vector.

The tandem or tracking flight problem can again be considered within an LQG framework. The requirement to remain at a fixed distance from the shadowee can be represented by introducing a new relative state, X^O , offset from the shadowee location as follows:

$$X^O = X^R + [d_x, d_y, 0, 0]' \quad (3.13)$$

where $[d_x, d_y]'$ is the desired displacement vector.

A guidance strategy can then be developed as a standard infinite-horizon LQG tracking problem.

Remarks

1. The motion camouflage strategy developed in this chapter assumes that the shadower has knowledge of the correct time-horizon for the engagement. As mentioned before, in genuine engagements with an oblivious target, this is not an entirely un-

realistic assumptions. However a reactive target may complicate the calculations considerably.

3.3 Results

3.3.1 General Example: Pursuit

Simulation studies of the proposed motion camouflage guidance were first performed in the setting of a generic pursuit problem, without the consideration of realistic biological constraints.

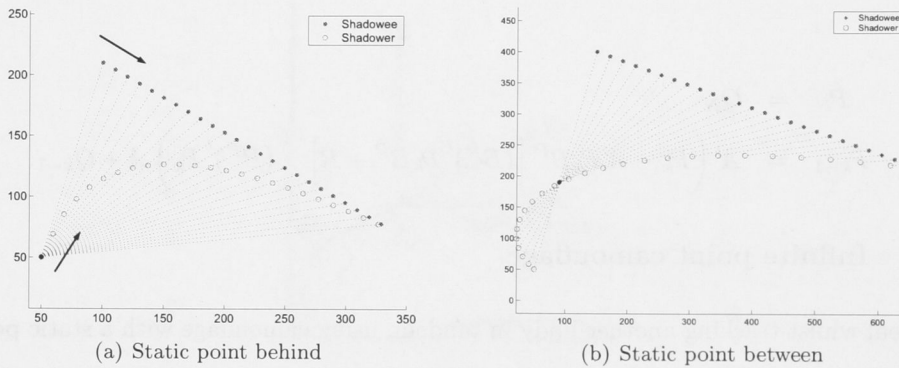
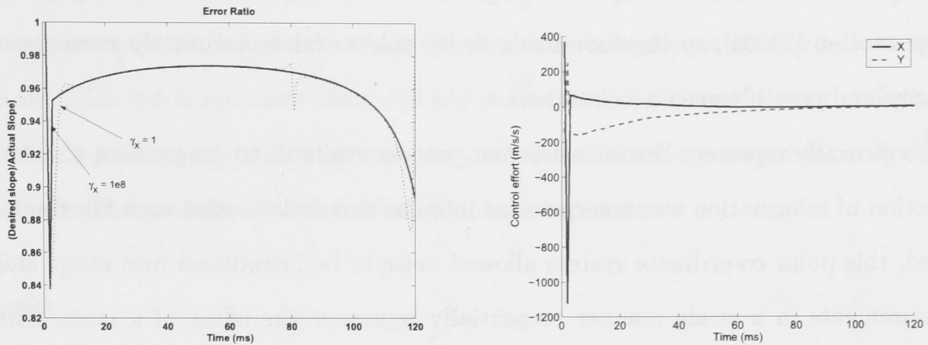


Figure 3.2: Examples of static point motion camouflage using a two-dimensional linear quadratic solution

Using a weighting factor of $\gamma_X = 1 \times 10^8$, initial shadowee and shadower states (in mm and mms^{-1}) of $[100, 210, 1300, -800]'$ and $[50, 50, 3000, 1500]'$, respectively, the proposed motion camouflage guidance algorithm was used to guide the shadower to a non-maneuvering shadowee. Figure 3.2(a) shows the resulting camouflaged trajectory, with the focal (static) point located at the starting position of the shadower. Figure 3.2(b) shows the resulting camouflaged trajectories when a point between the shadower and the shadowee ($\mathbf{r}_P = [80, 190]$) is used as a focal point. Initial conditions for the shadower are the same as Figure 3.2(a), the shadowee now starts at $[150, 400]$ with the same initial velocity.

A variety of initial conditions and focal point locations were tested, and the proposed control law could successfully camouflage a shadower for any predictable shadowee trajectory (an example of a known but nonlinear trajectory is shown in Figure 3.4).



(a) Error ratio between desired slope and that generated by the LQR controller ($\epsilon = 1$ indicates no error)

(b) Control acceleration for the controller

Figure 3.3: Error and Control Acceleration curves for Figure 3.2(a). Note that the error in the result is largely caused by the existence of an upper limit on the control acceleration, and the algorithm is sufficiently robust that only large variations in the weighting parameters produce visible increases in the error.

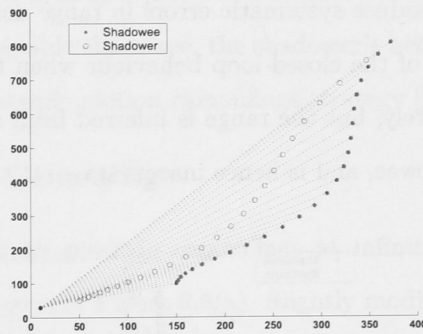


Figure 3.4: Example of a nonlinear target trajectory.

3.3.2 Mimicking Dragonfly Encounters: Realistic Constraints

In order to simulate the dynamic behaviour of dragonfly engagements more realistically, certain modifications were made to the simulation. Motion constraints were added to limit the allowable pursuer acceleration and velocity, to values that approximated those observed in genuine dragonfly interactions.

It is likely that insects have an excellent estimation of the apparent angular velocity of the shadowee [SPK99], but less is known about their acuity in measuring range [OWV00]. It is possible that dragonflies make assumptions about the size or speed [CL78] of the shadowee, and use these assumptions to infer range from dynamic cues. This corresponds

with other research indicating that dragonflies, like most insects, are very sensitive to image motion [FO95], so they are likely to be able to fairly accurately measure angular velocity and possibly even accelerations.

To partially represent the measurement process available to dragonflies, a polar representation of information was incorporated into the simulation. Although filtering was not added, this polar co-ordinate system allowed noise to be introduced into range and angle measurements in a crude manner to partially represent the effect of a state estimation process.

Let r be the range from shadowee to shadower, and θ be the angle of the line of sight vector between the two. Then the relative state vector is

$$X_R = \begin{bmatrix} r \cos \theta \\ r \sin \theta \\ \dot{r} \cos \theta - r \dot{\theta} \sin \theta \\ \dot{r} \sin \theta + r \dot{\theta} \cos \theta \end{bmatrix}. \quad (3.14)$$

In this way we can introduce systematic errors in range and velocity estimation. Figure 3.5 shows an example of the closed-loop behaviour when the angular position of the shadowee is known accurately, but the range is inferred from an (erroneous) assumption about the size of the shadowee, and is hence inaccurate.

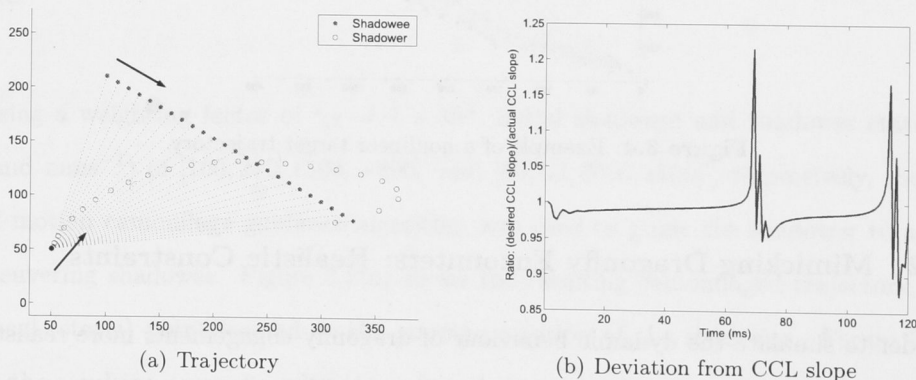


Figure 3.5: Trajectory with a (systematic) range estimation error: this figure shows the resulting trajectory and a plot of the deviation from the desired slope. Initial conditions were the same as Figure 3.2(a)

It can be seen that errors in range estimation produce an overshoot of the target (Figure 3.5(a)), and a slight deviation from the CCLs when a corrective acceleration is applied (Figure 3.5(b)). Here, we see that although the trajectory remains on the CCLs,

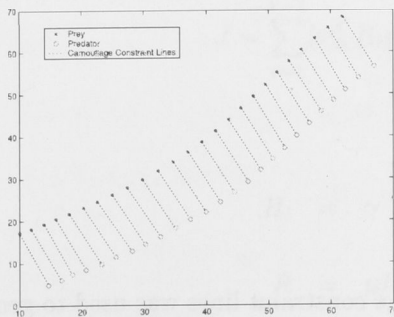
once the pursuer crosses the path of the shadowee it is no longer stationary from the shadowees perspective (ie in terms of our previous camouflage equations, $k > 1$, so motion lies on the CCL but is not camouflaged in any real sense). Hence unless range information is reasonably precise, a pursuit trajectory may require an auxiliary constraint or limitation to ensure it remains between the static point and the target.

Remarks

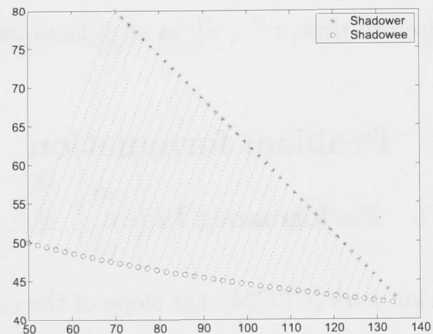
1. A systematic approach to estimating the required state information from the partial observations available to the dragonfly was not implemented in this study. A Kalman filtering approach to state estimation would seem to be one obvious approach.
2. A second, more subtle, issue is the prediction of future shadowee motion. It appears that some sort of prediction of future shadowee behaviour is required for successful guidance. However, it is known that when a shadower dragonfly encounters an aerially and tactically capable shadowee, the shadower's behaviour is more complicated than the presented simple motion camouflage strategy [MCS03].

3.3.3 Infinite Point Camouflage

The results of a program to generate camouflage at infinity, using an offset value as described in 3.2.5, can be seen in Figure 3.6(a). Slightly modified, the infinite camouflage algorithm will produce a successful capture, as in Figure 3.6(b).



(a) Tracking at constant distance



(b) Capture using camouflage at infinity

Figure 3.6: Either shadowing or capture can be accomplished using camouflage with a focal point at infinity.

3.4 LQR: Extension to 3 Dimensions

Previously [CFC04], we derived and tested a method of generating motion camouflaged trajectories using dynamic programming. This controller was limited to two dimensions, and engagements of finite length. Here, we first extend that work to three dimensions, then use a dynamic programming method with greedy cost constraints to develop an open-ended solution.

3.4.1 Dynamics of motion

Let the shadower position be designated $\mathbf{r}_D = [x^D(t), y^D(t), z^D(t)]$, and the shadowee position $\mathbf{r}_T = [x^T(t), y^T(t), z^T(t)]$. Similarly, the respective velocities are represented by $\dot{\mathbf{r}}_D = [\dot{x}^D(t), \dot{y}^D(t), \dot{z}^D(t)]$ and $\dot{\mathbf{r}}_T = [\dot{x}^T(t), \dot{y}^T(t), \dot{z}^T(t)]$. Then let the shadower state be written

$$\mathbf{r}^D = [x^D, y^D, z^D, \dot{x}^D, \dot{y}^D, \dot{z}^D]' \quad (3.15)$$

and the define the shadowee state similarly,

$$\mathbf{r}^T = [x^T, y^T, z^T, \dot{x}^T, \dot{y}^T, \dot{z}^T]' \quad (3.16)$$

The focal point of the engagement is written

$$\mathbf{r}^P = [x^P, y^P, z^P]' \quad (3.17)$$

The camouflage constraint lines are the vectors $\mathbf{r}^P - \mathbf{r}^T(t)$ at any particular time t , or in discrete time, $\mathbf{r}^P - \mathbf{r}_i^T$ at each time interval i .

3.5 Problem formulation

3.5.1 Performance Index

In prior work [CFC04], the slope of the camouflage constraint lines was used to generate a cost for the problem. Extending to three dimensions, we could use the normalized gradient of the constraint lines to obtain the equivalent information, however since the constraint vectors are straight lines, we can more simply use the normalized vector itself as a measure of the performance index. To do this, we need to augment the state of the shadower and

shadowee in a suitable fashion [Ber95]. So let

$$\mathbf{g}_i = \frac{\mathbf{r}^P - \mathbf{r}_i^T}{|\mathbf{r}^P - \mathbf{r}_i^T|} \quad (3.18)$$

then for a camouflaged trajectory, at any time interval i , the following holds true:

$$\mathbf{r}^P - \mathbf{r}_i^D = \frac{\mathbf{r}^P - \mathbf{r}_i^T}{|\mathbf{r}^P - \mathbf{r}_i^T|} |\mathbf{r}^P - \mathbf{r}_i^D| = \mathbf{g}_i |\mathbf{r}^P - \mathbf{r}_i^D| \quad (3.19)$$

Hence the running cost index for the problem can be written

$$((\mathbf{r}^P - \mathbf{r}_i^D) - \mathbf{g}_i |\mathbf{r}^P - \mathbf{r}_i^D|)^2.$$

We make a coordinate transformation ,

$$\mathbf{r}^N = \mathbf{r}^P - \mathbf{r}^D \quad (3.20)$$

and rewrite the cost accordingly:

$$(\mathbf{r}_i^N - \mathbf{g}_i |\mathbf{r}_i^N|)^2. \quad (3.21)$$

In order to write this running cost in the appropriate format, we need to augment the state equation for the controlled variable, so let

$$\mathbf{r}_A^N = [\mathbf{r}^N, |\mathbf{r}^N|]'. \quad (3.22)$$

Including an energy cost to limit excessive control action, the cost function for the problem can then be written [Ber95] as

$$J = \sum_{i=1}^{k-1} [\mathbf{r}_{Ai}^{N'} H_i \mathbf{r}_{Ai}^N + \mathbf{u}_i' R \mathbf{u}_i] + \mathbf{r}_{Ak}^{N'} H_k \mathbf{r}_{Ak}^N \quad (3.23)$$

where

$$\begin{aligned} H_i &= \gamma \left[\begin{array}{cc|c} I_3 & -\mathbf{g}_i & 0_4 \\ -\mathbf{g}_i' & \mathbf{g}_i' \mathbf{g}_i & 0_4 \end{array} \right] \\ R &= \mu I_4. \end{aligned} \quad (3.24)$$

3.5.2 Augmented dynamics

We are now in a position to define the discrete-time state equations associated with the system. Let

$$A = \begin{bmatrix} I_4 & \Delta t I_4 \\ 0_4 & I_4 \end{bmatrix} \quad (3.25)$$

$$B = \begin{bmatrix} 0_4 \\ \Delta t I_4 \end{bmatrix} \quad (3.26)$$

then the state equation for the system is

$$\mathbf{r}_{Ai+1}^N = A \mathbf{r}_{Ai}^N + B \mathbf{u}_i \quad (3.27)$$

where \mathbf{u} is the control vector for the system. The optimal control solution to the linear quadratic problem is

$$\mathbf{u}_i = -K_i \mathbf{r}_{Ai}^N. \quad (3.28)$$

The gain, K_i , is found by

$$K_i = [B' P_i B + R]^{-1} B' P_i A \quad (3.29)$$

where P is given by the appropriate Riccati equation [Ber95].

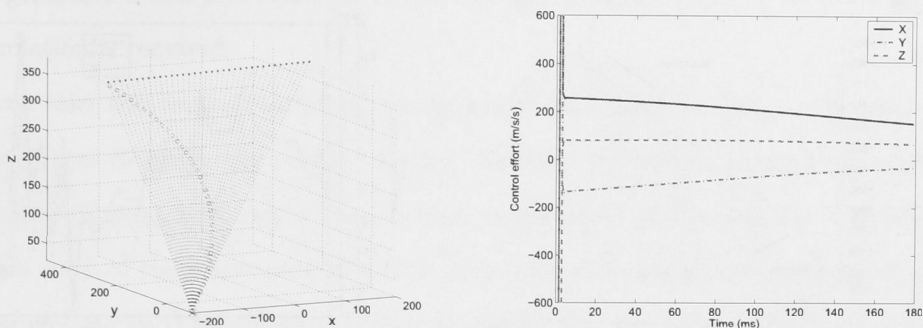
3.5.3 Results

The following graphs demonstrate optimized paths taken by the above control system in response to a linear (Figure 3.7) and nonlinear (Figure 3.8) shadowee path. For the sake of simplicity, the starting position of the active participant was assumed to be at the same location as the stationary point. For these examples, the weighting factors are as follows: $\gamma = 10^3$, $\mu = 10^{-5}$.

3.5.4 Spherical co-ordinate transformation

If we wish to simulate noise and sensor error in a manner similar to that used previously, it is easier to do so if the system is considered in the spherical frame, centred on the pursuer. We first write the system in a relative reference frame, $R = T - N$ (after the coordinate shift in (3.20) is taken into account). Then the necessary state equation can be written as

$$\mathbf{r}_{Ai+1}^R = A \mathbf{r}_{Ai}^R + B \mathbf{u}_i^D \quad (3.30)$$



(a) Example of 3D static camouflage using an LQR controller

(b) Control acceleration required for the path, in ms^{-2}

Figure 3.7: Examples of static point motion camouflage using a three-dimensional linear quadratic solution. Initial conditions, in mm and mm/s: $\mathbf{r}_P = \mathbf{r}_D(0) = [-200, 100, 20]$, $\mathbf{r}_T(0) = [200, 250, 380]$, $\dot{\mathbf{r}}_D(0) = [250, 440, 700]$, $\dot{\mathbf{r}}_T(0) = [-160, 130, -30]$.

where \mathbf{r}_A^R is the relative state vector ($\mathbf{r}_A^T - \mathbf{r}_A^N$), A and B are as before, and \mathbf{u}^D is the control acting on \mathbf{r}^N . Then the transformation to spherical co-ordinates is straightforward, and the augmented relative state vector can be explicitly written

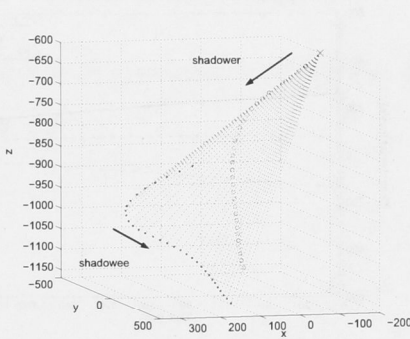
$$\mathbf{r}_A^R = \begin{bmatrix} r \cos \theta \sin \phi \\ r \sin \theta \sin \phi \\ r \cos \phi \\ r \\ \dot{r} \cos \theta \sin \phi + r(\dot{\phi} \cos \phi - \dot{\theta} \sin \theta) \\ \dot{r} \sin \theta \sin \phi + r(\dot{\phi} \cos \phi + \dot{\theta} \cos \theta) \\ \dot{r} \cos \phi - r \sin \phi \\ \dot{r} \end{bmatrix} \quad (3.31)$$

where r is the length of the relative vector $[x^R, y^R, z^R]$, θ is the azimuthal angle and ϕ is the angle of elevation.

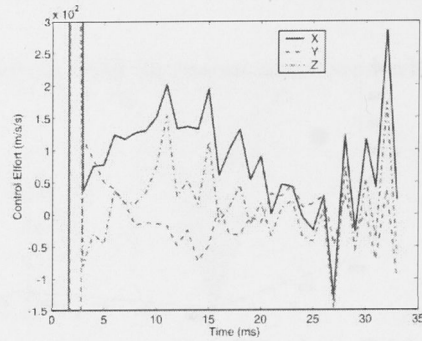
3.6 Greedy Optimal Control

3.6.1 Problems with LQR

The previous control equations depended on a cost function that was cumulative over the entire interaction, and thus required (a) a predictable shadowee path, and (b) a known end point for the engagement. The traditional finite-horizon LQR controller works by solving an appropriate Riccati equation for the desired end-point of the interaction and working backwards. While this can be converted into an infinite-horizon controller by continually recalculating the end-point as the state information is updated, doing so increases the



(a) Example against manoeuvring target



(b) Control acceleration required for the path

Figure 3.8: LQR against a manoeuvring target. Note the large control effort. In this simulation, no maximum cap on the control acceleration was used, so the solution was geometrically perfect. Initial conditions, in mm and mm/s, were: $\mathbf{r}_P = \mathbf{r}_D(0) = [-200, 100, -600]$, $\mathbf{r}_T(0) = [140, 107, -832]$, $\dot{\mathbf{r}}_D(0) = [2500, -280, -3000]$, $\dot{\mathbf{r}}_T(0) = [-3350, 462, -895]$.

processing power required enormously.

Greedy optimal control eliminates this problem by considering a piece-wise cost, optimized only over the immediate time interval. It thus removes the need for the shadowee path to be completely predictable, or for the time horizon of the engagement to be defined beforehand.

3.6.2 Problem formulation

Lavretsky [Lav00] outlines a useful greedy control method which can be adapted to this problem, also using dynamic programming. The difference is that the cost now takes the incremental form

$$J_k = u_k^T R u_k + x_{k+1}^T Q x_{k+1} \quad (3.32)$$

and at each time-step we attempt to minimise this cost without regard for the steps taken before or after. The gain is found by

$$K_k = [R + B^T Q B]^{-1} B^T Q A. \quad (3.33)$$

Note that the gain is similar in appearance to that based on the solution to the discrete forward-time Riccati equation [Ber95], however here the matrix representing the running cost Q takes the place of the Riccati solution P . When using the equation, then, it is not merely sufficient to redefine the cost appropriately, we must also ensure that Q has a form

which generates a non-zero solution. In the case of motion camouflage, we find that some reformulation is required.

If we take the control vector \mathbf{u}_k to be acceleration input as before, then our state matrix B acts directly only on the velocity. However the motion camouflage constraint is a geometric constraint, not a dynamic one, independent of the velocity. Therefore the resultant form of the state-space matrix H does not produce a solution under the greedy optimal equations. (It is trivial to demonstrate that the derivative of the cost constraint (3.9) is also not useful in defining a running cost matrix).

So we consider instead the control vector to be the velocity of the controlled body $\mathbf{u}_k = \dot{\mathbf{x}}_k^D$, and the (augmented) statespace equation is now:

$$\mathbf{x}_{k+1}^D = A \begin{bmatrix} \mathbf{r}_k^D \\ |\mathbf{r}_k^D| \end{bmatrix} + B \begin{bmatrix} \dot{\mathbf{r}}_k^D \\ |\dot{\mathbf{r}}_k^D| \end{bmatrix} \quad (3.34)$$

$$A = I_4$$

$$B = \Delta t I_4.$$

The cost matrices R and Q need to be defined. We let R represent a unity cost on the control,

$$R = \mu I_4 \quad (3.35)$$

where μ is the control cost weighting factor. Then Q must encapsulate the same geometric constraint previously included in H , however it must now be in a form that matches the incremental cost (3.32). Consider the constraint equation (3.9). The necessary geometric condition is then

$$\mathbf{r}_{k+1} = \mathbf{g}_{k+1} |\mathbf{r}_{k+1}| \quad (3.36)$$

so we need to obtain an estimate for \mathbf{g}_{k+1} (recall that the aim of greedy optimal control is to eliminate the necessity of complete predictability of the shadowee path, so that the system at future states is no longer known exactly).

To proceed: we minimize the time increment Δt^1 and assume the moment to moment acceleration undergone by the shadowee is relatively small. Then we can make the linear

¹In simulation we can choose the time increment to be as small as we like, so there is no lower bound and we can choose a Δt that is small enough to reduce error to negligible amounts. In practice, however, the minimum interval between measurements will be dependent on physical factors, for example delays and processing time within the system.

approximation

$$\mathbf{r}_{k+1}^T = \mathbf{r}_k^T + \Delta t \mathbf{v}_k^T$$

so

$$\mathbf{g}_{k+1} = \frac{\mathbf{r}_{k+1}^T}{|\mathbf{r}_{k+1}^T|} \approx \frac{\mathbf{r}_k^T + \Delta t \mathbf{v}_k^T}{|\mathbf{r}_k^T + \Delta t \mathbf{v}_k^T|}. \quad (3.37)$$

Call this approximation \mathbf{g}'_{k+1} , and let our running geometric cost constraint be

$$(\mathbf{r}_{k+1}^D - \mathbf{g}'_{k+1} |\mathbf{r}_{k+1}^D|)^2. \quad (3.38)$$

Our cost matrix now takes the form

$$Q = \begin{bmatrix} I_3 & -\mathbf{g}'_{k+1} \\ -\mathbf{g}'_{k+1}{}^T & \mathbf{g}'_{k+1}{}^2 \end{bmatrix}. \quad (3.39)$$

(The extension to polar co-ordinates for the new state vectors is a trivial reduction of Section 3.5.4 and thus is not detailed here).

3.6.3 Results

Again, we examine the response to a linear and a nonlinear shadowee path. No limit was placed upon the control acceleration, so the paths did not deviate from the camouflage constraint lines. However, capture of the target could only occur under a highly constricted set of starting conditions and target dynamics.

3.6.4 Analysis

As it stands, the system provides good camouflage, however it does not necessarily produce a capture or even pursuit path. Moreover, the control effort required may not differ significantly from that needed using a finite-horizon control. It may even be greater (see Figure 3.10(b)).

The crucial difference is that a greedy optimal trajectory, seeking to minimize immediate energy expenditure, will at each time interval seek the shortest path between two adjacent camouflage constraint lines (a perpendicular vector). We can see this is the case by examining the included angle between the shadower trajectory and the constraint lines, as in Figure 3.11(a). Compare with Figure 3.11(b), which plots the included angle for an LQR path using the same shadowee inputs and weighting scalars as the greedy case.

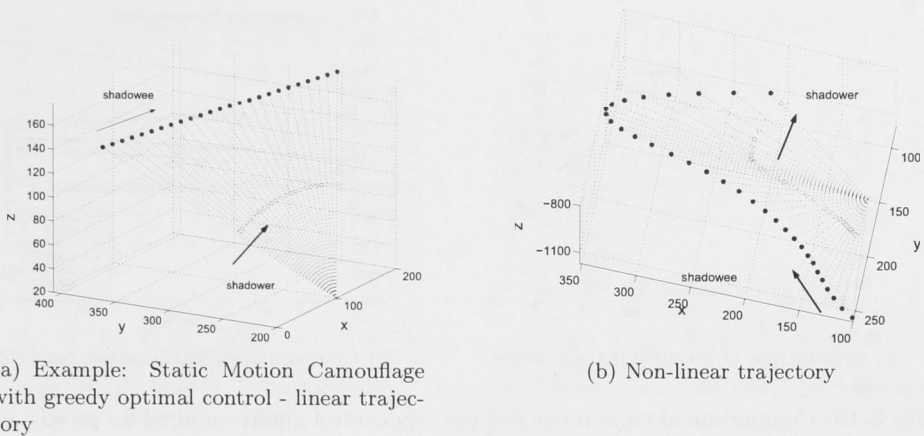


Figure 3.9: Greedy optimal control performance against (a) a nonmaneuvering target and (b) a manoeuvring target. Although in (b) the trajectory of the shadowee is such that it enables the shadower to achieve capture, this is not generally the case. (a) has initial conditions $\mathbf{r}_P = [-200, 100, 20]$, $\mathbf{r}_D(0) = [150, 225, 100]$, $\mathbf{r}_T(0) = [200, 250, 180]$, $\dot{\mathbf{r}}_D(0) = [190, 440, 140]$, $\dot{\mathbf{r}}_T(0) = [-60, 80, -30]$. (b) Starting points are $\mathbf{r}_P = [-200, 100, -800]$, $\mathbf{r}_D(0) = [144, 184, -980]$, $\mathbf{r}_T(0) = [140, 107, -832]$, $\dot{\mathbf{r}}_D(0) = [190, 440, 140]$, $\dot{\mathbf{r}}_T(0) = [330, 40, -90]$. Target trajectory in (b) is taken from an interaction filmed by Akiko Mizutani, 2003.

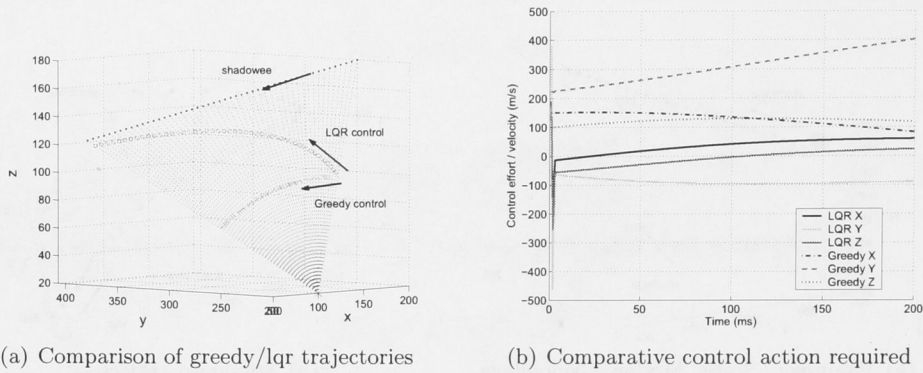
3.7 Implementing Force-based Control in Flexible Aerial Vehicles

In the preceding section we have examined higher level guidance methods for achieving motion camouflage. But how to implement these techniques, requiring a high degree of precision and flexibility? We here develop a force-based controller which may be used in conjunction with the methods presented both here and in Chapter 5.

Insects of all kinds hold a significant advantage over artificial craft in terms of maneuverability - unhindered by the weight, size and rigidity of inanimate aircraft, they can afford to undertake more acrobatically demanding tasks.

Our motivation stems from the fact that for a particular commanded inertial frame acceleration, there often exist multiple poses that will achieve the desired outcome. Descent, for example, may be accomplished either by pitching the nose down or by banking to either side, as shown in Figure 3.12. Most autopilots currently in use do not have the flexibility necessary to make use of more than one of these methods for any given command.

In contrast, we have designed an algorithm which takes a current or desired acceleration as input and extracts the attitude required for a fixed-wing body to achieve this



(a) Comparison of greedy/lqr trajectories

(b) Comparative control action required

Figure 3.10: Comparison of trajectories and velocity control inputs required for greedy and LQR trajectories. (a) has the same starting conditions as Figure 3.9(a). (b) Greedy control relies on a velocity control input, so the appropriate comparison is between the control required for a greedy solution and the velocity attained when using a traditional LQR solution

acceleration. In the case of multiple real solutions, a pose can be selected according to some defined optimal criteria. The algorithm can thus be used to estimate attitude from wind-frame forces, or to develop a trajectory for use in path-planning and navigation systems. It eliminates the need for the time- and process-intensive filtering of inertial data which is otherwise required to produce a force-based autopilot. It also takes into account the aerodynamic coupling between the roll and pitch, by considering the attitude as a single two dimensional construct, rather than by trying to control each separately. In addition, this procedure generates an energy-efficient series of commands, since it primarily operates by manipulating the gravity vector, minimizing any acceleration or deceleration due to thrust.

This method can not only be used to simulate a fixed-wing response to motion camouflage force-based guidance commands, it can also be used to analyze the inertial forces acting on a rigid body undertaking a known path in three dimensions. This gives us an excellent tool with which to examine the second-order differential equations governing patterns of insect flight.

Initially, we describe a method for determining attitude from provided wind-axis forces. Subsequently, we use desired acceleration inputs in the inertial frame to determine the attitude that will result in a controlled manoeuvre.

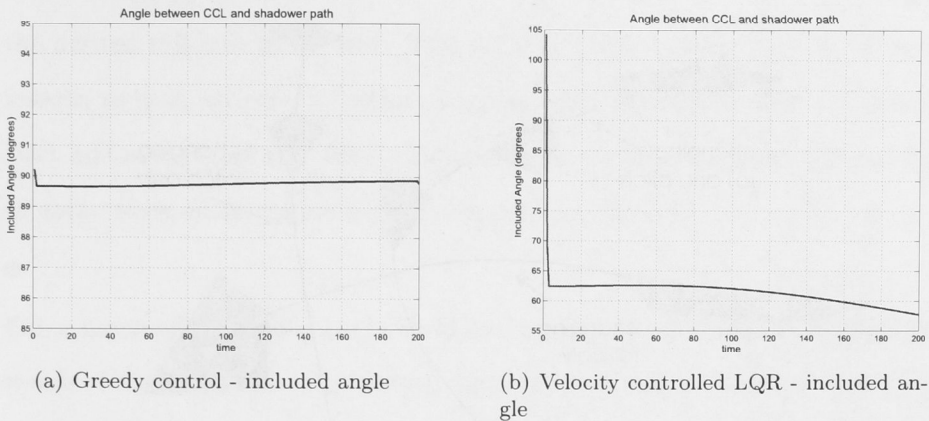


Figure 3.11: Angle comparison between greedy and LQR control: Comparing the angle between the course of the shadower and the camouflage constraint lines, it becomes clear that the greedy optimal control maintains a course perpendicular to the constraint lines.

3.7.1 Attitude from Wind-Axis Forces

We define the transformation matrix from the inertial frame to the body frame in the standard way [Ham63]:

$$B = \begin{bmatrix} \cos \theta \cos \gamma & \cos \theta \sin \gamma & -\sin \theta \\ \sin \phi \sin \theta \cos \gamma - \cos \phi \sin \gamma & -\sin \phi \sin \theta \sin \gamma + \cos \phi \cos \gamma & \sin \phi \cos \theta \\ \cos \phi \sin \theta \cos \gamma - \sin \phi \sin \gamma & \cos \phi \sin \theta \sin \gamma - \sin \phi \cos \gamma & \cos \phi \cos \theta \end{bmatrix}$$

To avoid singularities brought on by the high degree of non-linearity in the eventual controller, we work in quaternions rather than Euler angles [TW97]. So in quaternion form, for

$$\mathbf{q} = [q_0 \quad q_1 \quad q_2 \quad q_3]^T$$

$$B = \begin{bmatrix} 2(q_0^2 + q_1^2) - 1 & 2(q_1q_2 - q_3q_0) & 2(q_1q_3 + q_2q_0) \\ 2(q_1q_2 + q_3q_0) & 2(q_2^2 + q_0^2) - 1 & 2(q_2q_3 - q_1q_0) \\ 2(q_1q_3 - q_2q_0) & 2(q_2q_3 + q_1q_0) & 2(q_3^2 + q_0^2) - 1 \end{bmatrix} \quad (3.40)$$

See Appendix (C) for details on quaternions, their uses and the transformation between quaternions and Euler angles. Heading angle has no effect on the exerted forces in the body-frame, so we can derive some relationships between the four quaternion elements and thus reduce the number of independent variables to two, as follows:

The fundamental quaternion equation is

$$q_0^2 + q_1^2 + q_2^2 + q_3^2 = 1. \quad (3.41)$$

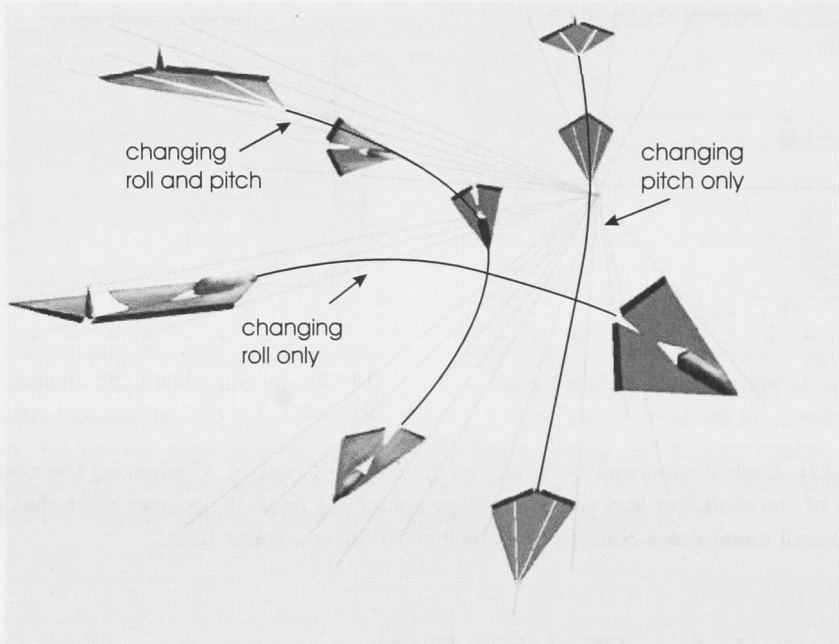


Figure 3.12: Various methods of losing altitude by changing the inertial orientation of the aircraft

Taking yaw to be zero, then from our knowledge of the structure of the rotation matrix, we can write

$$2(q_1 q_2 - q_3 q_0) = 0 \Rightarrow q_0 = \frac{q_1 q_2}{q_3}. \quad (3.42)$$

So using equations (3.41) and (3.42), the relationship between the quaternion elements can be described as

$$c = q_0^2 + q_1^2$$

$$q_3 = q_1 \left(\frac{1}{c} - 1 \right)^{\frac{1}{2}} \quad (3.43)$$

$$q_2 = q_0 \left(\frac{1}{c} - 1 \right)^{\frac{1}{2}}. \quad (3.44)$$

From the body-frame dynamics, we can write the two fundamental equations which will then enable us to solve for the attitude, based on the known variables [TW97].

$$\mathbf{a}_B = B\boldsymbol{\omega} \times \mathbf{v}_B + B\mathbf{g} \quad (3.45)$$

$$\mathbf{a}_I = B^{-1}\mathbf{a}_B. \quad (3.46)$$

We make some approximations and assumptions about the dynamics:

-
- When designing for an aircraft, we desire a steady, snap-to controller, so we define the desired roll-rate to be zero. This actually mimics the behaviour of free-flying insects, as their attitude adjustments around the longitudinal body axis tend to be swift and abrupt [R89], [SvH99]. Therefore it is not an unreasonable approximation to make when analysing insect flight trajectories. [Hen93]
 - For a manmade aircraft, the body-frame velocity occurs predominantly along the x-axis of the aircraft, so v_{z_B} and v_{y_B} are negligible and we assume velocity only in the forward direction.
 - As stated already, yaw (ψ) is considered to be meaningless, since heading angle exists only relative to an arbitrary external frame. In general, insects may use a celestial or geocentric compass [Hom04], [LM02] to orient themselves in a global reference frame, and this may impact upon navigation decisions. However such considerations are outside the scope of this thesis.
 - As the equations above stand, we have six equations but seven unknowns. We need to define an external acceleration which can be measured or determined independently from the body-frame orientation. So we choose a_{z_I} , the vertical inertial acceleration. In physical terms, this is equivalent to the vector sum of gravity and any inertial vertical forces produced by the thrust and lift generated by the wings of the body. In a fixed wing aircraft, we can use the physical characteristics of the plane to determine the lift co-efficient and hence the lift contribution of the aerodynamic forces. In the biological world, the procedure is not so simple. We can use previous studies [WE97], [BDD04] to make an approximation of the lift and thrust generated by the flapping wings of an insect. We find in practise that the controller is quite robust with regard to the inertial-frame z acceleration, so this approximation may be sufficient.

It is then a relatively straightforward procedure to rearrange the equations and solve for the quaternion-based attitude, using equations (3.43), (3.44), (3.45) and (3.46). In this way, we acquire non-linear functions for the attitude quaternion, \mathbf{q} , and the angular

velocity, ω :

$$\mathbf{q} = \mathbf{f}(\mathbf{a}_B, a_{z_I}, v_{x_B}, \mathbf{g}) \quad (3.47)$$

$$\omega = \mathbf{h}(\mathbf{q}, \mathbf{a}_B, a_{z_I}, v_{x_B}, \mathbf{g}) \quad (3.48)$$

where \mathbf{g} is the gravity vector. The exact solution depends on the type and capabilities of the body in question.

Example 1: Solving for the attitude of a rigid body aircraft

For this kind of problem, it is standard to assume that the velocity of the aircraft is primarily in the forward direction, ie $v_{x_B} \gg v_{y_B}, v_{z_B}$. We obtain the following fundamental equations for the problem:

$$a_{x_B} = 2g(q_1q_3 + q_2q_0) \quad (3.49)$$

$$a_{z_I} = 2a_{x_B}(q_1q_3 - q_2q_0) + 2a_{y_B}(q_2q_3 + q_1q_0) + a_{z_B}(2(q_3^2 + q_0^2) - 1) \quad (3.50)$$

$$q_0 = \frac{q_1q_2}{q_3} \quad (3.51)$$

If we let $c = q_0^2 + q_1^2$, then substituting into 3.49 we can solve for q_0 and the remaining values follow from 3.51 and the fundamental quaternion equation. So

$$c = \frac{1}{2} \pm \frac{1}{2g} \sqrt{g^2 - a_{x_B}^2} \quad (3.52)$$

where g is the magnitude of the gravity vector. Then

$$a_2 = 4(a_{y_B}^2 + \frac{a_{z_B}^2}{c^2}) \quad (3.53)$$

$$a_1 = 4 \left[a_{z_B} \left(\frac{a_{z_I}}{c} - 2a_{x_B} \sqrt{\frac{1}{c} - 1} \right) + ca_{y_B}^2 + \frac{a_{z_B}^2}{c} \right] \quad (3.54)$$

$$a_0 = (a_{z_I}^2 + a_{z_B}^2) - 4a_{x_B}c \left[(a_{z_I} + a_{z_B}) \sqrt{\frac{1}{c} - 1} - a_{x_B}(1 - c) \right] + 2a_{z_B}a_{z_I} \quad (3.55)$$

and

$$q_0^2 = \frac{1}{2a_2} (-a_1 \pm \sqrt{a_1^2 - 4a_0a_2}). \quad (3.56)$$

At least two distinct solutions for the attitude are thus discovered, perpendicular to each other in the roll plane. This method has the advantage of also providing the pitch and bearing rates of the flying body, if required.

3.7.2 Attitude from Inertial Acceleration

The above section establishes the basic procedure for establishing attitude from body forces. It is potentially of great use for an aircraft in flight to be able to assess its attitude given only gyroscopic input. However, it is in general more useful from a control point of view to be able to construct a future attitude from inertial force inputs, rather than reconstruct a current one from body force inputs. The former can be used for achieving a force-based trajectory, since inputs in the form of control accelerations are generally defined in terms of inertial forces.

We next determine the attitude necessary to accomplish some predetermined manoeuvre, i.e. an attitude that will result in a force operating in the appropriate direction. Hence the procedure developed in the preceding section is adjusted so as to take acceleration inputs in the inertial frame. The body-frame z acceleration, which is roughly equivalent to the centripetal forces experienced during the manoeuvre, acts as the controlling constraint. It can be set using the physical limitations of the modeled craft or body in conjunction with the desired shape of the trajectory.

Thus, whether the acceleration is commanded directly or derived from a path-planning algorithm, we need only concern ourselves with adding a qualitatively appropriate value for the turning force.

Methods for determining acceleration from a given path or waypoint system are explored in Example 4. In general, our fundamental equations now become

$$\mathbf{a}_I = \boldsymbol{\omega} \times (B^{-1}\mathbf{v}_B) + \mathbf{g} \quad (3.57)$$

$$\mathbf{a}_B = B\mathbf{a}_I \quad (3.58)$$

From there, the procedure is essentially the same, and we develop attitude and attitude-rate solutions of a similar form.

$$\mathbf{q} = \mathbf{f}'(\mathbf{a}_I, a_{z_B}, v_{x_B}, \mathbf{g}) \quad (3.59)$$

$$\boldsymbol{\omega} = \mathbf{h}'(\mathbf{q}, \mathbf{a}_I, a_{z_B}, v_{x_B}, \mathbf{g}) \quad (3.60)$$

Note

Naturally, the aircraft has a base speed (dependent on atmospheric conditions) which it is not desirable to fall below. In addition, it can be advantageous to attempt to maintain speed throughout a manoeuvre, as it reduces the necessity for consumption-heavy accelerations. Hence, when developing a series of acceleration commands, we can interpret these desirable speed conditions as a constant velocity constraint. This corresponds well with energy minimal control algorithms. In practise, the exact value of the velocity generally becomes irrelevant when considering the attitude, as long as the direction of that velocity is known.

Example 2: Direct control of attitude via inertial inputs

A test of the functions computing attitude from acceleration can be undertaken fairly easily, by coding the desired inertial accelerations directly into the attitude subfunctions. The following results were obtained by inputting the acceleration commands $A_I = [-5, 3, 24]^T$ and $a_{z_B} = 12$. After a pre-determined interval, the commands were changed to $A_I = [20, -5, 20]^T$ and $a_{z_B} = -9$. Figure 3.13 shows the relevant attitude of the aircraft. Since we are not attempting to control heading angle with this formulation, yaw was not included in the attitude figures.

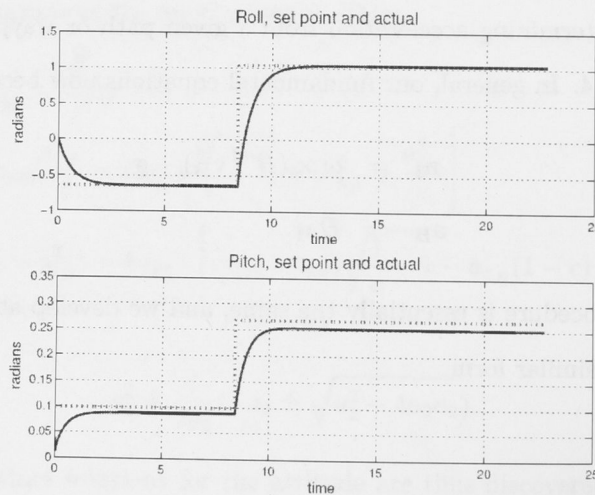


Figure 3.13: Attitude: output/setpoints derived from inertial inputs

Figure 3.14(a) shows the angular rates experienced by the aircraft, in radians per second. Figure 3.14(b) shows the actual acceleration experienced in the inertial plane. With the help of Saul Thurrowgood, an existing flight simulator based on an F16 aircraft [SL92] was modified and used to test the implementation of the derived algorithms. Figure 3.15(b) demonstrates the simulator in action under the command sequence described above. The attitude was held stable, even under a steep roll command.

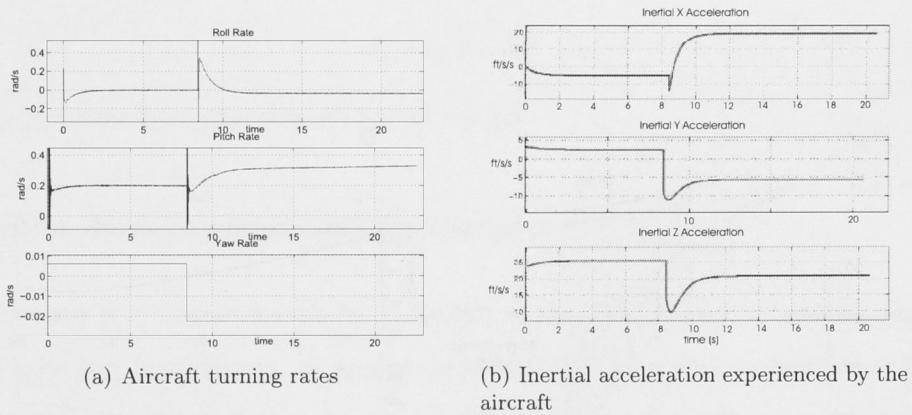


Figure 3.14: Angular rates and inertial accelerations for direct attitude control using an F16 flight simulator

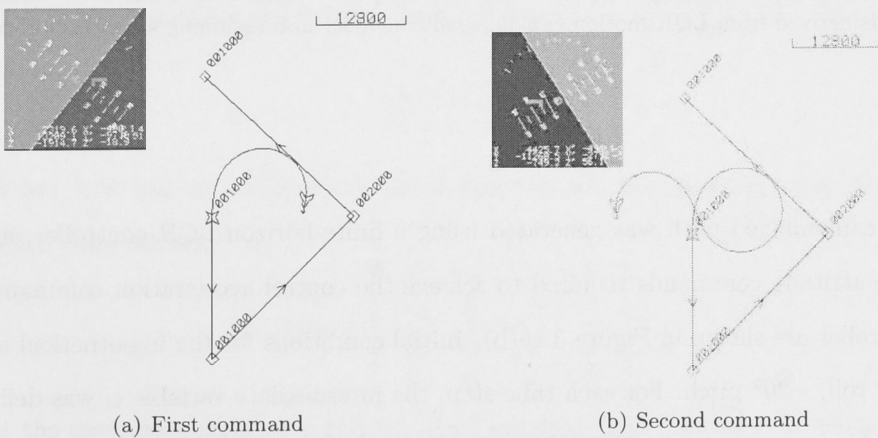


Figure 3.15: Screenshots from flight simulator. The inset in the upper left of each figure shows the artificial horizon output from the simulator cockpit at the moment the image was captured. The main figure shows the simulated plane as viewed from above. The starting point is marked with a star, and the trajectory traversed is shown as a line drawn from the star to the back of the aircraft.

Example 3: Attitude of rigid aircraft required for a motion-camouflaged LQR-derived path.

Using the above equations, we can simply input the control forces which will obtain a motion camouflaged path into a Matlab program, and acquire the desired attitude, as in Figure 3.16(a).

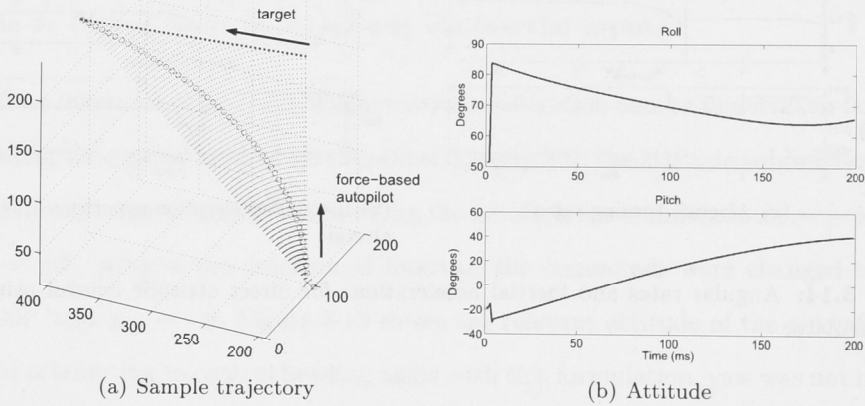


Figure 3.16: (a) LQR trajectory (b) the roll and pitch required to achieve it, using force-commands derived from LQR motion camouflaged controller and assuming a constant thrust.

The camouflaged path was generated using a finite-horizon LQR controller, and the requisite attitude commands required to achieve the control acceleration commanded by the controller are shown in Figure 3.16(b). Initial conditions for the hypothetical aircraft were 20° roll, -20° pitch. For each time step, the intermediate variable c_i was defined as

$$c_i = \frac{1}{2} \pm \frac{\sqrt{(a_{x_I}^2 + (g - a_{z_I})^2)^2 - a_{x_I}(a_{x_I}^2 + (g - a_{z_I})^2)}}{2(a_{x_I}^2 + (g - a_{z_I})^2)} \quad (3.61)$$

then the associated quaternion attitude components were found in the following manner:

$$q_{0_i} = \sqrt{\frac{-a_1 \pm \sqrt{a_1^2 - 4a_2a_0}}{2a_2}} \quad (3.62)$$

where

$$\begin{aligned} a_2 &= 4 \left[\left(2a_{x_I} \sqrt{\frac{1}{c} - 1} - a_{z_I} \left(2 - \frac{1}{c} \right) \right)^2 + \left(\frac{a_{y_I}}{c} \right)^2 \right] \\ a_1 &= 4 \left[\left(2a_{x_I} \sqrt{\frac{1}{c} - 1} - a_{z_I} \left(2 - \frac{1}{c} \right) \right) \left(a_{z_B} + a_{z_I} - 2a_{x_I} c \sqrt{\frac{1}{c} - 1} - \frac{a_{y_I}^2}{c} \right) \right] \\ a_0 &= \left(a_{z_B} + a_{z_I} - 2a_{x_I} c \sqrt{\frac{1}{c} - 1} \right)^2 \end{aligned}$$

and

$$q_{1_i} = \sqrt{c - q_{0_i}^2} \quad (3.63)$$

and q_{2_i}, q_{3_i} follow from equations (3.44) and (3.43).

Example 4: Path-planning using inertial inputs

The objective is to obtain a path in a parametric form which may be used to generate the requisite inertial equations, so we can use the problem formulation described in §3.7.2. Here, hermitian cubic splines have been used, which have the advantage of (approximately) minimizing path curvature [JC91].

The current attitude of the aircraft is obtained from instrument input, possibly by using the results arrived at in §3.7.1. Knowing the current forward body-frame velocity, we arrive at the initial inertial velocity quite simply:

$$\mathbf{v}_I = B^{-1} \mathbf{v}_B. \quad (3.64)$$

We are now free to set up the general matrices for this problem. Let M_H be the Hermitian basis matrix,

$$M_H = \begin{bmatrix} 2 & -2 & 1 & 1 \\ -3 & 3 & -2 & -1 \\ 0 & 0 & 1 & 0 \\ 1 & 0 & 0 & 0 \end{bmatrix} \quad (3.65)$$

and let the operand matrix of initial and final positions and velocities be designated G_H [dB01].

$$G_H = \begin{bmatrix} x_0 & y_0 & z_0 \\ x_n & y_n & z_n \\ v_{x_0} & v_{y_0} & v_{z_0} \\ v_{x_n} & v_{y_n} & v_{z_n} \end{bmatrix} \quad (3.66)$$

Then if $T = [t^3, t^2, t, 1]$ is the cubic parameter vector, the trajectory Q_H is found by

the matrix operation

$$Q_H = TM_HG_H. \tag{3.67}$$

Our initial assumptions include a constant velocity. Minimising acceleration along a curved path is equivalent to minimising the curvature of the path, and hence the following method for extracting acceleration commands was inspired by Jackson et al [JC91] and their Lagrangian method for constant speed trajectories.

We constrain the motion to a curved surface containing the spline path, and treat the acceleration minimisation as a cost constraint, expressed in terms of derivatives of the spline path. For a given path \mathbf{p} , the cost function is

$$J = \frac{1}{2} \int_{t=0}^{t_f} \ddot{\mathbf{p}}_I^T \ddot{\mathbf{p}}_I dt. \tag{3.68}$$

The physical interpretation of the parameters is shown in Figure 3.17.

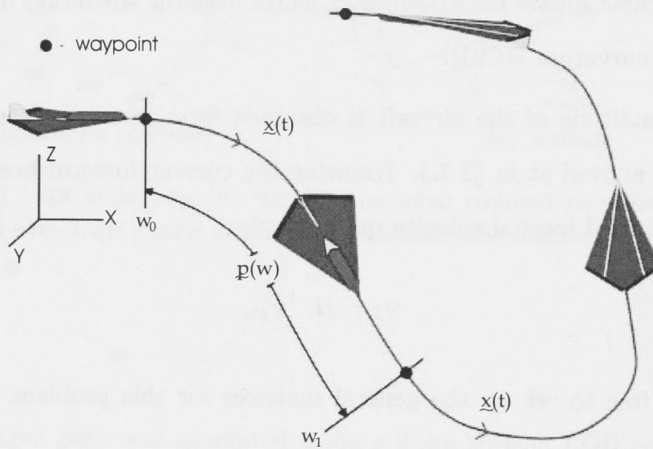


Figure 3.17: Parameterization of the waypoint paths

We develop a Lagrangian for the problem using this cost function, with the parameterized surface and velocity constraints expressed as Pfaffian constraints in terms of the first derivative of the spline path [Ros97]. Let A be the constraint matrix, and let $\mathbf{s} = \dot{\mathbf{p}}$, then

$$\mathcal{L} = \frac{1}{2} \dot{\mathbf{s}}^T \dot{\mathbf{s}} + \lambda A(\mathbf{s}) \dot{\mathbf{s}}. \tag{3.69}$$

λ is a Lagrange multiplier. Solving the Euler-Lagrange equations gives a solution

$$\ddot{\mathbf{s}} = (I - \mathbf{s}\mathbf{s}^T)\mathbf{c} - \kappa^T\mathbf{s} \quad (3.70)$$

for constant \mathbf{c} , where κ is the curvature of the path.

The control acceleration is then found by

$$\mathbf{u} = W \int \ddot{\mathbf{s}} dt \quad (3.71)$$

where W is a diagonal matrix of weighting constants dependent on the initial and final positions.

For each path segment, from point \mathbf{x}_N to \mathbf{x}_{N+1} , we use a discrete formulation of the problem, where the time to go is estimated by

$$t_f = \lfloor \frac{\|\mathbf{x}_{N+1} - \mathbf{x}_N\|}{\|\mathbf{v}_B\|} \rfloor \quad (3.72)$$

and then normalized to give a trajectory parameter. We then generate the control command and hence control acceleration at each time-step and use it as the inertial acceleration input to the attitude-based controller defined previously.

The waypoint algorithm was tested in Matlab, and the results demonstrated that the force-based control was comparable to other methods, as can be seen in the following figures. This example trajectory was generated by taking a series of waypoints comparable to that which would be encountered in the flight simulator, and an initial attitude, then following the procedure outlined earlier in §3.7.2.

The waypoints were located at the cartesian co-ordinates $[0, 0, 1000]$, $[-20000, 0, 1000]$, $[0, 20000, 2000]$ and $[20000, -500, 1000]$, where the scale is in feet, and the aircraft velocity was set at 500ft/s. The initial roll was 0, the initial pitch was 10 degrees. Figure 3.18(a) shows the paths generated by the original cubic spline, by direct integration of the Lagrangian-derived control acceleration, and by manipulation of the aircraft attitude in accordance with the method developed in §3.7.2. Figure 3.18(b) shows the aircraft attitude throughout the manoeuvre, and Figure 3.19 shows the control accelerations generated by the Lagrangian optimization method, and the actual accelerations experienced while traversing the generated path.

3.8 Discussion

In the first part of this chapter, we demonstrated that motion camouflage guidance could be achieved via the solution to a linear quadratic Gaussian control problem. Tracking behaviour was also considered.

The presented motion camouflage guidance strategies were examined in simulation studies involving a variety of camouflage focal points. These provide a preliminary illustration of the capabilities of the approach.

A force-based control system for an autopilot that uses direct attitude control to perform curved path maneuvers has been designed. For completeness, a method for using the control system along with a waypoint-based trajectory generation algorithm has also been included. The simulation demonstrates that a versatile force-based controller can be implemented with relative ease. The sample solutions presented here for attitude-based control were analytical, but more complex control algorithms can easily be obtained using iterative numerical methods.

Note that the force-attitude procedure is reversible and could be useful in reconstructing inertial forces on flying insects, if filmed at high enough resolution to accurately obtain roll and pitch. Moreover, the error between the attitude required to complete a manoeuvre

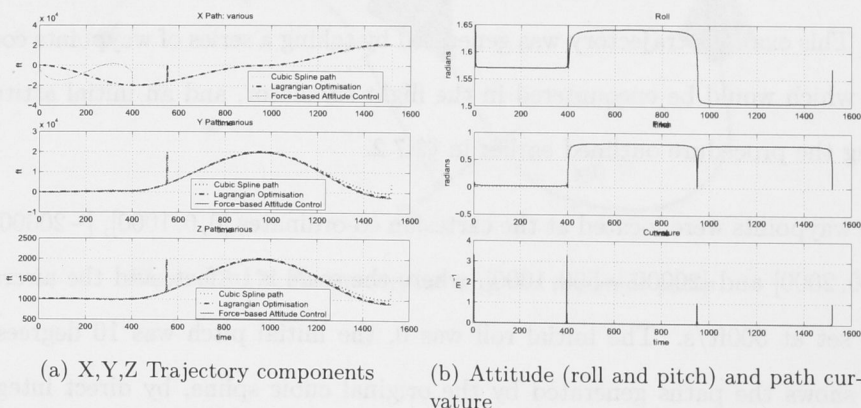


Figure 3.18: Results from a waypoint-following trajectory using non-linear attitude control. Note that although the first waypoint is achieved in the same time as the ideal cubic spline path, the path followed deviates along the x-axis from that proscribed by the spline. This is due to the existence of multiple attitudes which generate the same inertial forces. The controller in this case was instructed to take the first real solution presented, which did not match that envisioned by the cubic spline, yet still achieved the waypoint.

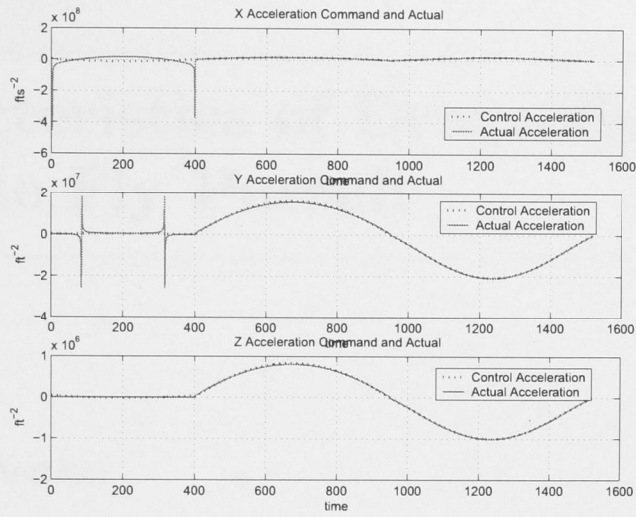


Figure 3.19: Control accelerations and resultant accelerations

ver using just inertial forces, and the attitude actually observed, can be subtracted to obtain a measurement of forces due to wing action, a procedure which is potentially simpler than the direct method of breaking down the aerodynamic forces acting on the wings themselves.



Figure 3.18: Results from a control experiment. The plots show the control signals and the system responses. The control signals are shown in the top row, and the system responses are shown in the bottom rows. The plots are labeled with letters (a) through (f) and numbers (1) through (6). The control signals are shown in the top row, and the system responses are shown in the bottom rows. The plots are labeled with letters (a) through (f) and numbers (1) through (6).

Characteristics of Dragonfly and Satellite Fly Pursuit

4.1 Introduction

Male dragonflies of the species *Hermianax papuensis* spend large portions of their time chasing and interacting with other insects in territorial patrols over bodies of water. These interactions may take the form of chasing prey, pursuing potential mates or warding off encroaching males. The first type of engagement often demonstrates incredible adeptness, but does not challenge the dragonfly in any serious physical sense, since prey insects are usually much less aerodynamically capable than dragonflies. Characteristics of the second type of flight vary depending on species, as does the receptivity of the females to mating flights of the male, but the number of male-female interactions counted over a day of filming tends to be significantly less than male-male [ES04], [PK87]. The third type of interaction is perhaps the most interesting. The behaviour seen between two male dragonflies of the same species most often resembles a dogfight between fighter planes, or a non-contact competition for aerial superiority. These engagements can be lengthy and are difficult to reproduce in a controlled environment, covering as they do a large territory at high speed. They are also, unfortunately, the hardest to define qualitatively, as we do not know what signals the start or end of such an engagement. As an introduction, we examine similar investigations into the guidance systems of other insects.

To catch and mate with females, male blowflies of the genus *Lucilia* engage in energetic high speed chases over short distances. Examining these chases in detail reveals two distinct behavioral modes - either the target is captured after a relatively short pursuit, or a fairly precise tracking path is chosen for up to several seconds, with no resulting capture [BKE03]. Other flies also demonstrate several chase modes, depending on the sex

or behaviour of the target [LC74], [CL75]. However, it has been demonstrated that for the blowfly at least, these two modes of behaviour can be explained as the consequence of a single control system. The system is calibrated to capture targets of an appropriate size and velocity, but can be fooled (and hence will exhibit other apparent behaviors) if the target is larger or faster than conspecifics [BE05]. In specific terms, the control of yaw rotation in the male fly is governed by the position of the target in the retina, where any offset from the central forward position elicits a turning response towards it [VR76]. Forward speed is governed by the size of the target on the retina, decreasing when the size is greater than a certain threshold value, but increasing if the retinal size is small [BKE03].

In certain species of hoverflies, a similar yaw response is engendered by target positional offsets [Col80b]. Others have been shown to manifest an interesting flight characteristic: when not aiming at any obvious goal, a hoverfly maintains the angular orientation of its body very constant [Col80b]. When attempting to catch a potential mate, however, they do not fly directly towards the target, but rather they adopt an interception course, accelerating in a uniform manner in the direction of target movement [CL78]. This appears to be a ballistic approach, rather than one under continuous control.

4.2 Variable definition

The following describe some of the more common angular variables used in this chapter:

List of Variables

| | |
|-------------------|----------------------------------------------------------------------------------------------------------------------------------|
| θ | Orientation of an insect's longitudinal body axis |
| α | Line-of-sight angle between one insect and another in the (2-dimensional) inertial reference frame |
| $\alpha - \theta$ | Line-of-sight angle relative to the body axis |
| ψ | Direction of flight |
| β | Line of sight angle relative to the flight direction |
| | Sign convention: As is standard, counter-clockwise rotation is presumed to be positive, clockwise rotation is taken as negative. |

4.3 Method

Free flying adult dragonflies of the species *Hermianax papuensis* and *Hemicordulia tau* were filmed on sunny days over natural bodies of water during the late morning and mid-afternoon. Territorial behaviour amongst these insects can be observed over most of the

day if the weather is fine, so the filming periods were chosen to maximize the natural light available, and to minimize the interference of shadows cast by environmental features. For the same reason, filming was restricted to days with little wind activity, which also helped to minimize camera shake and ensured the insects were not operating under particularly arduous external forces. The inertial reference frame was assumed to be oriented as in Figure 4.1.

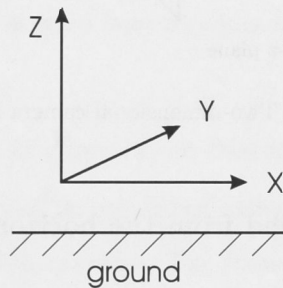


Figure 4.1: Inertial, or world axes

The filming was conducted in several stages, depending on available equipment.

4.3.1 Monoscopic filming in the horizontal plane

With Akiko Mizutani, I filmed trajectories from a side view, as shown in Figure 4.2(a). The camera used was a Sony XC-HR58, framerate 200fps, attached to a tripod and set up on a stable, predominantly flat plane at the water's edge and aligned with the horizontal plane using a spirit level.

4.3.2 Monoscopic filming in the vertical plane

With Jochen Zeil, dragonflies were filmed from overhead using a tripod and arm attachment, as in Figure 4.2(b), using a Sony DSR-PD170P camcorder. The equipment used for the previous data collection was not available at this time. The frame-rate was 50fps, the exposure time was 5ms. Both types of monoscopic footage were uploaded onto a computer and converted to .avi format using the program *VirtualDub*. Extraction of the position information of the insects was done manually frame-by-frame, using *Matlab 6.5*.

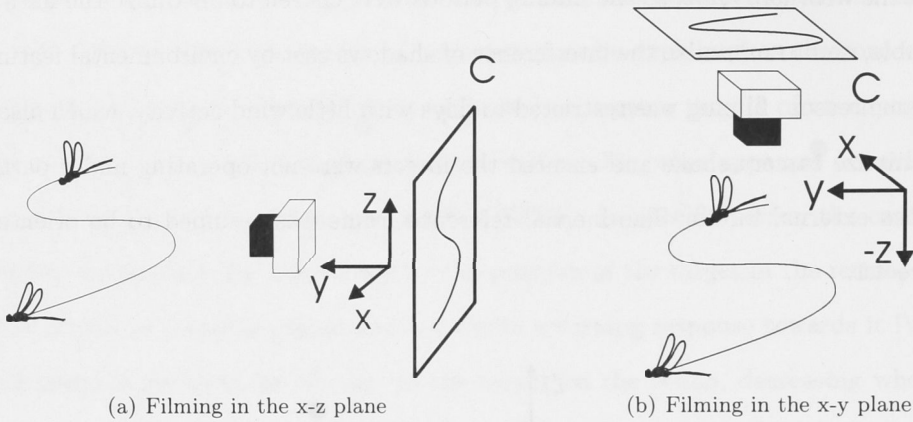


Figure 4.2: Two-dimensional camera arrangements

4.3.3 Stereo footage, filmed from the horizontal plane

Two Pulnix cameras, frame-rate 50fps, were mounted inside an aluminium frame, 30cm apart along the y-axis. An anemometer was mounted to the top of the box to record wind speed. At first, the cameras were mounted on a static tripod. Later, a 2DOF rotating joint was added to allow the camera to pan and tilt. Potentiometers connected to the rotary joints measured the degree of rotation, which was also recorded in real time on the linked laptop. The cameras were synchronized using a patented telemetry system (APN 2003245110) to imprint each recording with the time (to within $10 \mu\text{s}$), the frame number, the anemometer reading and, later, the output from the potentiometers measuring the yaw and pitch of the tripod joint. The film from each camera was then recorded to a tape in a double slot VCR recorder, uploaded to a PC and converted to avi format using a Matlab toolbox.

4.3.4 3D reconstruction from stereo cameras

The cameras are mounted such that their optical axes are coplanar and parallel (Figure 4.3).

The missing dimension can be reconstructed from such a arrangement using the following equation:

$$y = f - \frac{fL}{d} \quad (4.1)$$

where f is the focal length of the camera, d is the displacement between camera frames,

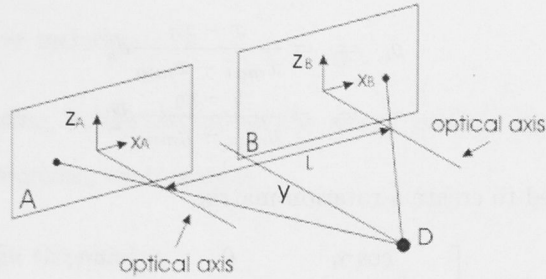


Figure 4.3: Reconstruction of depth from images generated by two parallel cameras

and L is the camera separation, as shown in the diagram.

Calibration of the cameras was accomplished using a regular checkerboard pattern, placed in the viewing field of both cameras. The frames from this stereo sequence were used to calibrate the cameras in accordance with Bouguet's Camera Calibration Toolbox for Matlab (cite!). This enabled us to reconstruct the left to right camera transformation, and hence the images could be converted into parallel camera geometry, enabling us to solve the correspondence problem using the epi-polar constraint

4.3.5 Data processing

In three dimensions with the pan and tilt information available, the camera rotation was accounted for using the following algorithm:

We attached potentiometers to the rotational axes, and take a reading at the minimum and maximum extremes of rotation. For rotation around the camera x-axis (pitch), the minimum potentiometer reading (x_{min}) was 16385, the maximum (x_{max}) was 47180. The total span of rotation around the x-axis (d_s^x) was 114 degrees, between -24 and 90 degrees as measured from the inertial frame. We determine the potentiometer reading corresponding to 0 degrees as follows:

$$x_0 = \frac{x_{max} - x_{min}}{d_s^x} + x_{min} \quad (4.2)$$

We also define a pitch constant, $\rho_0 = \frac{x_{max} - x_{min}}{d_s^x}$.

We followed a similar procedure for rotation around the y-axis (yaw). $d_s^y = 118$, between -59 and 59, $y_{min} = 15742$, $y_{max} = 52100$. We define the yaw constant, $\gamma_0 =$

$\frac{y_{max}-y_{min}}{d_s^y}$. Then for each frame i , we obtain the corresponding pitch and yaw readings,

$$\rho_i = \frac{x - x_0}{x_{max} - x_{min}} d_s^x \quad (4.3)$$

$$\gamma_i = \frac{y - y_0}{y_{max} - y_{min}} d_s^y \quad (4.4)$$

These values are used to create a rotation matrix,

$$R_i = \begin{bmatrix} \cos \gamma_i & 0 & \sin \gamma_i \\ \sin \gamma_i \sin \rho_i & \cos \rho_i & -\cos \gamma_i \sin \rho_i \\ -\sin \gamma_i \cos \rho_i & \sin \rho_i & \cos \gamma_i \cos \rho_i \end{bmatrix}.$$

For each point of interest \mathbf{x}_i^j in the camera frame, we apply the rotation matrix to obtain the corresponding point in the reconstructed world frame,

$$\mathbf{y}_i^j = R\mathbf{x}_i^j. \quad (4.5)$$

When processing the raw position information, post-digitization, an $\alpha - \beta$ filter was used to smooth the first-order data. This is a special case of a Kalman filter, and is generally considered suitable for most tracking applications due to its simplicity and computational efficiency [Bro98]. The filtering procedure is as follows: Let X be the array of position information, in two or three dimensions, of length n . Then

$$[V_i] = [X_{i+1} - X_i], i = 1, \dots, n. \quad (4.6)$$

Let $v_1 = V_1$, $x_1 = X_1$. Then for $i = 1, \dots, n - 1$,

$$v_{i+1} = v_i + \frac{b}{T}(X_i - x_i) \quad (4.7)$$

$$x_{i+1} = x_i + Tv_{i+1} + a(X_i - x_i). \quad (4.8)$$

The values chosen for the filter variables were $a = 0.2, b = 0.01, T = 1$.

Second-order data processing was done using an approximate differentiation process. For example, the velocity for a particular dragonfly D was determined by filtering the position information using a three-frame window, as follows

$$\mathbf{v}_i^D = \frac{\mathbf{x}_{i+1}^D - \mathbf{x}_{i-1}^D}{2\Delta t}$$

where Δt is the time interval between frames, or the inverse of the framerate.

4.3.6 Error sources

Possible sources of error include:

1. inconsistent lighting, light reflected off the water, and moving shadows induced by wind in the surrounding environment
2. lens aberration in the camera
3. noise in the recording device
4. wind shaking or moving the camera
5. video tape jitter
6. human error in manual selection of digitized insect positions.

To eliminate some of the higher-frequency errors caused by video jitter, a low pass alpha-filter was applied to the position information before analysis. The frequency of the filter was ascertained by filming a stationary object and assessing the frequency of the deviations in position. It was assumed that errors in orientation generated by manual inaccuracies were at most 1° per frame, so any changes in direction of less than $200^\circ/\text{s}$ were ignored.

4.4 Results from Dragonfly Interactions

4.4.1 Results from monoscopic data

Fixation

Dragonflies have fully articulated heads providing high mobility in the roll, pitch and yaw planes [Gor99]. During pursuit, some dragonflies have been shown to hold the absolute angle to the prey constant while the abdominal axis error angle changes, suggesting dragonflies stabilize their head against rotation during prey capture [Gor95]. However, for a non-perching species in regular flight, this arrestor system does not necessarily activate and the head may remain free to rotate [Sta81]. Either way, without precise information about the head orientation, we cannot be certain where the image of the other participant appears on the retina. Nevertheless, using the orientation of the longitudinal axis of the body, we can approximate the horizontal retinal position of the other participant. We do this by subtracting the body orientation from the absolute line of sight angle, as in Figure

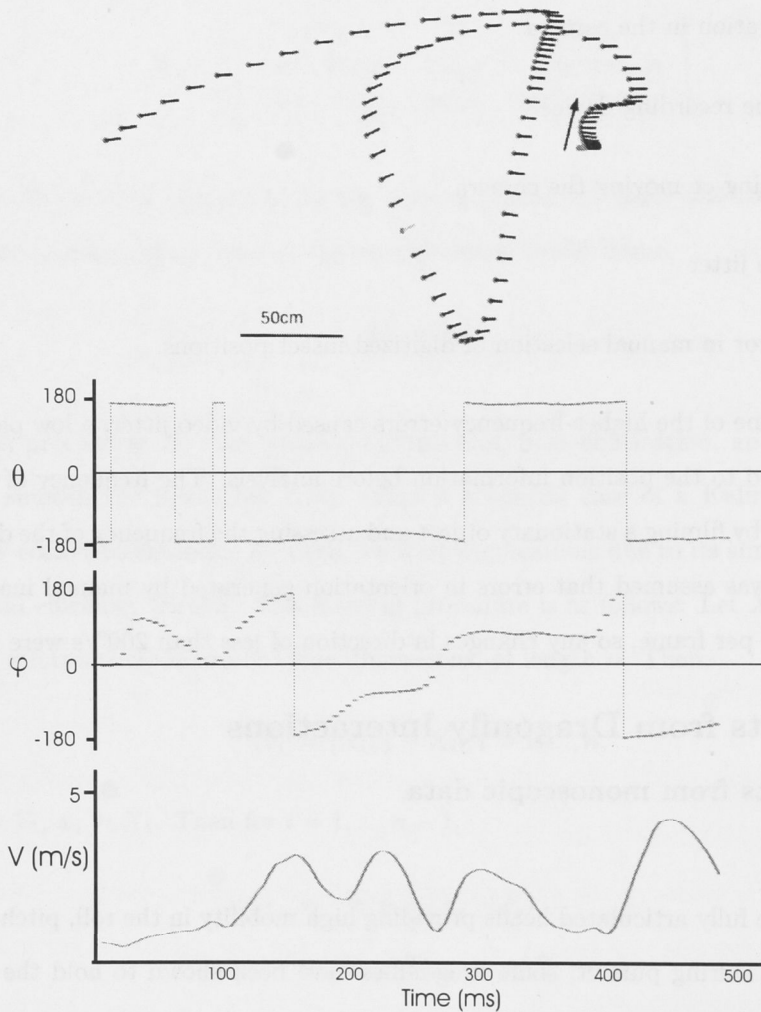


Figure 4.4: Lateral movement of *Hemicordulia tau*. Top: x-y position of a dragonfly every 20ms during a 0.5s flight. Note that the dragonfly can move both along and laterally to the body axis. Bottom: plots of longitudinal body axis angle, flight direction and the velocity in the direction of flight. Discontinuities in angular position caused by transferring from the negative to positive half of the unit circle are marked by a vertical line.

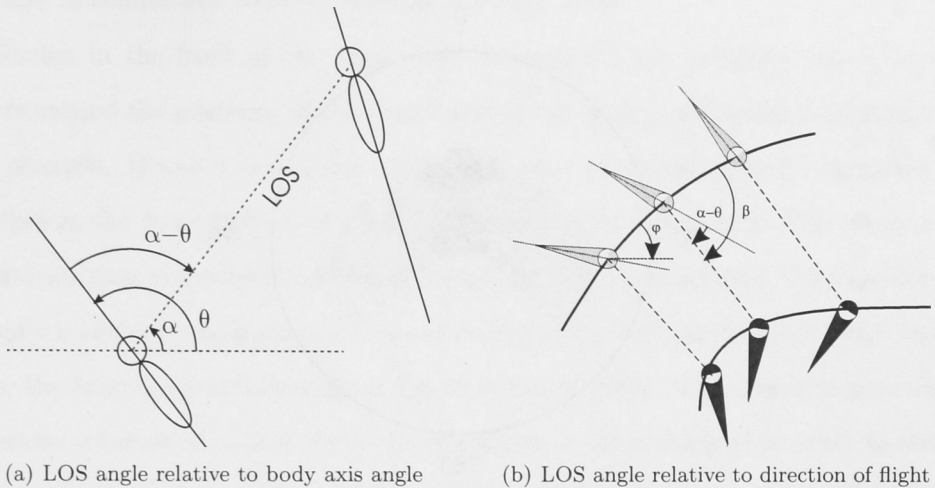


Figure 4.5: Actual retinal angular position and position if the body were aligned with the flight direction. Although head angle is still not accounted for, $\alpha - \theta$ is a far more accurate measure of angular target position than the approximation β . However the measure of LOS relative to the flight direction, r , is useful in determining the amount of fixation due to changes in body angle, compared to the amount occurring due to changes in flight direction.

4.5(a). The body orientation is derived from the three-dimensional reconstruction of the head and tail position, which can be used to determine body axis information.

Dragonflies also have the ability to move laterally without changing their longitudinal orientation, therefore changes in body orientation in response to changes in the line of sight angle are not necessary to enact a dynamic response to the movement. Such shifts may therefore indicate an attempt to fix the other participant in some particular retinal location. For example, Olberg et al [OWV00] found that the rolling component of the dragonfly *Leucorrhinia intacta*'s head movement in prey pursuit is such that the image of the prey is aligned along the midline of the dorsal acute zone of the eye.

Retinal position therefore may or may not be influenced by the chosen trajectory. The position due to the trajectory can be separated from that due to body orientation by considering the hypothetical retinal location of the pursued insect should the body axis be aligned with the flight direction for the entirety of the interaction.

Figure 4.4 shows the path generated by a single dragonfly filmed from overhead - note how it frequently moves laterally for significant portions of its flight. This lateral movement may be due to manipulation of gravity and wing-beat forces, the dragonfly producing a sideways thrust by rolling, in the same way as that described for an automated craft

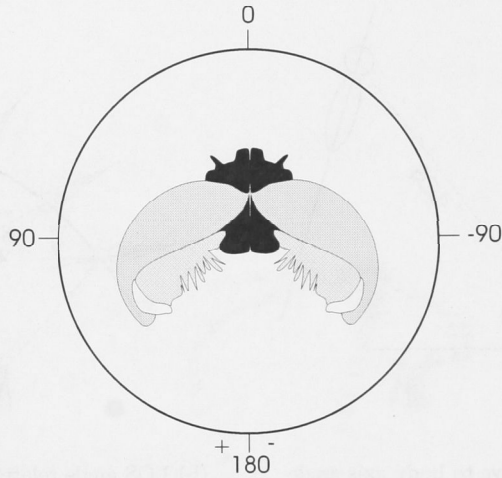


Figure 4.6: Retinal position, in degrees. The angles move from positive to negative in a counter-clockwise direction.

in Chapter 3. Alternatively, if no roll along the longitudinal axis is present, sideways thrust may be generated by asymmetry in the wing-beat pattern [R89]. To distinguish which mechanism predominates (for they are not mutually exclusive), higher resolution footage would be needed. Nevertheless, we can discern that the insect's body axis direction remains reasonably constant throughout the flight. In this study, we wish to examine this axis orientation when another dragonfly is in close proximity.

Figure 4.5(b) demonstrates the difference between the body axis angle and the course angle. $\alpha - \theta$ is the angle between the LOS and the body axis angle, β is the LOS angle relative to the flight direction. I define the angle of flight at time t as being the direction of the tangent vector to the trajectory at time t . This tangent is approximated in the discrete-time analysis by the vector between the head positions of the dragonflies in question at sequential time intervals. Figure 4.6 describes the orientation of the the co-ordinate system used in the results. The longitudinal axis is chosen as the 0/180 line, where 0 is directly in front of the insect at the anterior visual position, and ± 180 is directly behind. As in the conventional Euclidean unit circle, the positive direction of rotation is counter-clockwise.

Figure 4.7 shows histograms of the retinal position of one dragonfly as seen by the other for eight typical trajectories. Compare the actual retinal position $\alpha - \theta$ with that which would occur were the pursuing insect aligned with its direction of flight, β . Overall, the eccentricity (error angle) of the leading fly on the tracking fly's retina is fairly large,

especially in comparison to other tracking insects [CL75].

Clusters in the front of the visual field (around 0°) are generally concurrent with clusters around the posterior of the visual field of the other participant, indicating a true chase scenario. However this is not always the case - on occasion, both dragonflies have the other in the front portion of their visual field, as in Figure 4.7C. The clusters in β demonstrate that even when body orientation is not taken into account, the trajectory of a dragonfly is such that an opponent tends to be placed centrally in the visual field. In other words, the target is positioned along the direction of flight. The disparity between the histograms demonstrates that the body orientation is often changed in order to increase this anterior placement, and we can say that at least some degree of visual fixation is occurring. (For comparison, see the satellite fly fixation results in section 4.5).

Visual Tracking of a moving target - control of body axis orientation

We attempt first to quantify the visual tracking mechanism being used by a pursuing dragonfly. Note that angular tracking can be summarized by the expression

$$\dot{\theta} = k(\alpha - \theta) \quad (4.9)$$

where k is a gain constant [Col80a].

The complexity of the flight patterns observed complicated the analysis significantly. Body axis angle was frequently unresolvable when the insects were filmed from the side, as the dragonflies would often orient along the camera axis. However filming from above had its own problems - the dragonflies would often cross paths above or below each other in the vertical plane. Combined with the low frame rate used when filming from this direction, this meant care had to be taken not to inadvertently 'swap' the dragonflies during one of these cross-overs. Moreover, a third factor could complicate the analysis even when neither of the error sources were present - the roles of 'target' and 'pursuer' were not always well-defined during a sequence. The dragonflies would frequently swap the roles of pursuer and target¹, making it much more difficult to extract reaction delays, for example, as which insect was initiating and which was reacting would change, sometimes more than once. As

¹Perhaps when considering dragonfly conspecific interactions, especially those between males, 'initiator' and 'reactor' are more appropriate terminologies, especially since capture of the 'target' does not appear to be a goal of the pursuer.

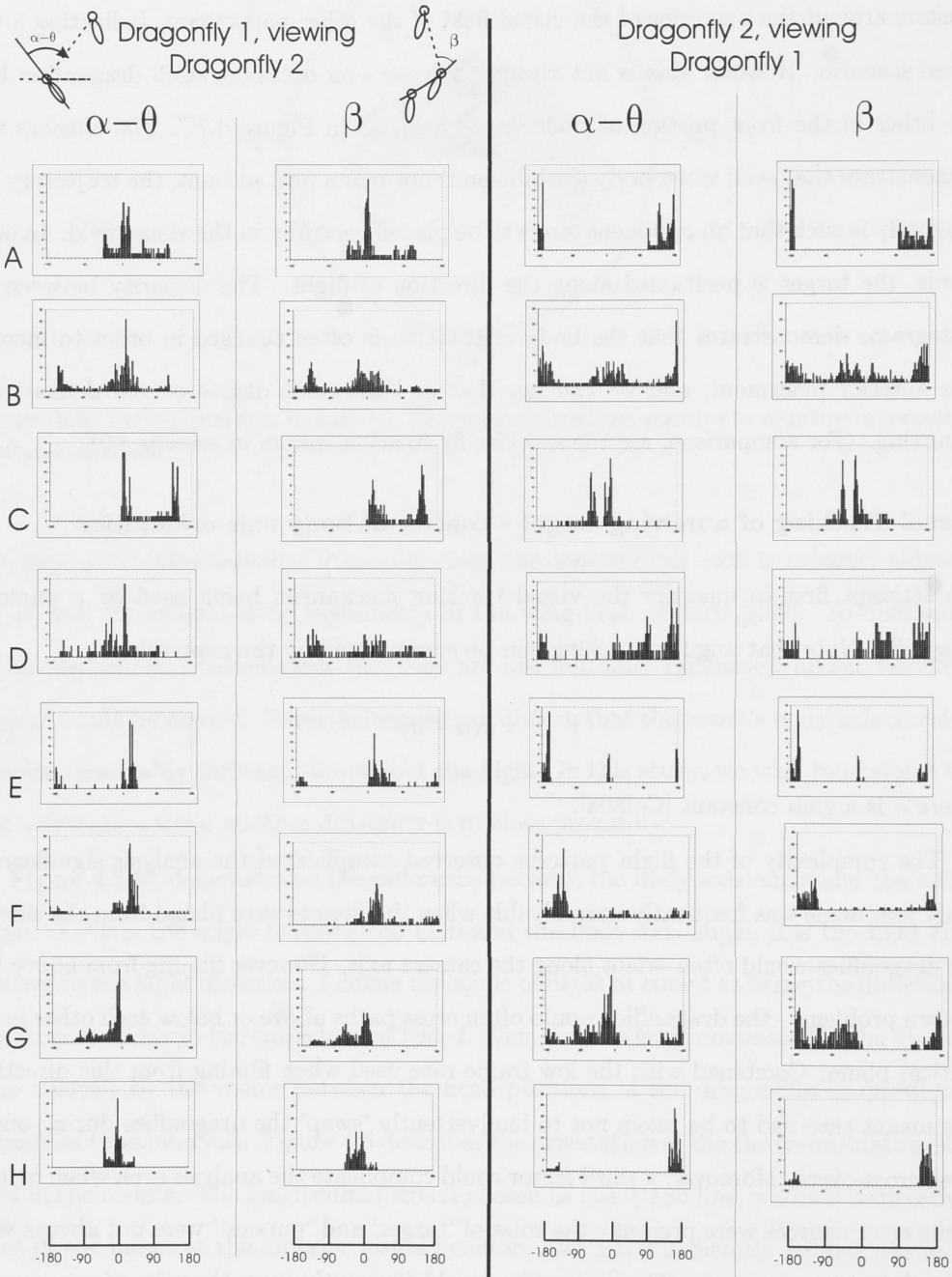


Figure 4.7: 2D data: Line-of-sight retinal position, compared with the position if the body were aligned with the flight angle, for both dragonflies in eight two-body trajectories. At least one participant, and occasionally both, maintain a degree of anterior fixation in all examples.

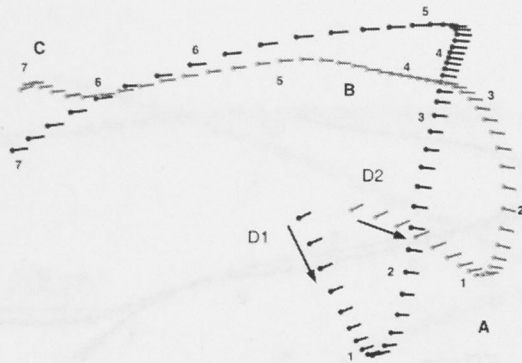


Figure 4.8: An example of pursuer and target swapping roles partway through a pursuit. Numerals mark every 200ms. At point A, D2 is tracking D1. By point B, D1 has become the pursuer (reactor), but then around point C, we observe D2 once again becoming the reactor (rather than the initiator).

a consequence, trajectories where body axis information was not available for more than one or two frames, where the pursuer and target were not visibly distinguishable for the entire period, or where the roles of the pursuer and target were swapped were not included in the analysis.

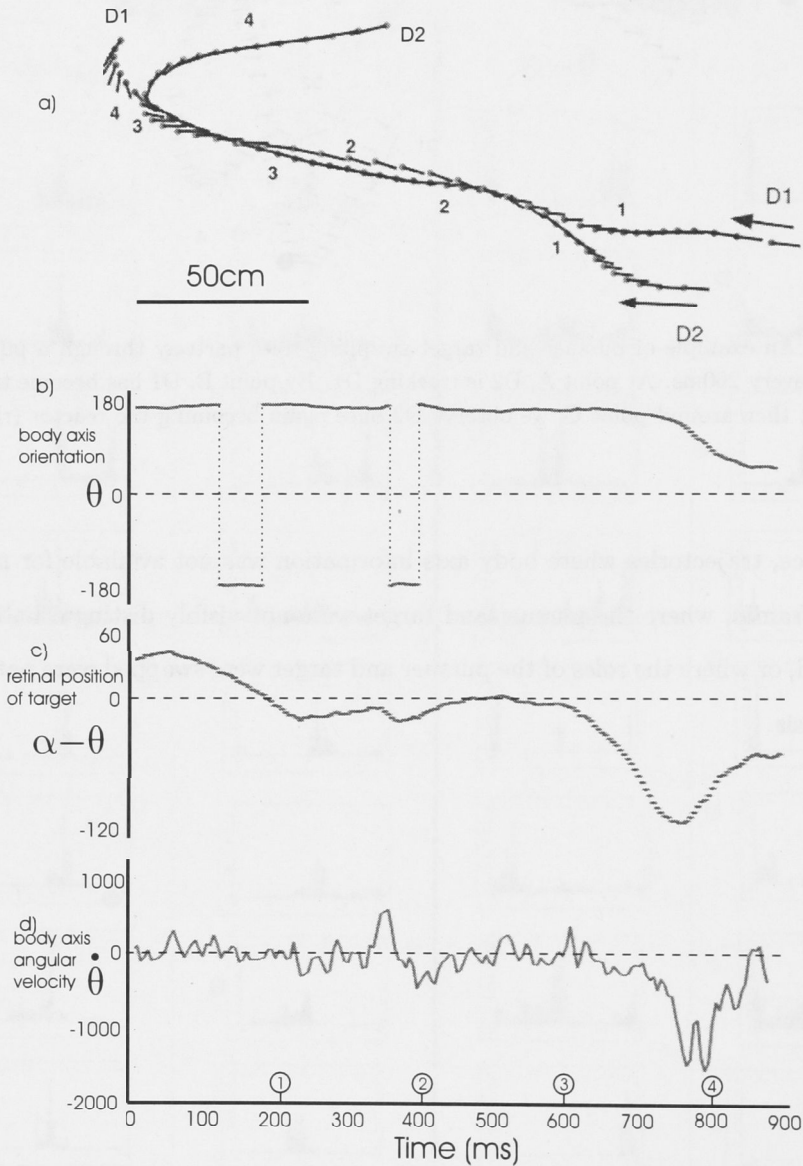


Figure 4.9: (a) Flight trajectory of a two-dragonfly chase, filmed from the side. The head of the dragonfly is marked by solid dots, the bodies by lines along the longitudinal axis. Numerals mark every 200ms. For clarity, the insect positions are shown only every 20ms, although the recording framerate was 200fps. (b) Longitudinal body axis angle (θ) for the pursuer, D1, in degrees. (c) Line-of-sight error angle ($\alpha - \theta$) for D1, in degrees. (d) Body axis angular rate ($\dot{\theta}$) for D1, in degrees per second.

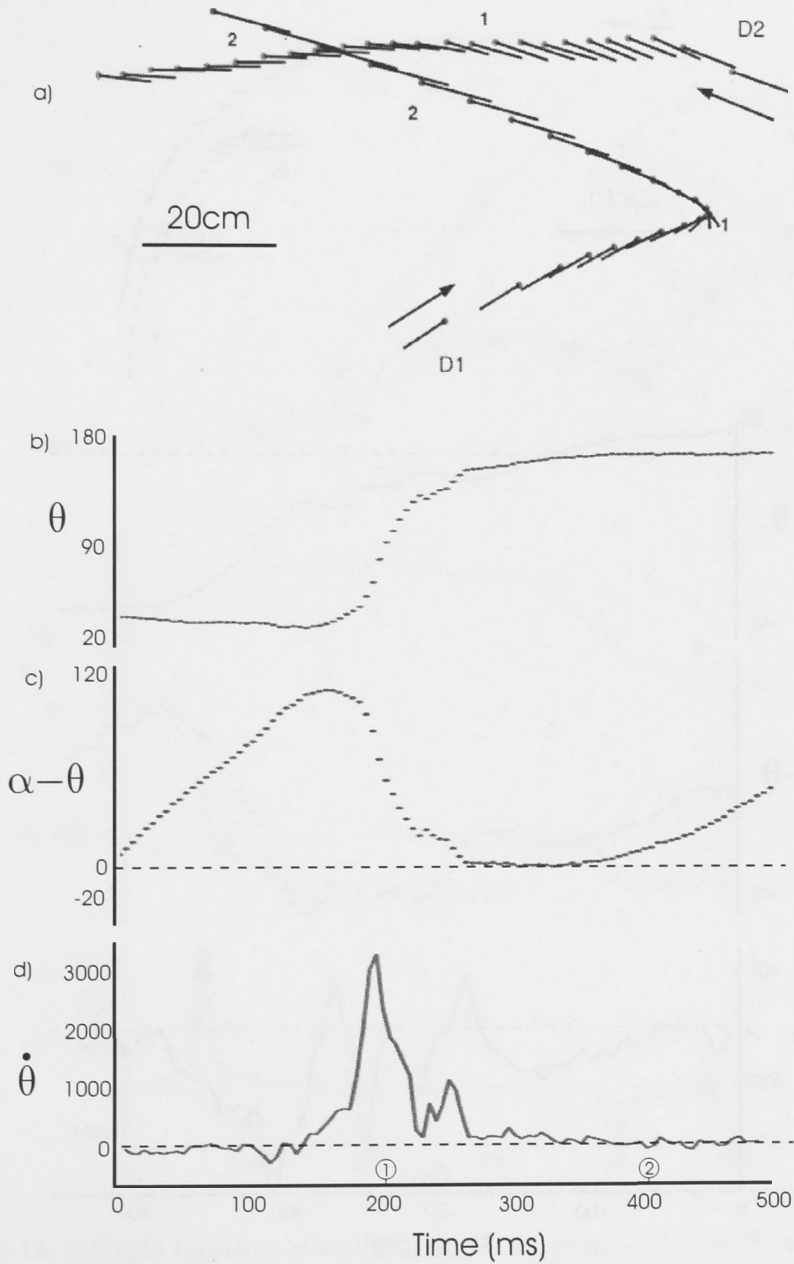


Figure 4.10: Filmed from the side: (a) Flight trajectory. As before, numerals mark every 200ms and the insect positions are shown every 20ms. Interestingly, D1 makes no correction to its body axis orientation until the line of sight error angle is quite large ($\geq 90^\circ$). (b) Longitudinal body axis angle of D1 (θ), in degrees. (c) Line-of-sight error angle of D1 ($\alpha - \theta$), in degrees. (d) Body axis angular rate of D1 ($\dot{\theta}$), in degrees per second.

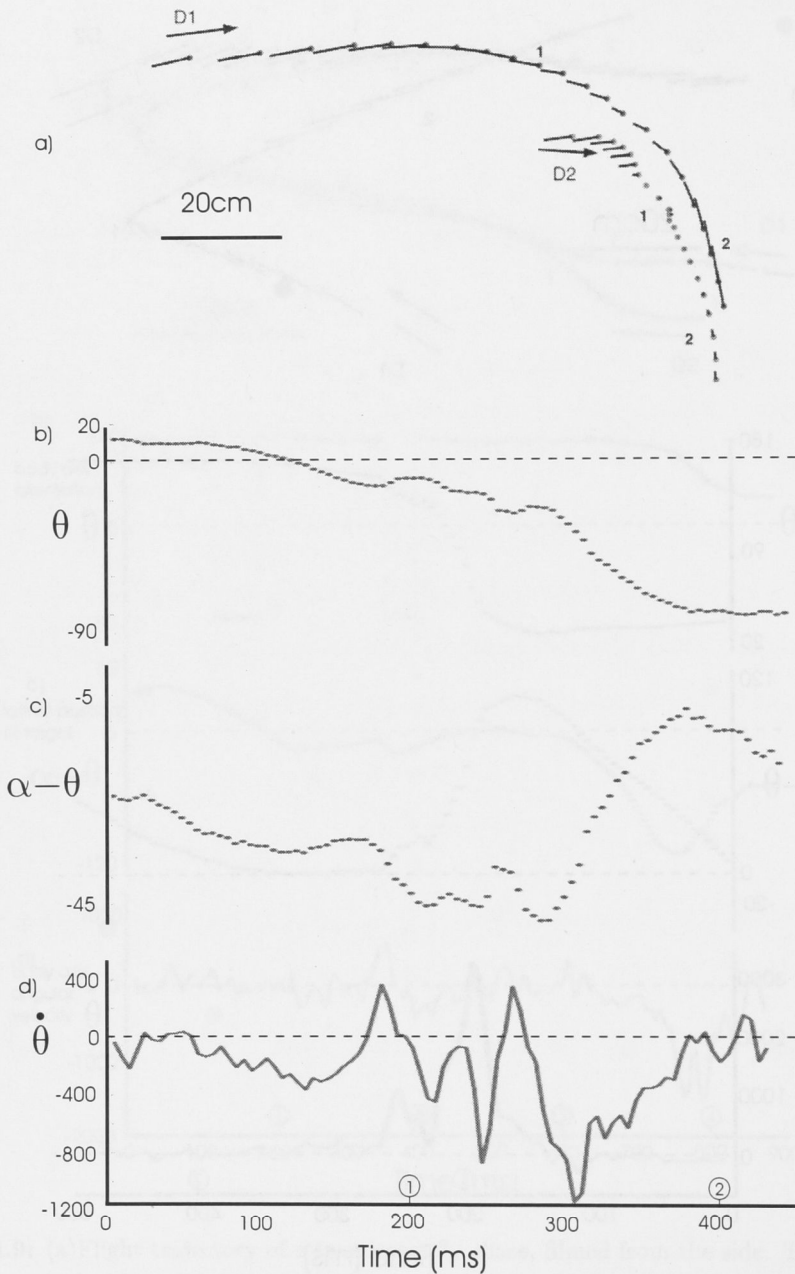


Figure 4.11: Filmed from the side: (a) Flight trajectory for both dragonflies. As before, numerals mark every 200ms and the insect positions are shown every 20ms. (b) Longitudinal body axis angle in D1 (θ), in degrees. (c) Line-of-sight error angle of D1 ($\alpha - \theta$), in degrees. (d) Body axis angular rate of D1 ($\dot{\theta}$), in degrees per second.

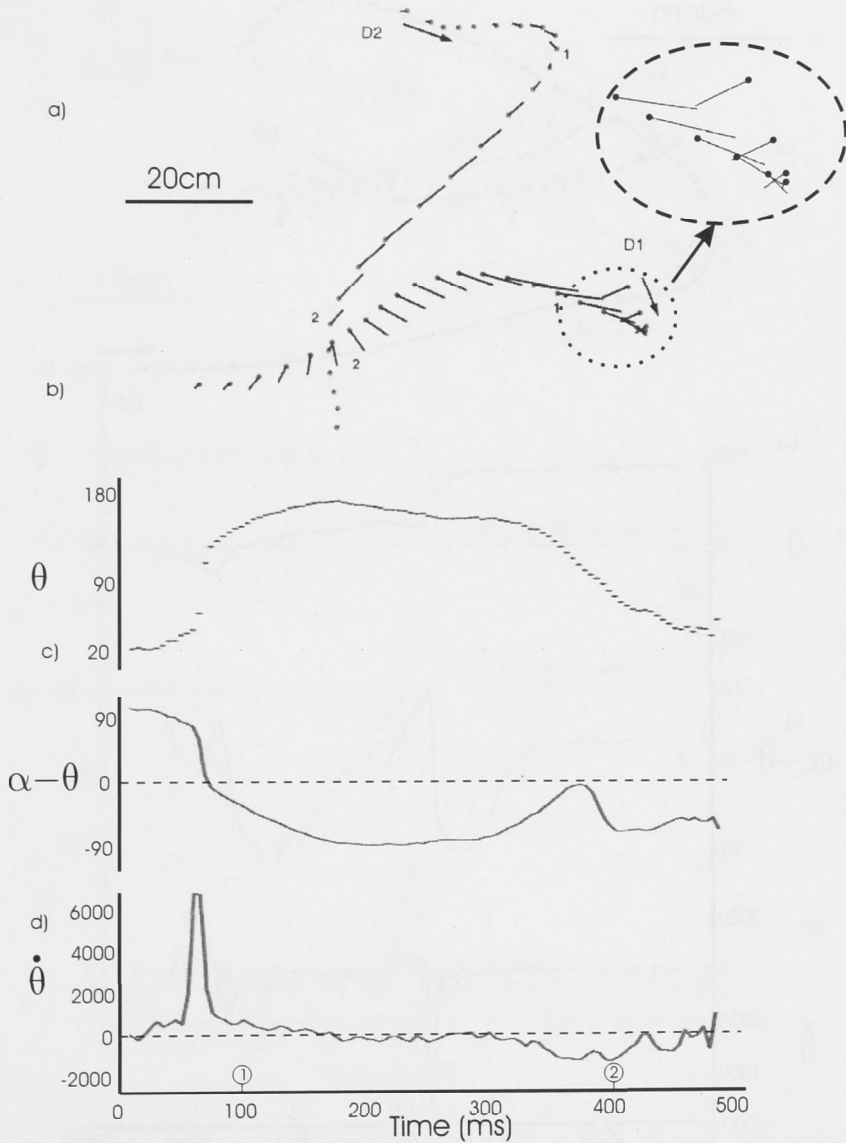


Figure 4.12: (a) Flight trajectory of both dragonflies, filmed from the side. As before, numerals mark every 200ms and the insect positions are shown every 20ms. (b) Longitudinal body axis angle of D1 (θ), in degrees. (c) Line-of-sight error angle of D1 ($\alpha - \theta$), in degrees. (d) Body axis angular rate of D1 ($\dot{\theta}$), in degrees per second.

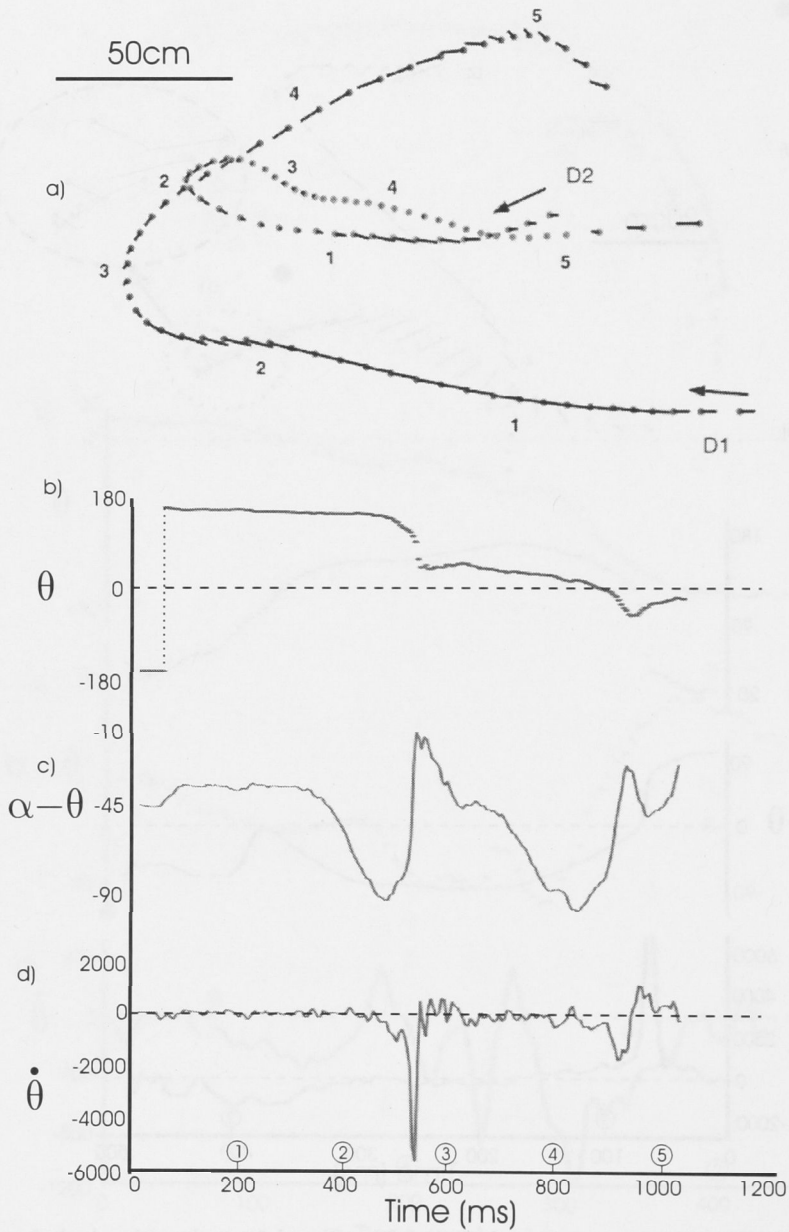


Figure 4.13: Filmed from the side: (a) Flight trajectory of both dragonflies. As before, numerals mark every 200ms and the insect positions are shown every 20ms. (b) Longitudinal body axis angle of D1 (θ), in degrees. Dotted vertical lines mark the discontinuity as the angle switches from negative to positive. (c) Line-of-sight error angle of D1 ($\alpha - \theta$), in degrees. (d) Body axis angular rate of D1 ($\dot{\theta}$), in degrees per second.

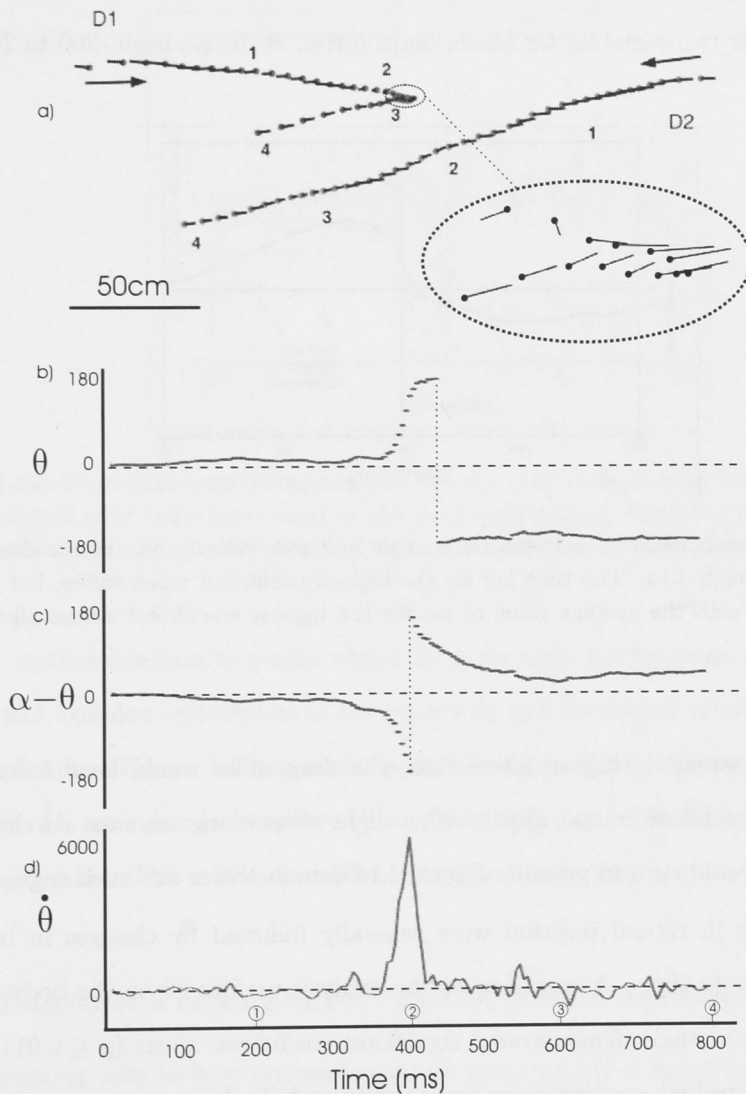


Figure 4.14: (a) Flight trajectory of both dragonflies, filmed from the side. As before, numerals mark every 200ms and the insect positions are shown every 20ms. The pursuing dragonfly (D1) initially is on a collision course with the target, which changes to a pursuit as the target position moves across the retina. The inset gives an exploded view of the turn made by the pursuer at about 400ms. (b) Longitudinal body axis angle of D1 (θ), in degrees. Dotted vertical lines mark the discontinuity as the angle switches from negative to positive. (c) Line-of-sight error angle of D1 ($\alpha - \theta$), in degrees. (d) Body axis angular rate of D1 ($\dot{\theta}$), in degrees per second.

The analysis was therefore restricted to several longer sequences which demonstrated as few of the problems described above as possible. Figures 4.9 - 4.14 show these sequences, the body axis angle of the pursuing dragonfly over the length of the interaction, the LOS error angle and the body angular velocity. Figure 4.15 shows the correlation coefficients between the latter two variables for all six trajectories, at delays from -200 to 200ms.

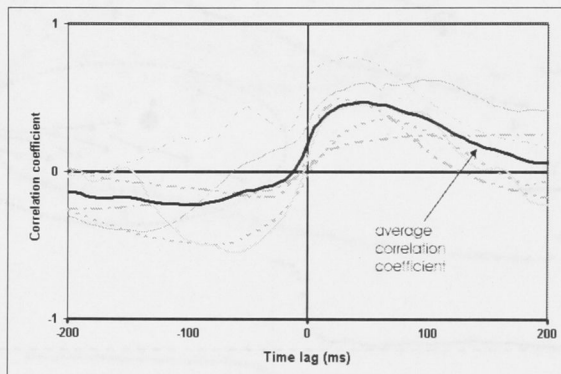


Figure 4.15: Cross-correlation between error angle and yaw velocity for the six chases shown in Figures 4.9 through 4.14. The time lag for the highest coefficient value varies, but is usually between 30-40ms, with the average value of lag for the highest co-efficient across all six chases being 35ms.

On many occasions during an interaction, the dragonflies would head towards each other on almost a collision course, albeit with a slight offset along one axis. As they passed each other, one would turn in pursuit. Figure 4.14 demonstrates one such engagement.

Large changes in retinal position were generally followed by changes in body axis orientation within 30-40ms. A cross-correlation analysis performed on the body axis rate and the line-of-sight angle demonstrated significant coefficient values ($p \leq 0.01$) at these delays. The LOS retinal position error was usually stabilized to some value, though not always at 0° , by changes in the yaw velocity of the pursuing insect. Hence it is likely that the angular velocity of the body axis of the pursuing dragonfly is governed at least partially by the position of the target on the retina.

However, given the large spread of eccentricity, can this alone be governing the body axis angle? Changes in the flight direction of chasing muscid flies [LC74] have a yaw velocity directed by both angular position and angular velocity. It could be that this, too, is a second order system. Cross-correlations between pursuer body axis velocity and error

angle velocity of the target were dominated by the negative correlation due to error angle changes caused by body axis changes, however the maximum positive correlation was in some interactions found at a delay of around 40-50ms (Figure 4.16).

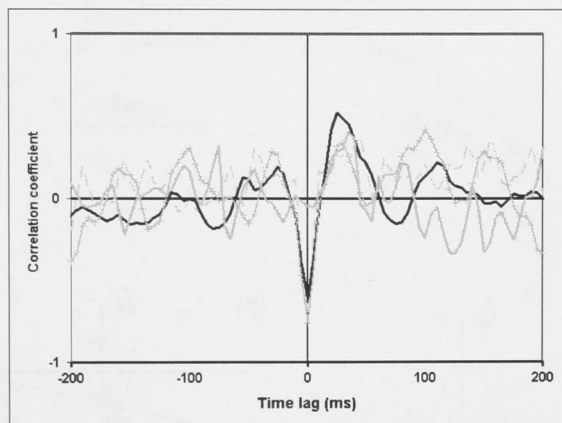


Figure 4.16: Error angle rate influencing yaw velocity. The strongly negative peak at 0ms is due to the change in error angle rate caused by the body itself turning. For many chases, there seemed to be a positive correlation peak between these variables at around 40ms delay.

If we restrict the data to points where the error angle lies between -30 and 30 degrees [Lan97] and examine scatterplots of the error rate and rotational velocity of the body at a delay of 40ms (Figure 4.17), a slight positive relationship is observed. This could be indicative of a second-order response that is only triggered when the error angle is below a threshold value. This is not dissimilar to the first-order response observed in hoverflies [CL75].

Visual Pursuit of a moving target - control of flight direction

Visual tracking tells us how dragonflies might govern their orientation, but as shown in Figure 4.4, it may reveal little of the policy controlling the flight direction of the insect.

Again, several sequences with clear view of body axis direction for the pursuing dragonfly were analyzed, this time examining the change in flight direction to changes in line-of-sight and line-of-sight velocity. The trajectories and traces are shown in Figures 4.18 to 4.21.

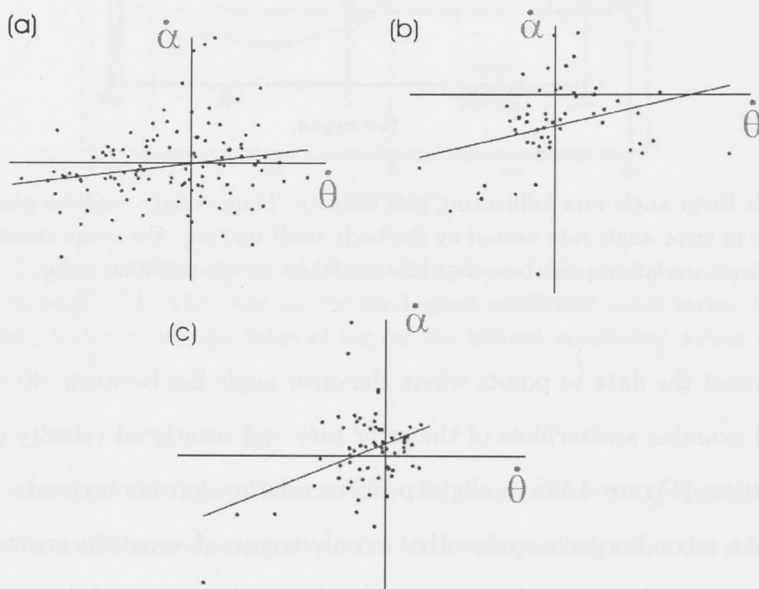


Figure 4.17: Scatter diagrams showing LOS velocity and body axis angular velocity for the paths illustrated in Figures 4.9, 4.11 and 4.14, showing only those points for which the error angle ($\alpha - \theta$) lay between -30° and 30° . A linear line of best fit has been included on each graph.

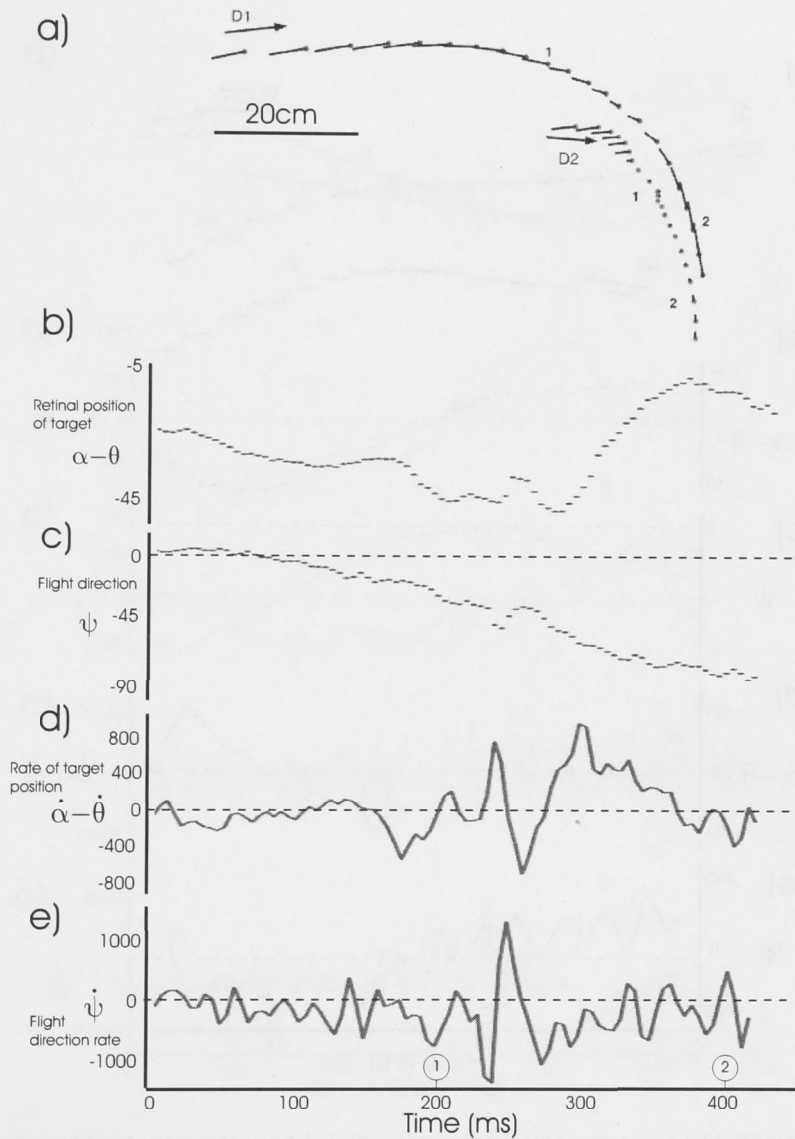


Figure 4.18: (a) Flight trajectory of two dragonflies, filmed from the side. As before, numerals mark every 200ms and the insect positions are shown every 20ms. (b) Line-of-sight error angle for D1 viewing D2 ($\alpha - \theta$), in degrees. (c) Flight direction for D1 (ψ) in degrees. (d) Line-of-sight error angle rate for D1 ($\dot{\alpha} - \dot{\theta}$), degrees per second. (e) Flight direction rate for D1 viewing D2 ($\dot{\psi}$), degrees per second.

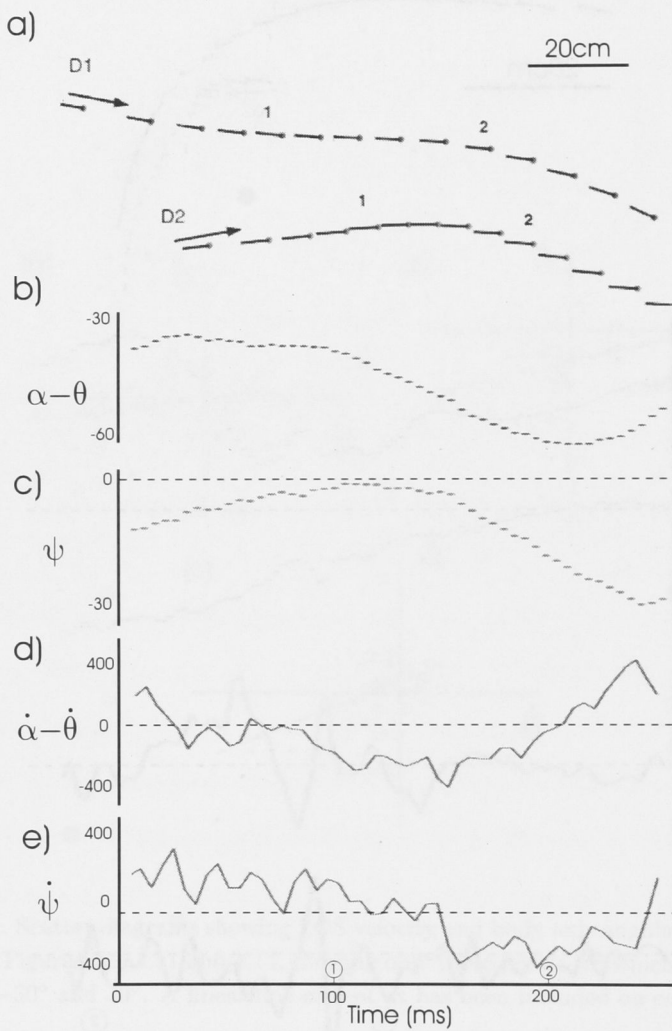


Figure 4.19: (a) Flight trajectory of two dragonflies, filmed from the side. In this case, numerals mark every 100ms though the insect positions are still shown every 20ms. (b) Line-of-sight error angle ($\alpha - \theta$), in degrees. (c) Flight direction (ψ) in degrees. (d) Line-of-sight error angle rate ($\dot{\alpha} - \dot{\theta}$), degrees per second. (e) Flight direction rate ($\dot{\psi}$), degrees per second.

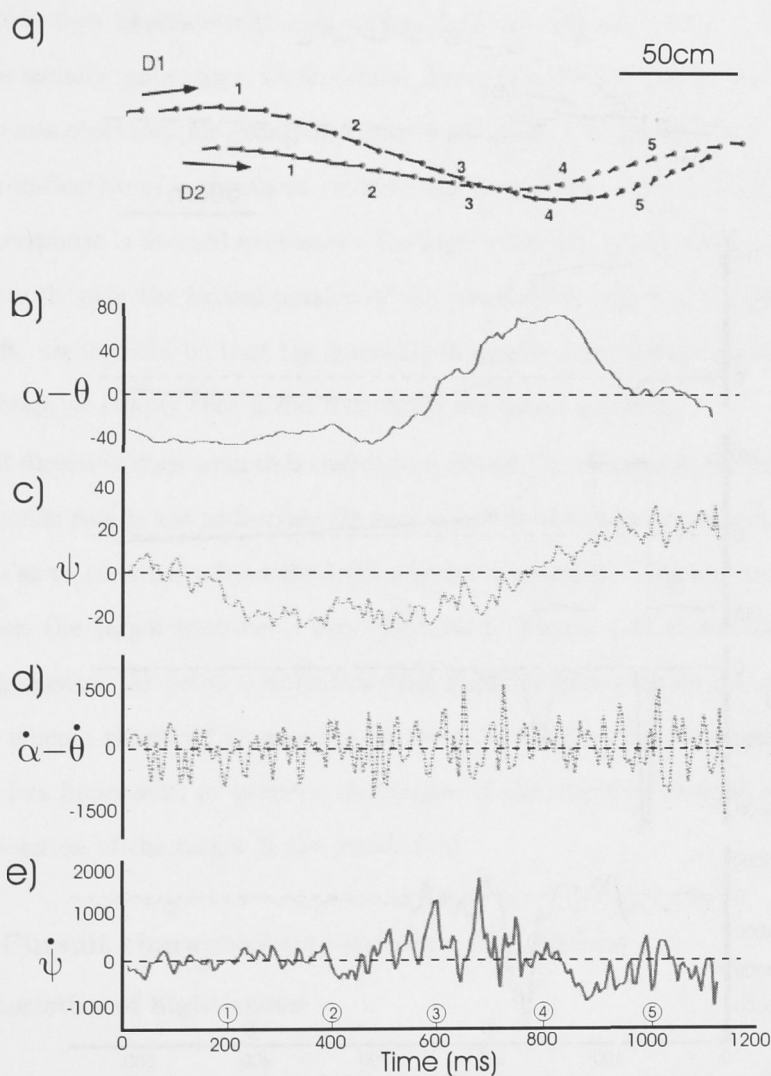


Figure 4.20: (a) Flight trajectory of two dragonflies, filmed from the side. As before, numerals mark every 200ms and the insect positions are shown every 20ms. (b) Line-of-sight error angle for D1 viewing D2 ($\alpha - \theta$), in degrees. (c) Flight direction of D1 (ψ) in degrees. (d) Line-of-sight error angle rate for D1 viewing D2 ($\dot{\alpha} - \dot{\theta}$), degrees per second. (e) Flight direction rate of D1 ($\dot{\psi}$), degrees per second.

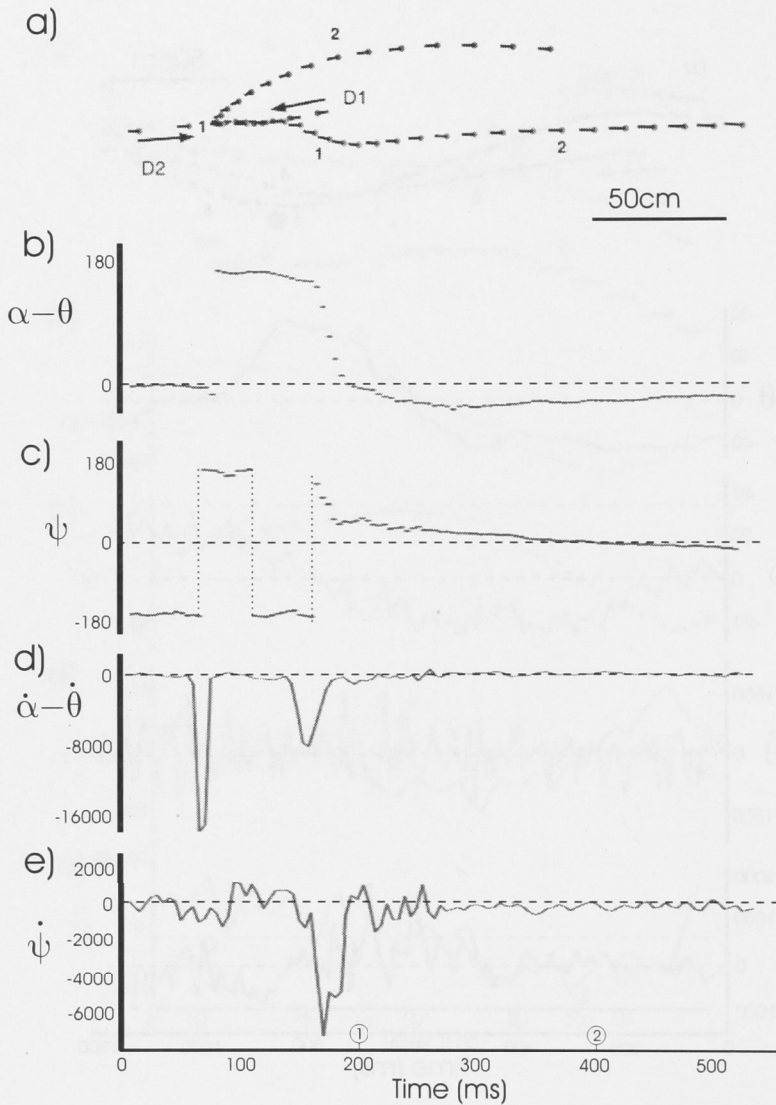


Figure 4.21: (a) Flight trajectory of two dragonflies, filmed from the side. As before, numerals mark every 200ms and the insect positions are shown every 20ms. (b) Line-of-sight error angle for D1, viewing D2, ($\alpha - \theta$), in degrees. (c) Flight direction of D1 (ψ) in degrees. (d) Line-of-sight error angle rate for D1 viewing D2 ($\dot{\alpha} - \dot{\theta}$), degrees per second. (e) Flight direction rate of D1 ($\dot{\psi}$), degrees per second.

Changes in flight direction generally had the effect of stabilizing the line of sight error angle, although not necessarily to zero. Looking at the first derivatives of the variables, in order to eliminate offset in the eccentricity, we see a correspondence between error angle velocity and the flight angular velocity. The correlation coefficients for the latter variables in the above four figures reveal a significant peak at delays of 5-30ms, (Figure 4.23). The delay was usually quite short, within about 15ms, however on occasion a large delay of up to 100ms was observed (for example, Figure 4.21). Figure 4.22 shows one such flight. This could be indicative of a threshold on the angular position offset tolerated by the insect before a response is deemed necessary - the flight direction is not changed until the target is significantly past the frontal portion of the visual field, and then the responsive turn is very swift. Or it could be that the pursuing dragonfly was responding to more than one moving body, or simply that it did not notice the target initially.

Flight direction does seem to be influenced directly by changes in the line of sight angle. However, this rule is not universal. On rare occasion the pursuer will actually change its course so as to turn *away* from the LOS angular movement. This appears to occur more often when the target executes a very tight turn. Figure 4.24 shows some examples of this phenomenon. As yet it is unknown what might inspire such an inverted response. It could be when a threshold is exceeded on the LOS velocity, the direction of the response becomes less important, or perhaps the nature of the response changes according to the general position of the target in the visual field.

4.4.2 Pursuit characteristics in three dimensions

Characteristics of flight speed

The footage gleaned from stereo filming was unfortunately too low in resolution to consistently identify the body axis orientation of the dragonflies. However, using stereo information we can gather a more accurate assessment of variables such as range, range-rate and forward speed of both insects. Hence we can attempt to unravel some of the cues governing the forward velocity of a dragonfly during pursuit.

Range to the target and apparent target size have been observed to impact the flight speed of pursuing insects [OWV00], [BKE03]. The angle subtended by a target insect on the pursuers retina is one of the simplest visual range cues available to insects. Other

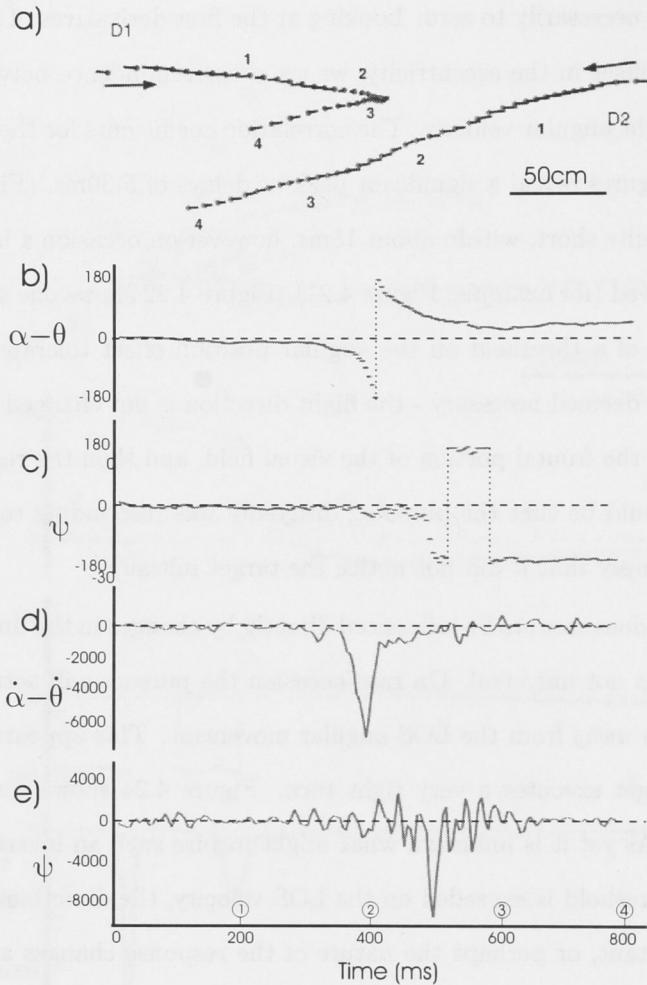


Figure 4.22: Example of significant lag between a change in LOS angular velocity and a corresponding change in flight direction

means of measuring range using visual cues do exist [Hor86], but their contribution to the task of range estimation by dragonflies is not yet known. So instead we examine the relationship between range and forward speed, without concerning ourselves with how the range information is extracted. Some three-dimensional trajectories and the corresponding traces for range and forward speed are shown in Figures 4.25 to 4.29.

In the flight sequences thus examined, an increase in range was generally marked by a corresponding decrease in responsive velocity. Some, perhaps all, manifestations of this inverse relationship may be explained phenomenologically. Looking at the flight direction, it can be seen that the local minima in forward speed generally correspond with changes

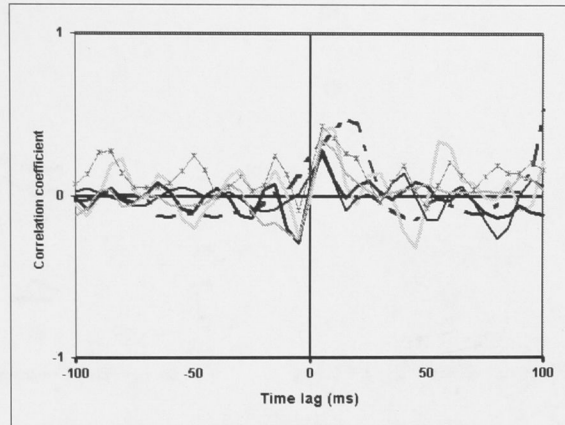


Figure 4.23: Cross-correlation between error angle velocity and flight angle velocity.

in flight direction. Olberg [OWV00] found evidence that the apparent size of a target will affect a pursuing dragonfly's response, so there is some likelihood that range or size measurements do play a part in driving the guidance system in use. However the data set used in this analysis is not sufficient to disambiguate such a response from the natural dynamics of a moving body.

The speed profiles of the pursuing dragonfly seen here are all qualitatively similar. The

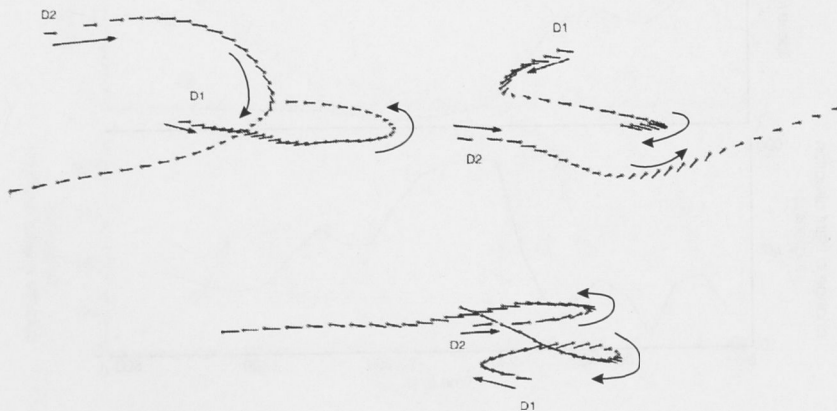


Figure 4.24: A few sequences demonstrated a strange behaviour by the pursuer, where a manoeuvre by the target was matched by a turning response counter to the direction of the LOS error motion.

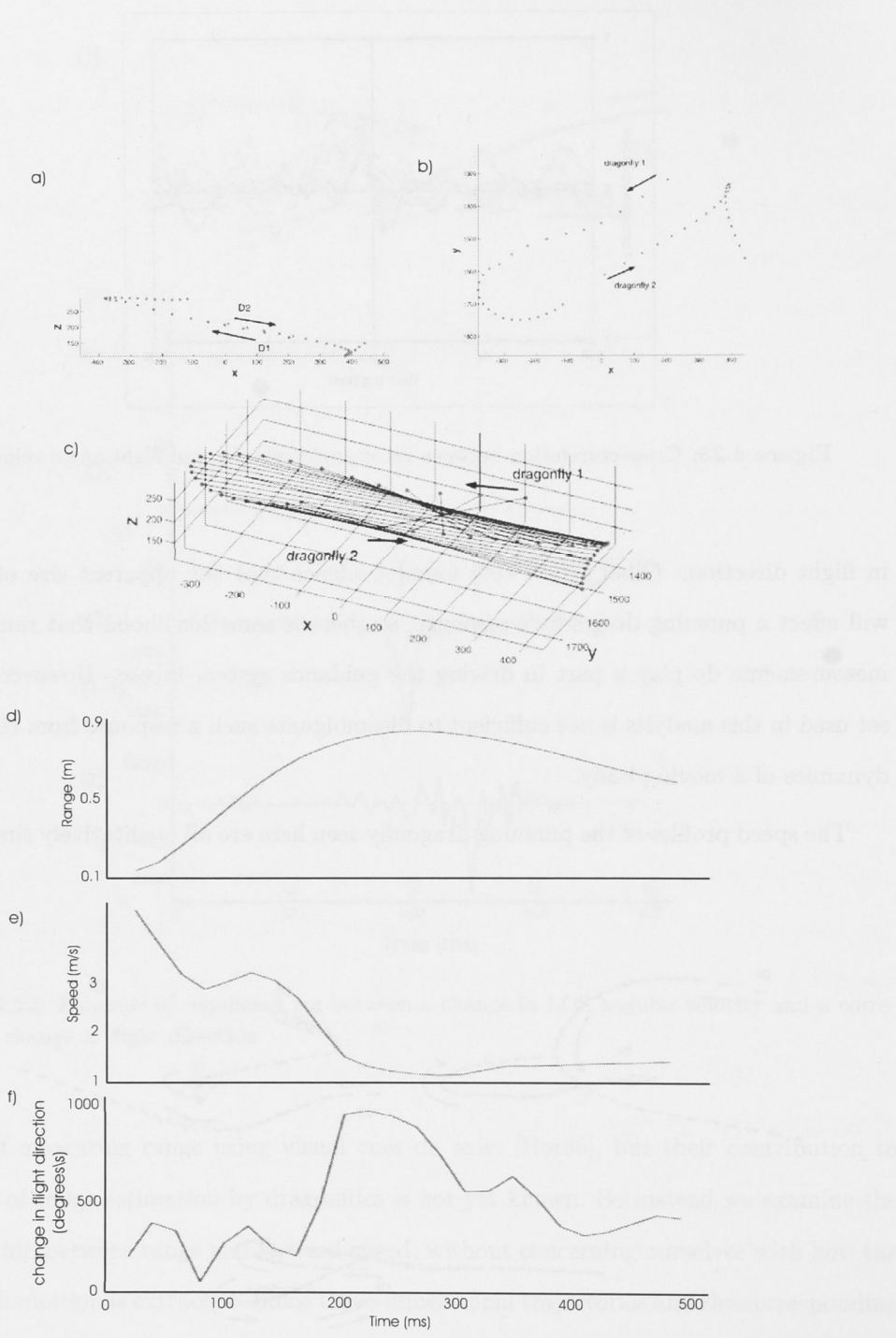


Figure 4.25: (a) Side view, (b) Top view, (c)3 dimensional chase, (d) Range (in m), (e) Forward speed (in m/s), (f) Change in flight direction, in degrees/s

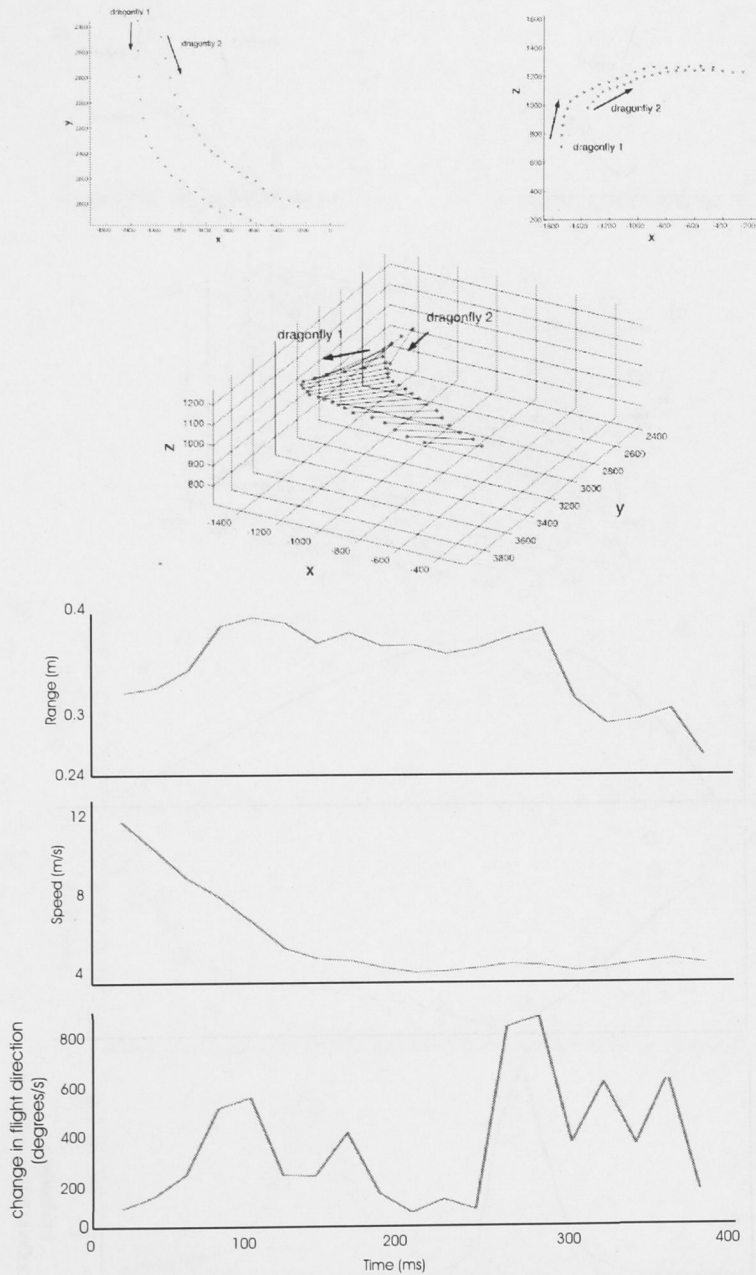


Figure 4.26: (a) Side view, (b) Top view, (c) 3 dimensional chase, (d) Range (in m), (e) Forward speed (in m/s), (f) Change in flight direction, in degrees/s

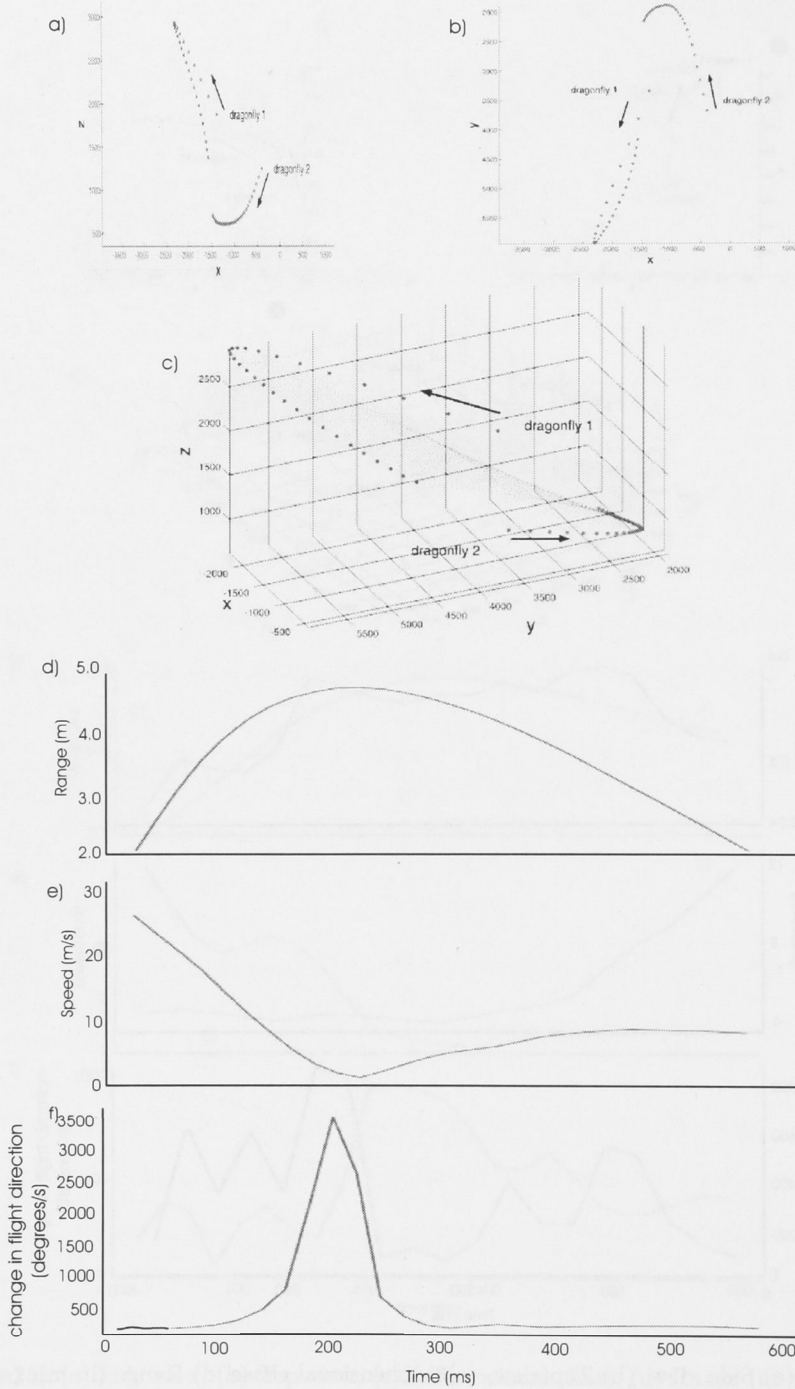


Figure 4.27: (a) Side view, (b) Top view, (c) 3 dimensional chase, (d) Range (in m), (e) Forward speed (in m/s), (f) Change in flight direction, in degrees/s

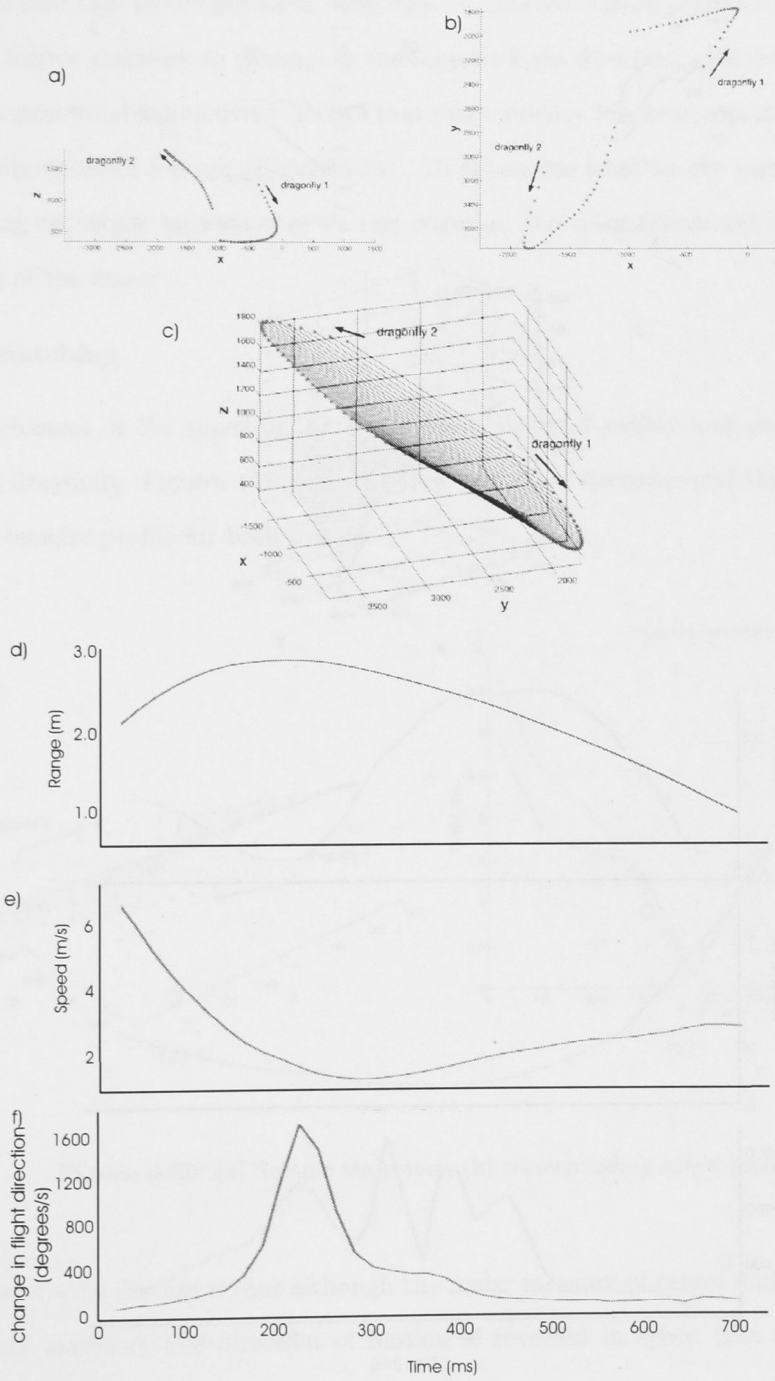


Figure 4.28: (a) Side view, (b) Top view, (c) 3 dimensional chase, (d) Range (in m), (e) Forward speed (in m/s), (f) Change in flight direction, in degrees/s

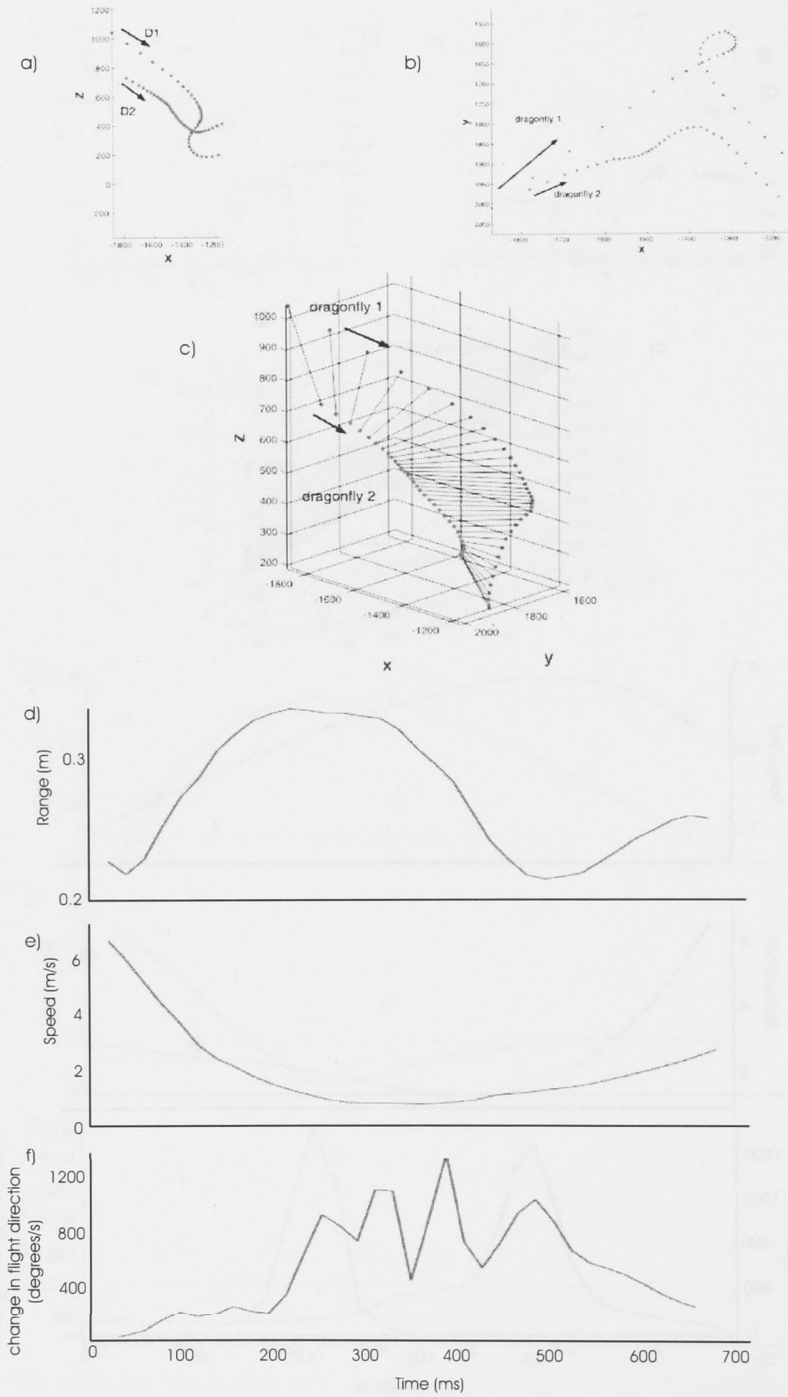


Figure 4.29: (a) Side view, (b) Top view, (c) 3 dimensional chase, (d) Range (in m), (e) Forward speed (in m/s), (f) Change in flight direction, in degrees/s

high-speed segments seems to occur when the insects move past each other in opposite but often parallel courses. The flight speed then decreases rapidly, corresponding with a change in direction of the pursuing dragonfly. A notable feature is that this change often seems to mirror response to changes in the target's flight direction, creating beautiful and almost symmetrical manoeuvres. Recall that this tendency was also sometimes observed in the two-dimensional footage (Figure 4.24). To determine whether the pursuer is actually responding to target manoeuvres, we can compare the total speed and change in flight direction of the insects.

Speed matching

Indeed, changes in the speed of the target were matched swiftly and accurately by the pursuing dragonfly. Figures 4.30 and 4.31 show sample trajectories and the corresponding forward velocity profile for both insects.

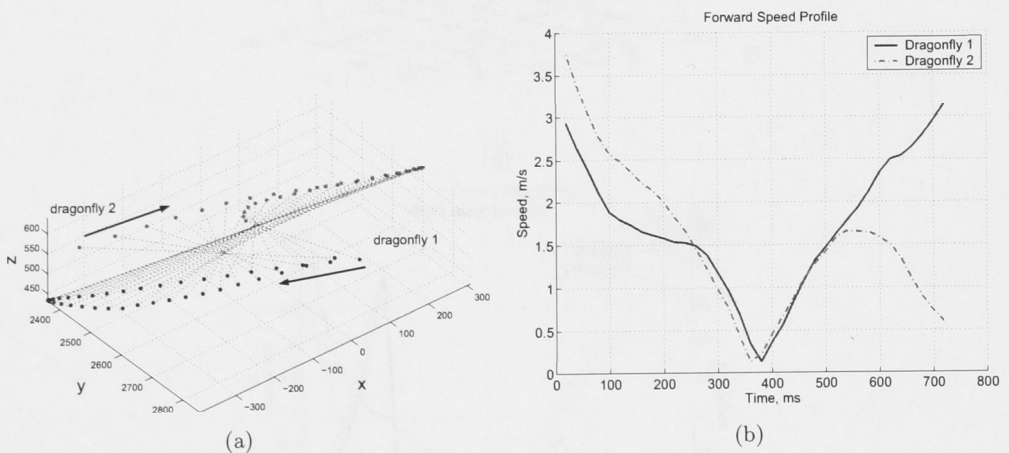
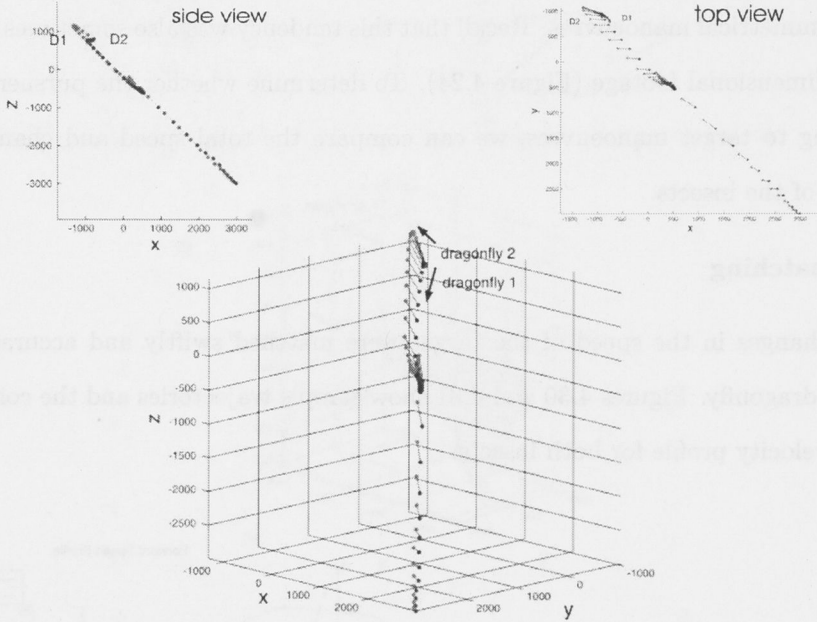


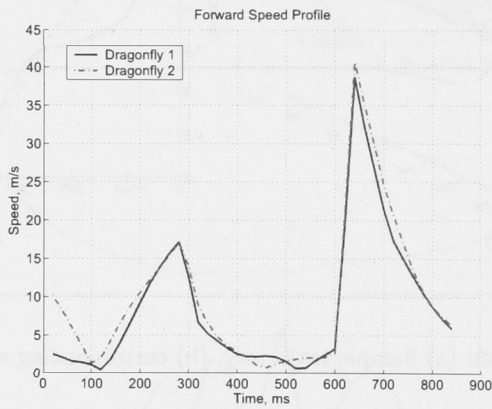
Figure 4.30: (a) Sample trajectory, (b) corresponding speed profiles

A noteworthy feature is that although the scalar measure of target and pursuer speeds are closely matched, the direction of motion is reversed in space (the mirroring effect alluded to earlier).

Moreover, the relative velocity between the insects tended to be small when compared to the forward speed of the target. Figure 4.33 shows the average relative speed between the pursuer and target corresponding to specific target speeds (incrementing in 10cm/s).



(a)



(b)

Figure 4.31: (a) Sample trajectory, (b) corresponding speed profiles

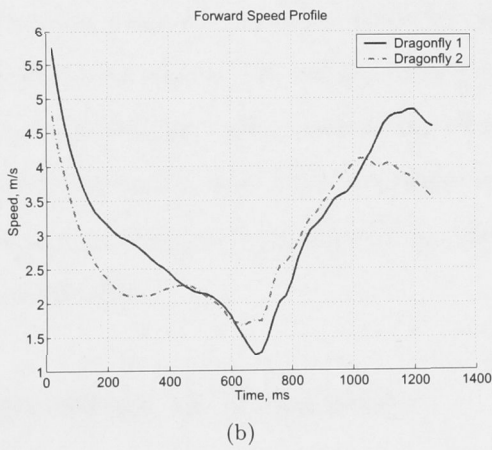
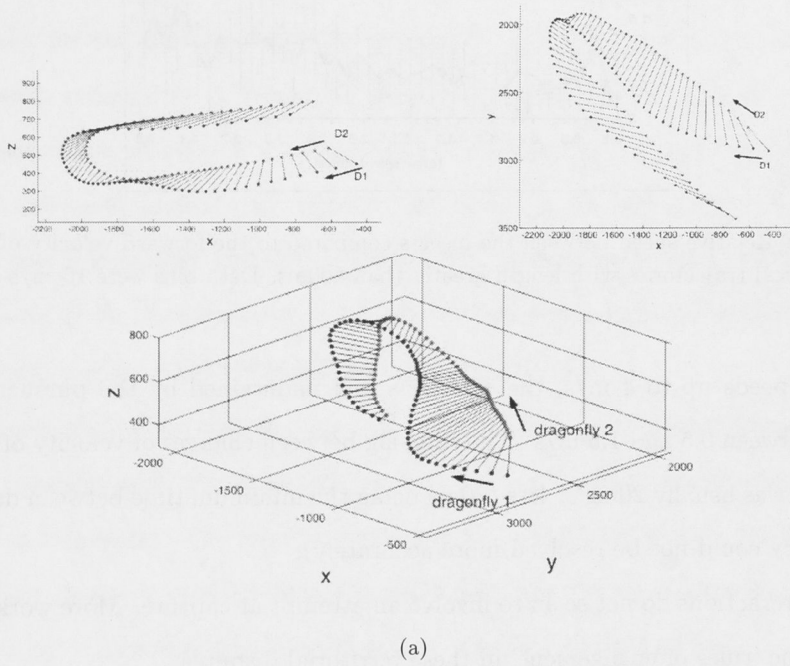


Figure 4.32: (a) Sample trajectory, (b) corresponding speed profiles

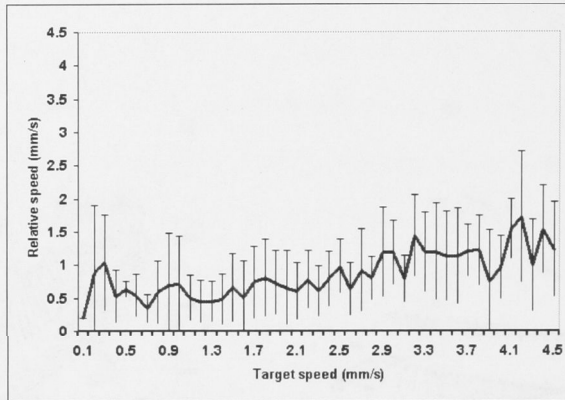


Figure 4.33: Relative speed between the insects compared to the forward velocity of the target, across 23 typical trajectories with length greater than 400ms. Data bins were 10cm/s in width.

For target speeds up to 4 m/s, the *relative* speed maintained by the pursuer generally remained between 0.5 and 1.5 m/s. The time lag between changes of velocity of the target and pursuer was usually 20ms or less (20ms being the minimum time between data points, so the latency could not be resolved more accurately).

These interactions do not seem to involve an attempt at capture. More work is needed to unravel the ‘rules of engagement’ in these territorial disputes.

4.5 Results from Satellite Flies

To assess the success of dragonfly fixation, we can compare the results from section 4.4.1 to similarly generated results for satellite flies (*Sarcophagidae miltogramminae*) stalking wasps (*Cerceris*) (Figure 4.34). Satellite fly/wasp interactions have the advantage of clearly defined roles for the participants. The satellite fly reacts to the behaviour of the wasp, and the wasp remains predominantly oblivious to the fly. This enables us to examine the dynamic characteristics of a system with similar parameters but reduced complexity, since only one participant is truly reactive. By studying the similarities and discrepancies between these interactions and that of dragonflies, we can make some observations about the additional levels of complexity added by multiple maneuverable, reactive bodies. Note that shadowing of wasps involves tracking, but not pursuit.

In satellite flies, if we compare the actual line of sight to that engendered if the flight direction coincides with the body axis, we perceive a far greater discrepancy between the two than in dragonflies. The implication is that the orientation change producing fixation of the target (wasp) is distinct from the flight direction chosen. Moreover, the degree of target fixation is significantly better than that observed in dragonflies.

The differences between the fixation behaviours of the two species suggests that the line-of-sight angle is important not only to the angular orientation of the dragonfly, but also to the course chosen while tracking, unlike satellite flies where changes in the line of sight angle impact the body orientation only. Ergo it is likely that in dragonflies, retinal position influences the pursuit system used to chase the target insect, but the same cannot necessarily be said for satellite flies..

4.6 Motion Camouflage in Dragonflies

Previous research has established the presence of instances of motion camouflage in hoverflies chasing mates [SD95], in dragonflies warding off encroaching males from their territory [MCS03], and in bats attempting to track prey by echolocation [Gho94]. It is yet to be determined whether these manifestations of the phenomena occur by design, or as an incidental byproduct of an overall, more conventional guidance strategy, or simply as a quirk of the geometry under certain dynamic conditions.

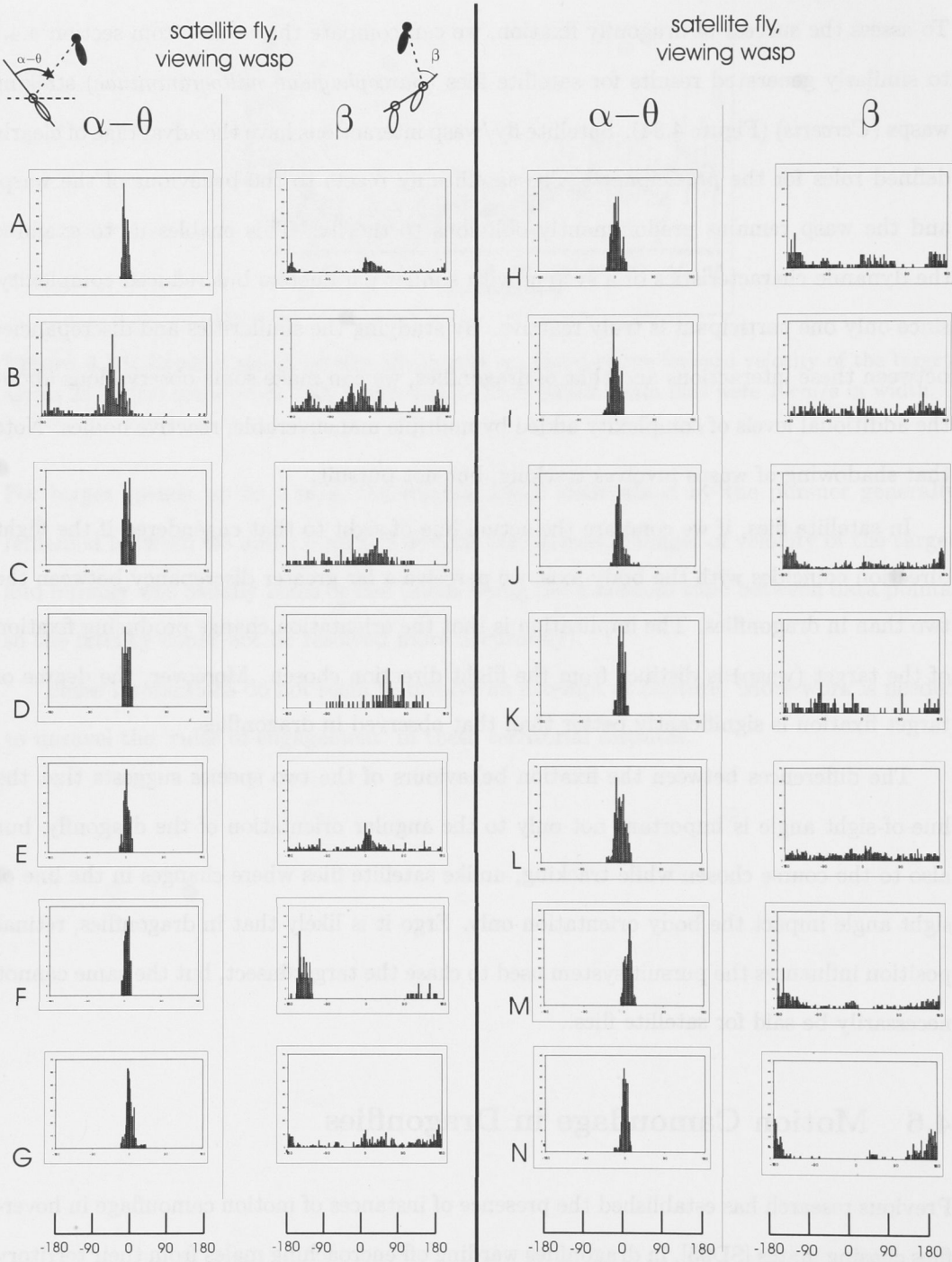


Figure 4.34: LOS retinal position with body orientation accounted for, compared with the retinal position when the body is assumed to be aligned with the flight direction, for fourteen separate satellite fly/wasp interactions

4.6.1 Method for determining camouflaged sequences

To identify instances of motion camouflage, a method is needed to monitor the apparent location of a pursuer from the point of view of the target. Figure 4.35 shows a sequence of two moving bodies and the lines of sight between them. P is the pursuer, T the target. Taking the initial positions, P_1 , T_1 , and the intersection point of the lines drawn between them, I_1 , as the start of a camouflaged encounter, the following positions at discrete time intervals were examined relative to the initial condition. For a camouflaged trajectory, the intersection point of the lines-of-sight defines the static point of that trajectory, and thus the apparent location of the pursuing insect. Assuming an image on an insect eye cannot be properly resolved if it subtends at the retina less than 1° , then the trajectory was said to be camouflaged if the intersection points I_1, \dots, I_n are not separated by more than 1° when viewed by the target. Note: In the cartesian frame, it may seem natural to group the intersection points based on the absolute distance between them. By using the angular, rather than physical, distance between the points as a measurement, we allow for the possibility that the intersection points have a large spread in an elliptical direction facing radially away from the target. In this case, the distances between intersection points might be quite large, but this movement would not be apparent to the target except as a change in size. Camouflage sequences of less than 80ms were discarded as trivial and too short for useful analysis.

Excerpts of Matlab Code for determining motion camouflage sequences

Determining the intersection points of the line-of-sight vectors between the insects

```

k = p(1); % p(1) is the length of the trajectory
intersect(1,:) = [0 0 0]; % initialise the vector that will store
% the intersection points

for t=1:k-1
    X1 = [PCOPY(t,1), PCOPY(t,2), PCOPY(t,3)]; % Target position at t1
    X3 = [PCOPY(t+1,1), PCOPY(t+1,2), PCOPY(t+1,3)]; % Target position at t2
    X2 = [DCOPY(t,1), DCOPY(t,2), DCOPY(t,3)]; % Pursuer position at t1
    X4 = [DCOPY(t+1,1), DCOPY(t+1,2), DCOPY(t+1,3)]; % Pursuer position at t2

    AV = X2-X1; % Vector between participants at t1
    BV = X4-X3; % Vector between participants at t2
    CV = X3-X1; % Vector between target positions at t1 and t2

    temp = dot(cross(CV,BV), cross(AV,BV))/norm(cross(AV,BV))^2;

```

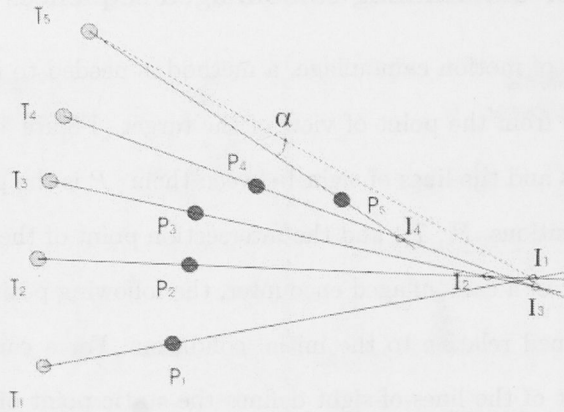


Figure 4.35: Determining a motion camouflage interaction. The points T_n represent the position of the target at time n , the points P_n represent the position of the pursuer. The points I_n are the intersection points of the lines of sight between the target and the pursuer. As long as α is less than 1° we add that segment of the trajectory to the motion camouflaged period. As soon as α becomes greater than 1° , the motion camouflage segment is said to have ended.

```
intersect(t,:) = X1 + AV*temp;           % Intersection point
end
```

Measuring the angular distance between the line-of-sight intersection points and storing those sequences deemed to be camouflaged in an array:

```
% Variable initialisation: big_arc is the resolution of the insect eye,
% chosen to be 1 degree
big_arc = 1*pi/180;
alpha1(1)=0;
alpha2(1)=0;
lengthP_1(1)=0;
lengthP_2(1)=0;
lengthD_1(1)=0;
lengthD_2(1)=0;
dist_c(1) = 0;
tally=0;
j=k;
counter=1;
store(counter) = 0;
count1 = 1;
count2= 1;
alphasum = 0;
```

```
% Working backwards from the end of the entire sequence, each LOS pair
% has its intersection point compared with that prior. The angular
% distance between them is summed. If that sum is less than the
% resolution size defined earlier, the positions and velocities of the
% insects, and the LOS intersection point, are stored as the count2'th
```

```

% segment of the count1'th camouflaged path. When the sum exceeds 1
% degree, that camouflage sequences is considered to be finished and
% the variable count1 is incremented.

for t=k-2:-1:2
    lengthP_1 = PCOPY(j,:)-intersect(j-1,:);
    lengthP_2 = PCOPY(j,:) - intersect(t-1,:);
    lengthD_1 = DCOPY(j,:) - intersect(j-1,:);
    lengthD_2 = DCOPY(j,:) - intersect(t-1,:);
    dist_c = norm(intersect(j-1,:) - intersect(t-1,:));
    temp1 = dot(lengthP_1, lengthP_2)/(norm(lengthP_1)*norm(lengthP_2));
    temp2 = dot(lengthD_1, lengthD_2)/(norm(lengthD_1)*norm(lengthD_2));
    alpha1(t) = acos(temp1);
    alpha2(t) = acos(temp2);
    alpha_min(t) = min(norm(alpha1(t)), norm(alpha2(t)));
    alphasum = alphasum + alpha_min(t);
    if alpha_min(t) < big_arc
        store(counter)=j;
        camP(count1,count2,:) = PCOPY(t,:);
        camD(count1,count2,:) = DCOPY(t,:);
        camPT(count1, count2, :) = PTCOPY(t,:); % PT and DT - positions
        camDT(count1, count2,:) = DTCOPY(t,:); % of the tails of the two
        camDvel(count1, count2, :) = DVEL(t,:); % participants
        camPvel(count1, count2,:) = PVEL(t,:); % PVEL, DVEL - velocities.
        inter(count1, count2,:) = intersect(t,:);
        count2=count2+1;
        store(counter+1) = t;
    else
        j=j-1;
        count1=count1+1;
        count2=1;
        counter=counter+2;
    end
end

```

4.6.2 Results

Various forms of motion camouflage behaviour were observed in almost all recorded flights between dragonflies (Figure 4.36), although some sequences were too short to be of use. An immediately noticeable attribute of the static point encounters is that they occur predominantly when the dragonflies are passing each other in opposite directions, a feature we return to in the discussion at the end of the chapter §4.8. Dynamic analysis on the sequences was performed using two dimensional information, for the sake of simplicity and also because the higher frame rate meant angular velocity measurements were more accurate.

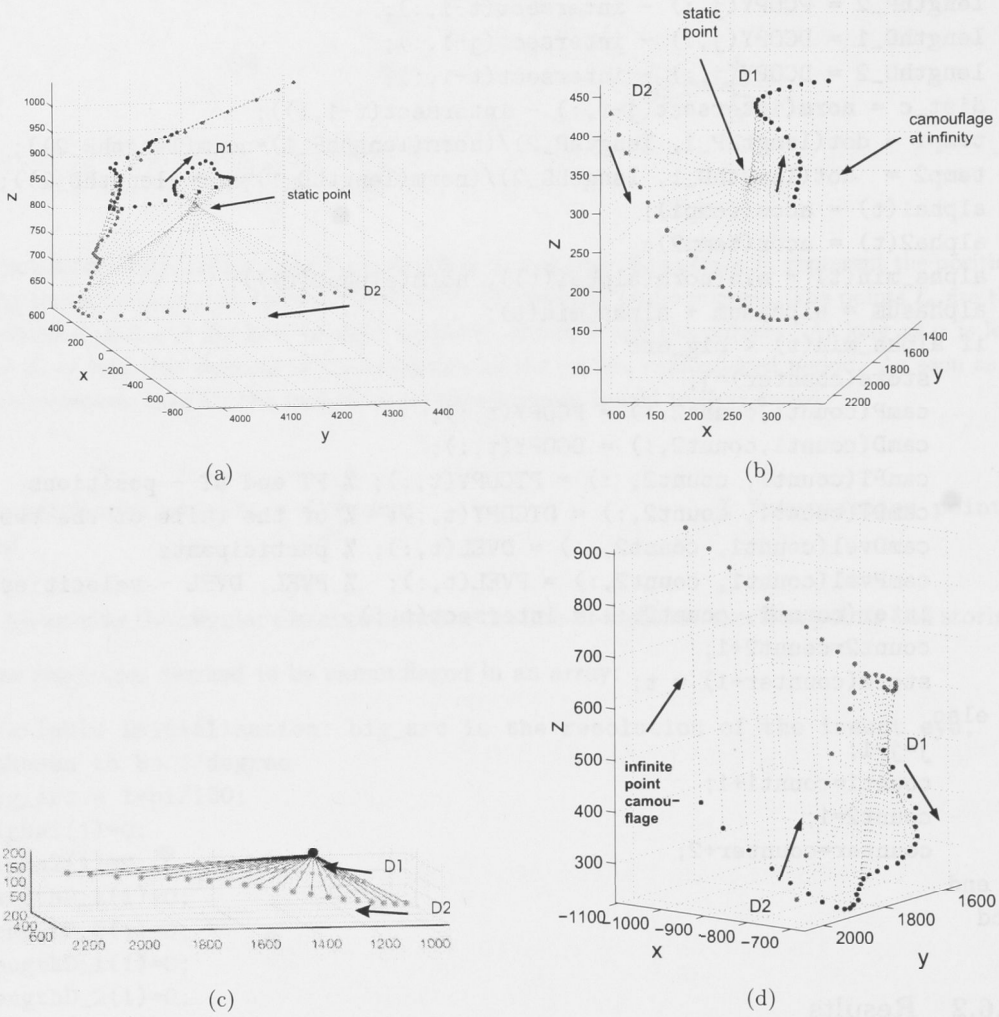


Figure 4.36: Distances along the axes are in mm. (a) Motion camouflage with a static point between the participants (b) Movement is initially camouflaged with a static point between the participants, later the motion changes to camouflage at infinity, or parallel tracking (c) Camouflage with a static point behind the pursuer (d) Again, camouflage at infinity occurs about halfway through the interaction.

Recall the geometric condition for camouflage, $\mathbf{r}_P - \mathbf{r}_D = k(\mathbf{r}_P - \mathbf{r}_T)$, and note that if $k = 0$ the result is a trivial solution, where $\mathbf{r}_D(t) = 0 \forall t$, i.e. the pursuer remains stationary at the static point of the engagement. The angular criterion on the other hand, $\Omega_P^D = \Omega_D^T = \Omega_P^T$, established in §2.2, excluded this trivial condition. By examining the angular velocity of camouflaged sequences with respect to the static point, we can eliminate trivial camouflage occurrences. Figures 4.37 - 4.39 show examples of camouflage interactions between dragonflies and the corresponding angular velocities of both insects relative to the static point.

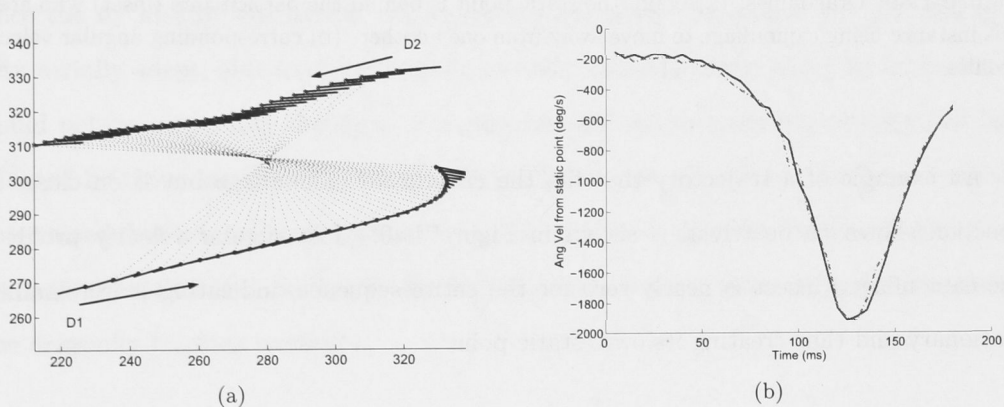


Figure 4.37: Dragonflies: (a) Motion camouflage with static point between participants (b) corresponding angular velocity profiles, as measured from the static point.

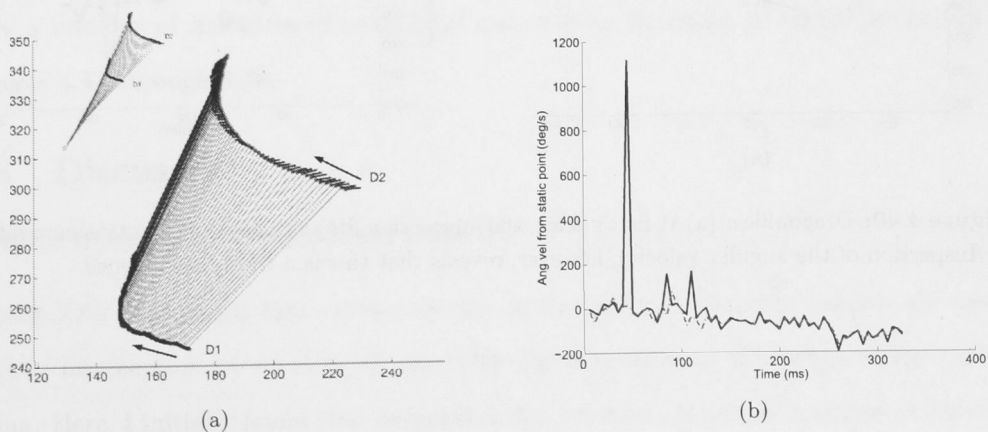


Figure 4.38: Dragonflies: (a) Motion camouflage with static point behind the participants. Inset shows trajectory including static point, main image shows detailed view of pursuer and target. (b) corresponding angular velocity profiles.

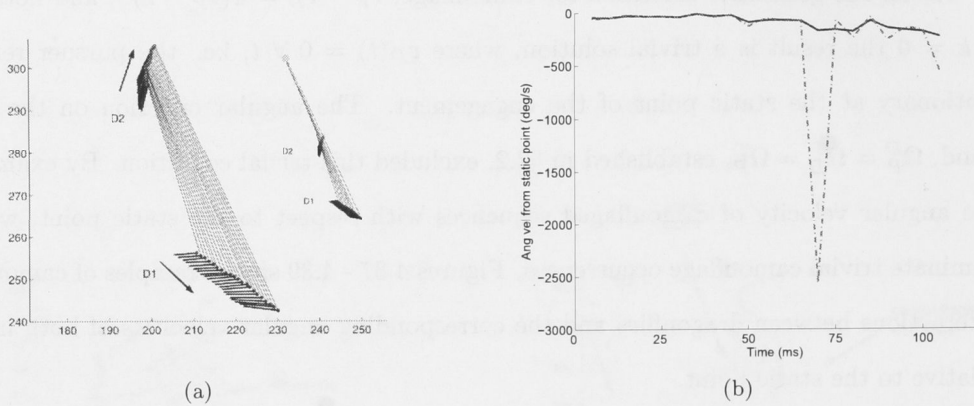


Figure 4.39: Dragonflies: (a) Again, the static point is behind the participants (inset) who are in this instance using camouflage to move away from one another. (b) corresponding angular velocity profiles

An example of a trajectory that fits the criteria for camouflage but is on closer inspection shown to be trivial is shown in Figure 4.40. The angular velocity profile of the camouflaged insect is nearly zero for the entire sequence, indicating it is remaining stationary and thus creating its own ‘static point’.

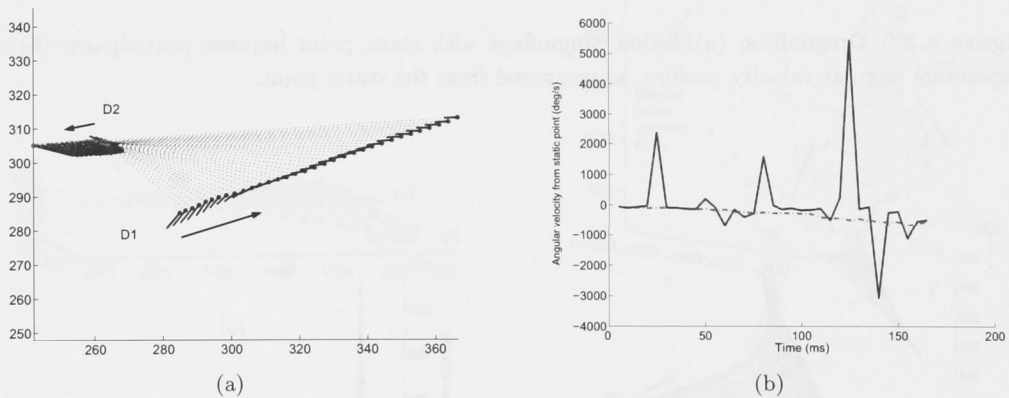


Figure 4.40: Dragonflies: (a) At first glance, the interaction fits the criteria for motion camouflage (b) inspection of the angular velocity, however, reveals that this is a trivial occurrence.

4.7 Motion Camouflage in Satellite Flies

As mentioned in 4.6, there are a number of possible reasons why motion camouflage might occur with some frequency in the interactions of multiple insect and animal species. One insect which might assist in discriminating between these possibilities is the satellite fly, genus *Sarcophagidae*. Female flies wait near the burrows of digger wasps, and larviposit on the prey of provisioning wasps before they enter their nests [Eva70]. This parasitic behaviour requires an excellent angular tracking mechanism, since the fly must be prepared to react very quickly. Stealth is also an important element of the tracking procedure, since the fly ideally will remain undetected by the wasp. Moreover, the satellite fly is very aerially adept, able to move laterally as well as longitudinally along its body axis. It would not be surprising, therefore, if motion camouflage as a stealth strategy had been adopted by these insects. The satellite fly guidance strategy has not yet been explicitly determined, but it is probably distinct from that used by dragonflies. As already described, the retinal fixation of a satellite fly shadowing a wasp is much more accurate than that of one dragonfly tracking another.

4.7.1 Results

Examining footage of satellite flies tracking wasps, we determined that instances of motion camouflage are also observed in these interactions. Most of those observed, however, were trivial cases where the satellite fly remained stationary or very nearly stationary. There were a number of instances of non-trivial camouflage, examples of which are shown in Figures 4.41 through 4.44.

4.8 Discussion

Retinal fixation and directional response

Olberg [OWV00] found that certain species of dragonfly fly directly towards the point of prey interception by steering to minimize the movement of the prey's image on the retina. Here, I initially found that dragonflies did indeed demonstrate a degree of anterior fixation in their target during a pursuit (§4.4.1). Usually, this was evident in only one of the participants, but occasionally both would face each other (note that this did not necessarily result in a closing trajectory), or pursuer/target roles would swap during an

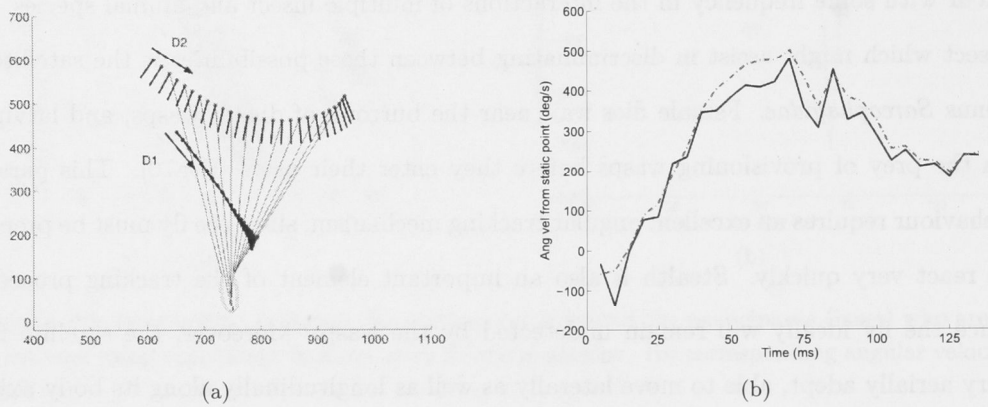


Figure 4.41: Satellite flies: (a) A non-trivial motion camouflage instance between a satellite fly and a wasp. Framerate is 200fps, line-of-sight vectors are shown every 10ms for the sake of clarity. (b) Angular velocity of both insects.

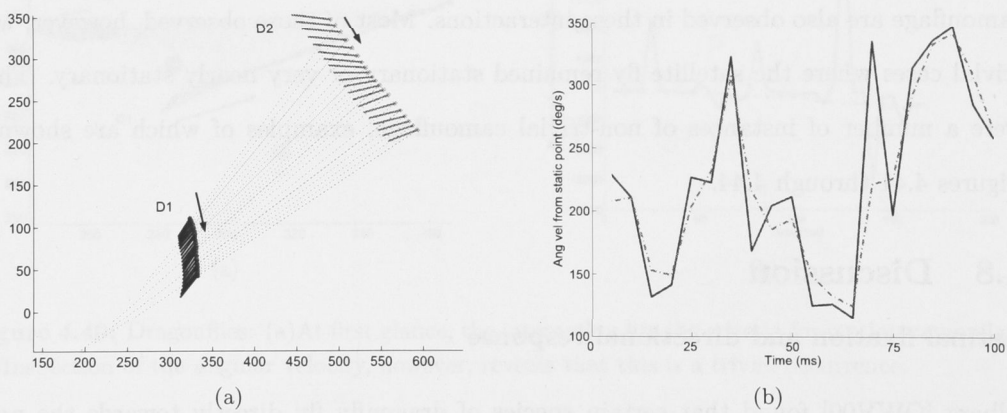


Figure 4.42: Satellite flies: (a) A non-trivial motion camouflage instance between a satellite fly and a wasp. Framerate is 200fps, line-of-sight vectors are shown every 10ms for the sake of clarity. (b) Angular velocity of both insects.

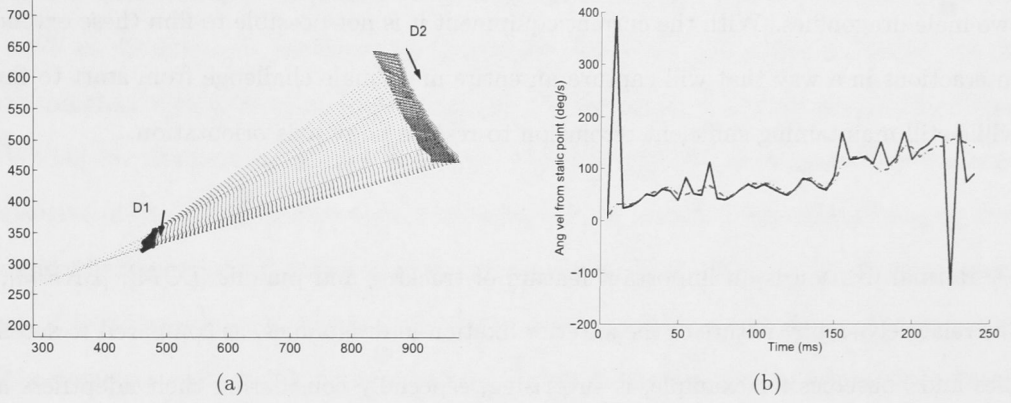


Figure 4.43: Satellite flies: (a) A non-trivial motion camouflage instance between a satellite fly and a wasp. Framerate is 200fps, line-of-sight vectors are shown every 10ms for the sake of clarity. (b) Angular velocity of both insects.

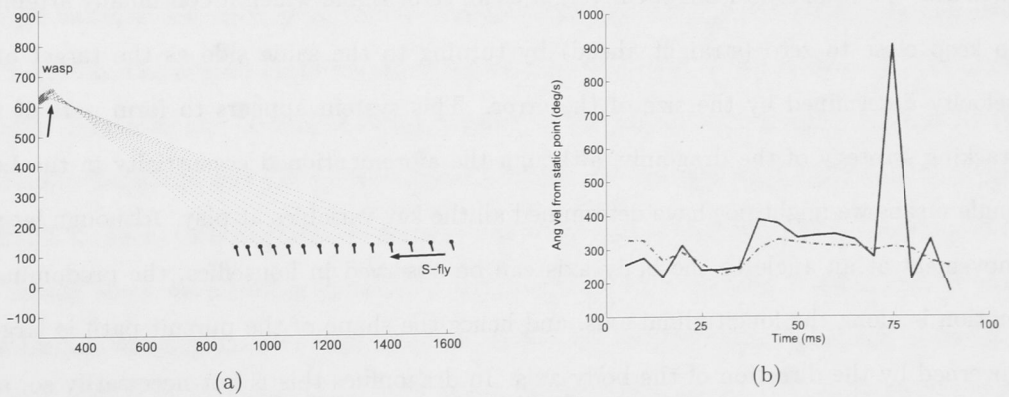


Figure 4.44: Satellite flies: (a) A non-trivial motion camouflage instance between a satellite fly and a wasp. Framerate is 200fps, line-of-sight vectors are shown every 10ms for the sake of clarity. (b) Angular velocity of both insects.

engagement. The recorded sequences were usually only segments of an overall interaction which could span tens of metres and many seconds. It is likely that the roles of pursuer and target are often reversed, perhaps even several times, during an aerial pursuit between two male dragonflies. With the current equipment it is not possible to film these extended interactions in a way that will capture an entire male/male challenge from start to finish while still maintaining sufficient resolution to resolve body axis orientation.

Retinal fixation is an important feature of tracking and pursuit [LC74], [BKE03], so the relatively sloppy nature of the anterior fixation in dragonflies, as compared to satellite flies and houseflies for example, is surprising, especially considering their adeptness and accuracy of movement in other pursuit-related tasks. It may be that the head orientation, not resolvable with the limitations of the current equipment, is compensating for changes in the retinal position of the target insect. Alternatively, perhaps fixation (anterior or otherwise) is not a necessary component of the tracking and pursuit strategy being used.

In flies, tracking is archived by a reflex in which the retinal eccentricity of the target governs the pursuing fly's angular velocity with a lag of 10 to 20 ms [BKE03]. The fly thus uses the retinal position of the target as an error signal which it continually attempts to keep close to zero (straight ahead) by turning to the same side as the target at a velocity determined by the size of the error. This system appears to form part of the tracking strategy of the dragonfly, although the aforementioned eccentricity in the LOS angle means we might not have determined all the key variables at play. Although lateral movement at an angle to the body axis can be observed in houseflies, the predominant motion is along the longitudinal axis, and hence the shape of the pursuit path is largely governed by the direction of the body axis. In dragonflies this is not necessarily so, and we have found some evidence that the flight direction is in fact governed by the velocity of the line-of-sight vector, ie

$$\dot{\psi} = G(\dot{\alpha} - \dot{\theta}). \quad (4.10)$$

Some of the ramifications of this differential guidance law, should it be valid, are explored in the next chapter.

General flight characteristics

By examining the gross flight characteristics of two-body dragonfly flight in all three cartesian dimensions, we can draw some conclusions about the way velocity magnitude, as well as direction, is governed by the target dynamics. Changes in target velocity were matched within 20-40ms by the pursuer, corresponding with results found by Olberg [OWV00] for dragonflies in prey pursuits. Angular velocity, as measured by the time-derivative of the absolute course angle, tended to have a much longer delay, ranging from around 20-60ms in the horizontal plane to anywhere up to 100ms in the vertical plane. Part of this increase in apparent response time is probably due to the secondary nature of the response, since in the three-dimensional reconstruction used to measure the overall angular response, the changes in body axis angles could not be resolved. In addition, the dragonfly must first pitch upwards before it can change its elevation, incurring a reaction delay. In the horizontal plane, no change in yaw direction is required to make a course angle change, although an adjustment to roll angle may be necessary. Depending on the organization of the flight motor and musculature of the insect, this may account for the greater delay in responses to a vertical movement by the target.

The strong correlation between the flight direction of the pursuer and target supports the notion that flight direction in the vertical plane is governed by the change in apparent target velocity just as it is in the horizontal plane (as observed in earlier experiments). In addition, the overall flight speed of the pursuer was heavily influenced by that of the target. Increases and decreases in flight speed of the target were closely matched by the pursuing dragonfly, and the relative speed between the two was kept fairly low. In a pure pursuit scenario with capture as the goal, one would not expect the correspondence to be so strong since maintaining speed at a maximum level, or at least a value greater than the target, would guarantee capture more often. On the other hand, pursuing dragonflies do not appear to maintain a constant range between themselves and conspecifics, which would be expected if the goal was simply to chase and match the movements of the target [LC74]. Moreover, while quantitatively the flight direction of the pursuer was generally close to that of the target, in many cases a qualitative analysis reveals that the changes in flight direction were mirrored rather than matched.

The guidance system governing velocity magnitude, then, may have simple overall

features but has complex behavioral ramifications, resulting in neither capture nor precise mimicry of the target trajectory, but something akin to an attempt to match overall aerial maneuverability.

Motion camouflage in dragonflies and satellite flies

When attempting to maintain camouflage, the direction of flight is the most important variable. A shadower must remain on the camouflage constraint lines, which can change rapidly depending on target motion. The most important clue in assessing current target motion or predicting future motion is the angular position and movement of the line-of-sight vector between the target and pursuer. In the free flights observed amongst dragonflies, with or without the presence of camouflaged segments, there did seem to be a relationship between the flight direction and the line-of-sight angle, or more accurately between the first derivatives of those variables.

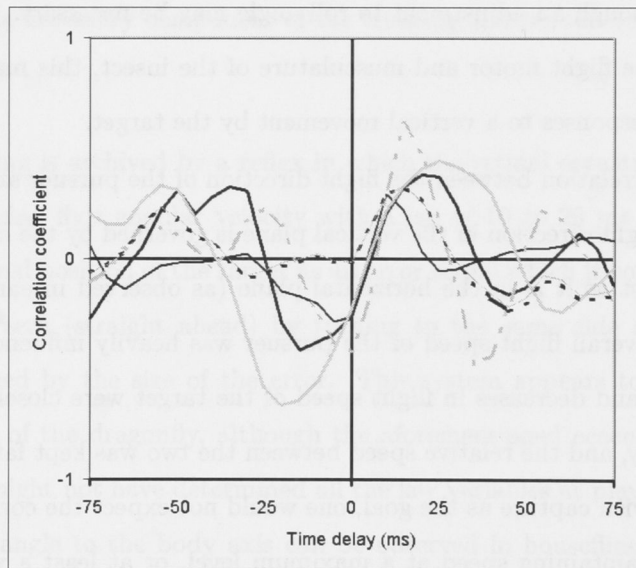


Figure 4.45: Cross-correlation between changes in flight direction and changes in LOS angular position, for motion camouflaged sequences between satellite flies and wasps.

In general, we found the flight direction of satellite flies to be unrelated to the change in position of the wasp. Examining the correlation between the change in flight direction in the satellite fly and the LOS angular velocity during *only* camouflaged sequences, however, revealed a positive relationship. Changes in LOS angular velocity within those segments

were usually responded to by changes of the satellite fly flight direction within 30ms (Figure 4.45). Likewise, changes in flight direction in dragonflies exhibited a positive relationship to the LOS angular velocity during camouflaged sequences, also at delays of 30-40ms (Figure 4.46).

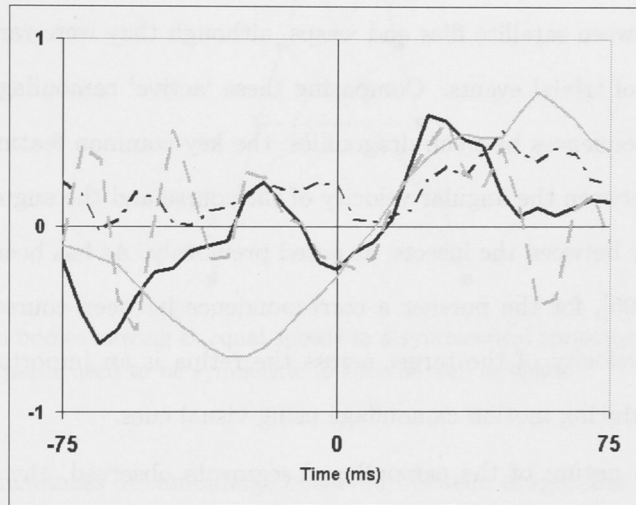


Figure 4.46: Cross-correlation between changes in flight direction and changes in LOS angular position, for motion camouflaged sequences between dragonflies.

Limiting the analysis to only camouflaged sequences in both the dragonfly and satellite fly / wasp interactions, we find a significant change in the flight direction occurs in response to changes in the line of sight velocity. As discussed, dragonflies tended to change flight direction in response to LOS velocity changes. However most of the time, satellite flies did not exhibit a clear correspondence between flight direction and line-of-sight angular velocity to the wasp, probably because the flies place more priority on angular tracking.

Examining the sequences of camouflaged behaviour exhibited by the satellite flies, it was observed that they tended to remain close to the nominal ‘static point’ of the sequence, resulting in a passive camouflage state that did not truly qualify under the angular condition established in Chapter 2. Moving not at all, or at most a very small distance around a set ‘node’, is perhaps the easiest way of producing a camouflaged sequence if target capture is not an objective, especially if the distance between shadowee and shadower is relatively large. Satellite flies tend to keep a relatively constant distance between themselves and the target wasp, which reduces the angular movements necessary to keep the

target image on the insects' fovea [RW69].

The above describes a good reason why the satellite fly may maintain itself in a moderately stationary position at some distance from the target and change positions by rotating around a central 'node'. The fact that these are also ideal conditions for static point camouflage is simply a feature of the geometry. However, instances of non-trivial camouflage were observed between satellite flies and wasps, although they were rare when compared with the number of trivial events. Comparing these 'active' camouflage traces with 'active' camouflage sequences between dragonflies, the key common feature seemed to be a correspondence between the angular velocity of the course and the angular velocity of the line of sight vector between the insects, as noted previously. As has been suggested in the past [AM03], [SD95], for the pursuer a correspondence between course angular velocity and the angular velocity of the target across the retina is an important, possibly vital component of producing motion camouflage using visual cues.

Regarding the nature of the camouflaged segments observed, the crucial feature of camouflaging motion to note in many instances is that it is a purely geometric phenomenon. Hence, given the right conditions between two moving bodies, it can occur without either participant even being aware of the other. Consider, for example, two cars moving at a constant speed on a highway:

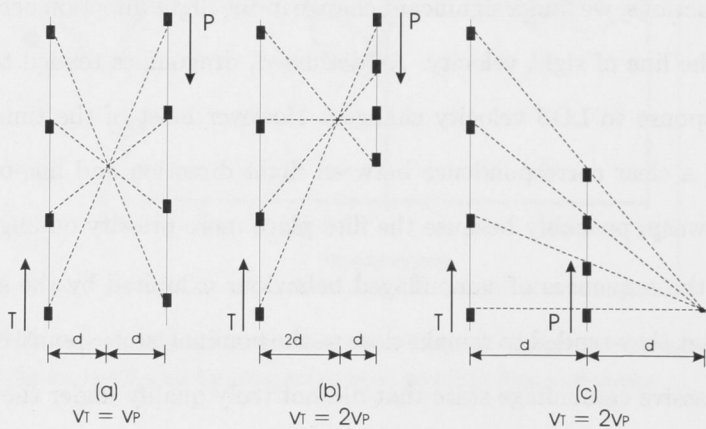


Figure 4.47: (a) Two oblivious bodies moving at constant speeds in opposite directions, $v_T = v_P$; (b) Two oblivious bodies moving at constant speeds in opposite directions, $v_T = 2v_P$; (c) Two oblivious bodies moving at constant speeds in the same directions, $v_T = 2v_P$;

Given constant speed and a mirrored inversion symmetry in the geometry, motion

camouflage patterns are produced whether or not the participants are actively attempting to generate them. (Not all geometrical symmetries will produce camouflage - see, for example, Figure 4.48).

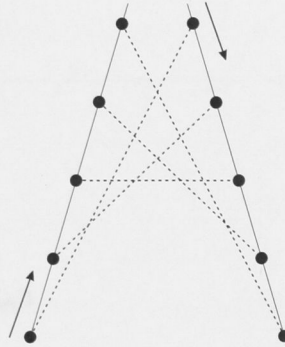


Figure 4.48: Two bodies moving at equal speeds in a symmetrical trajectory that is not motion-camouflaged - the paths need to be symmetric in time as well as space.

Many of the instances of camouflage observed between dragonflies matched in quality those described in Figures 4.47(a) and 4.47(b) - that of the participants moving in contrary directions while maintaining an approximately constant velocity. The question then becomes - why do dragonflies so often engage in behaviour which incidentally leads to the geometric condition of motion camouflage? One of the notable things about camouflage with a static point between participants, of course, is that both dragonflies will appear static to each other in an angular sense. Are the insects perhaps merely trying to get a good look at one another?

...the pursuit of a dragonfly and a satellite fly. The dragonfly is the predator and the satellite fly is the prey. The dragonfly is a large, powerful insect with a long, segmented body and six legs. It is a voracious predator and is known for its speed and agility. The satellite fly is a smaller, more delicate insect with a long, thin body and six legs. It is a common pest and is known for its annoying behavior. The pursuit of the dragonfly and the satellite fly is a fascinating and complex behavior that has been studied extensively by scientists. The dragonfly is able to track its prey with remarkable accuracy and is able to catch it in a matter of seconds. The satellite fly is able to evade its predator for a short time, but eventually it is caught and eaten. This pursuit is a classic example of predator-prey behavior in the animal kingdom.

...the pursuit of a dragonfly and a satellite fly. The dragonfly is the predator and the satellite fly is the prey. The dragonfly is a large, powerful insect with a long, segmented body and six legs. It is a voracious predator and is known for its speed and agility. The satellite fly is a smaller, more delicate insect with a long, thin body and six legs. It is a common pest and is known for its annoying behavior. The pursuit of the dragonfly and the satellite fly is a fascinating and complex behavior that has been studied extensively by scientists. The dragonfly is able to track its prey with remarkable accuracy and is able to catch it in a matter of seconds. The satellite fly is able to evade its predator for a short time, but eventually it is caught and eaten. This pursuit is a classic example of predator-prey behavior in the animal kingdom.

...the pursuit of a dragonfly and a satellite fly. The dragonfly is the predator and the satellite fly is the prey. The dragonfly is a large, powerful insect with a long, segmented body and six legs. It is a voracious predator and is known for its speed and agility. The satellite fly is a smaller, more delicate insect with a long, thin body and six legs. It is a common pest and is known for its annoying behavior. The pursuit of the dragonfly and the satellite fly is a fascinating and complex behavior that has been studied extensively by scientists. The dragonfly is able to track its prey with remarkable accuracy and is able to catch it in a matter of seconds. The satellite fly is able to evade its predator for a short time, but eventually it is caught and eaten. This pursuit is a classic example of predator-prey behavior in the animal kingdom.

Proportional Navigation and Insect Flight

5.1 Variable definition

The following table describes the variables used in this chapter:

| List of Variables | |
|-------------------|--------------------------------------------------------------------------------------------|
| \mathbf{r} | Position vector |
| \mathbf{v} | Velocity vector |
| \mathbf{a} | Acceleration vector |
| $\Delta\rho$ | Angular distance moved across the pursuers retina by the target over one time interval |
| σ | Horizontal direction of flight (pursuer) |
| β | Horizontal direction of flight (target) |
| ψ | Vertical direction of flight (pursuer) |
| ϑ | Vertical direction of flight (target) |
| θ | Horizontal line-of-sight angle between pursuer and target |
| ϕ | Vertical line-of-sight angle between pursuer and target |
| η | Angle between the pursuer's acceleration vector and the vector normal to the line-of-sight |
| ζ | Angle between the target's acceleration vector and the vector normal to the line-of-sight |

5.2 Introduction

In Chapter 3 we explored various linear cost-optimal solutions to the motion camouflage problem. Although effective, they were cumbersome, required a very thorough knowledge of the target states, and often performed sub-optimally against maneuvering targets due to the necessary cost constraint on the control effort.

In Chapter 4 we analyzed the interactive behaviour of dragonflies and established some of the key variables which appear to influence the guidance and dynamics of free-flying dragonflies and satellite flies engaged in non-predatory chases. Now, using this

information, I seek to establish a model for a possible guidance system driving such a camouflaging insect. I then approach a camouflage solution using a guidance law based around the capabilities of this biomimetic control algorithm.

Pursuit models based on visual control of flight direction have been examined to different degrees in various insects. Land and Collett [LC74] modeled the chasing engagements of patrolling houseflies using a line-of-sight dependent angular velocity model. Reichardt and Poggio [PR81] suggested a more situationally-dependent control algorithm, wherein alterations to the overall form of the dynamic strategy were made depending on the geometry of the engagement - for example, a control system for angular tracking of a target might not kick in unless the line-of-sight error angle is increasing, or greater than a threshold value, or some other geometric or dynamic condition. Boeddeker and Egelhaaf [BE05] designed a decoupled system to model chasing behaviour in blowflies. This simulator was designed along similar principles to the one initially developed in this chapter, controlling orientation and forward velocity by separate mechanisms.

Most controllers developed to describe insect guidance systems' focus on goal-specific flight control, namely that of target capture. It is possible, of course, that like those of the housefly, the dragonfly interactions observed begin as capture attempts, perhaps with the pursuing dragonfly mistaking the target for a female or prey. However the length¹ and close-range nature of the interactions argues against this, and it is known that the dragonflies in question are highly territorial and will attempt to drive off encroaching males [PK87].

5.3 Decoupling the Control Systems

A useful approach for initial analysis is to decouple the guidance system into two control pathways, one governing direction and the other speed. This deconstruction may be a little artificial but it enables us to more easily estimate the influences of the various aspects of the target's appearance and behaviour on different dynamic variables in the pursuer. For the sake of simplicity, we consider the control problem in two dimensions, at least initially.

¹Observed interactions often lasted for many seconds, however they ranged over such distances that generally only a small portion of the interaction was recorded. Moreover, we would often see several distinct engagements with the same participants

5.3.1 Forward Speed Control

Recall the following information from Chapter 3:

- the speed of the pursuer is related to the apparent speed of the target across the retina
- a qualitative analysis seems to indicate that the pursuer, or reactive dragonfly, attempts to match the magnitude of the dynamic output of the target, keeping the relative (translatory) speed small, no matter the absolute speed of the target.
- At least a rough ability to estimate range is required to define a ‘territory’, and it is probable that dragonflies are using range information gleaned from a number of sources [OWV00]. Range data may affect the speed and behaviour of pursuer and target.

In our simulation we therefore want the velocity to approximately match that of the target, in the inertial frame. However, the absolute velocity of the target will not be available to a moving insect, only the apparent velocity. If the model incorporates a scaling factor dependent on range, the absolute speed of the target can be approximately reconstructed.

As a first approximation, I choose the characteristic equation of the speed controller during an engagement to be

$$v_D = \gamma_1(v_0 + r^\epsilon \Delta\rho) \quad (5.1)$$

where v_0 is an estimate of the pursuer’s own speed, r^ϵ is an estimate of the range and ρ is the angle the target tracks across the pursuer’s retina over one time interval. γ_1 is a gain factor, and is likely to be near 1 in a conflict between similarly capable insects.

5.3.2 Directional Control

In a simple predatory or amorous pursuit, the goal is straightforward to define and we may assume the directional control is in some way related to the error angle between the velocity vector of the insect and the position of the target. However when the goal is not interception, we must be wary of making assumptions about the reaction to positional change on the retina. Moreover, whereas in artificial systems the velocity vector is often assumed to align itself along the body axis, so forward velocity dominates the dynamics, in

dragonflies and other aerodynamically capable insects velocity direction is not necessarily related to body axis direction. In other words, a dragonfly may head towards a target even when it is not positioned frontally on the retina. In Chapter 4, we demonstrated that the frontal fixation of a target in a responding dragonflies retina is much less marked than that of a wasp's in a responding satellite fly, for example.

Looking at high-speed films of trajectories, we found that for some flights there exists a correlation between the error angle velocity and that of the flight direction of the pursuer. We put forward an hypothesis that change in flight direction is linearly related to error angle velocity. Land and Collett [LC74] found a similar relationship was a good model for angular velocity control in houseflies.

$$\begin{aligned}\dot{\sigma} &= \gamma_2 \dot{\theta} \\ \sigma &= \gamma_2(\theta + \theta_0)\end{aligned}\tag{5.2}$$

The scalar gain γ_2 determines the gain of the course orientation change. σ is the flight direction, θ is the line of sight error angle, and θ_0 is an offset angle. The latter is included because the position fixation which has been observed in dragonflies does not necessarily seem to be in the anterior of the visual field, so the offset acts as a non-zero set-point which we can drive the system towards.

5.3.3 Implementing a Decoupled Control System

Discretizing the equations derived in the previous section, we apply the velocity control to a point mass imitating the location of the dragonfly, in a direction determined by a discrete approximation of the differential equation (5.2). At this stage we do not concern ourselves with body axis orientation. From the results in Chapter 3, we use a lag in the relative velocity measurement of 20ms, and a lag in the measurement of change in error angle rate of 15ms. Choosing four sequences where the relationship between flight direction and LOS angle was clearly shown (Figures 5.1 - 5.3), we tested the decoupled controller to see how well it matched the real trajectories used by the dragonflies.

The simulation can be adjusted using the two gain factors and the offset angle, θ_0 . This angle at which the course stabilizes varies between, and even within, sequences. Initial conditions at the start of the filmed sequence were used to set the offset, since as yet no

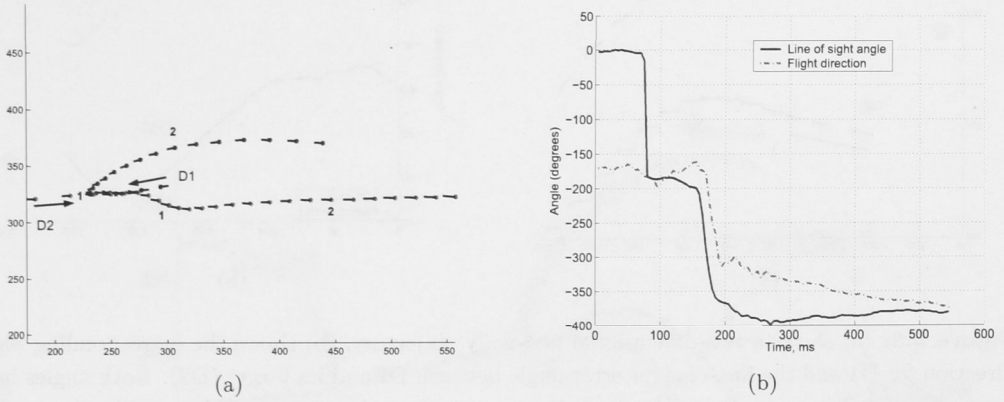


Figure 5.1: (a) shows a two-dimensional two-body trajectory, (b) shows the corresponding flight direction for D1 and the line-of-sight error angle between D1 and its target (D2). Both angles have been unwrapped so as to remove jumps between negative and positive angular positions, and thus show the correspondence between the variables more clearly.

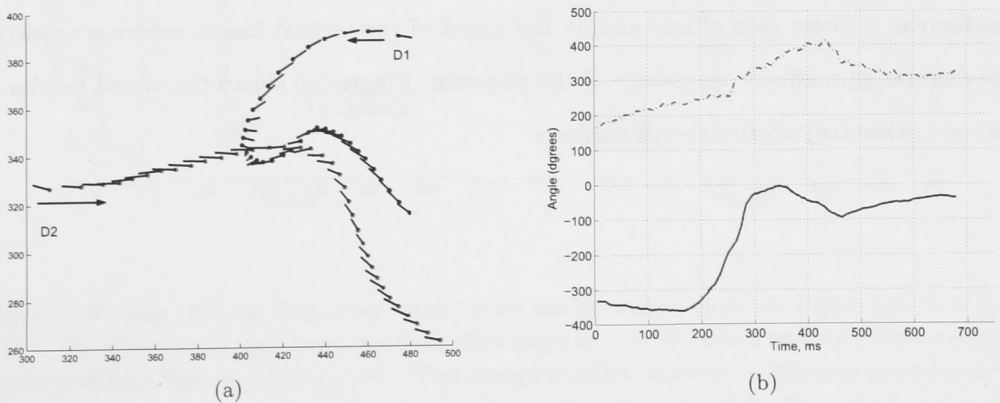


Figure 5.2: (a) shows a two-dimensional two-body trajectory, (b) shows the corresponding flight direction for D1 and the line-of-sight error angle between D1 and its target (D2). Both angles have been unwrapped so as to remove jumps between negative and positive angular positions, and thus show the correspondence between the variables more clearly.

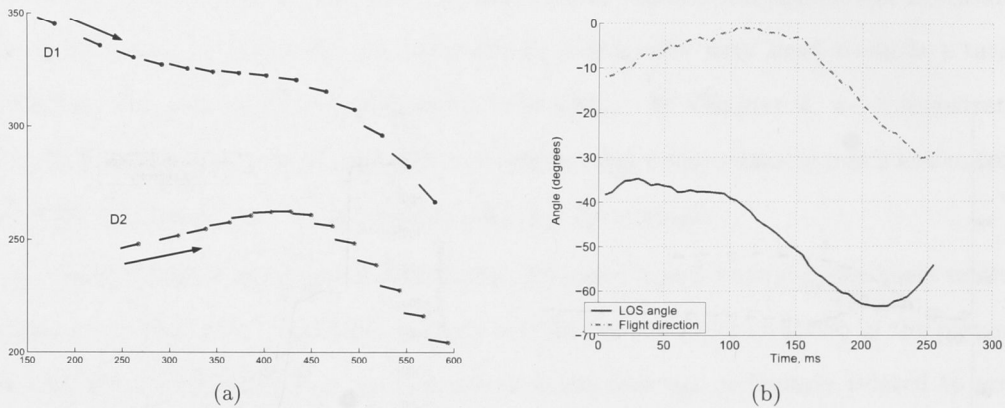


Figure 5.3: (a) shows a two-dimensional two-body trajectory, (b) shows the corresponding flight direction for D1 and the line-of-sight error angle between D1 and its target (D2). Both angles have been unwrapped so as to remove jumps between negative and positive angular positions, and thus show the correspondence between the variables more clearly.

provision has been made for changing the angle during a pursuit.

Initial position and velocity conditions of the model dragonfly were matched to the recorded data for the first few frames of the interaction, until sufficient previous data existed for the time delay to be incorporated. Figure 5.4 shows the performance of the tuned controller. From the point of view of trajectory matching this is an open-loop system, so deviations from the biological flight path we are trying to track will not be corrected. Adjusting the velocity gain affects simply the speed of the virtual insect, whereas adjusting the angular gain affects the nature of the response. Figure 5.5 shows the tuned results for the two other trajectories shown earlier.

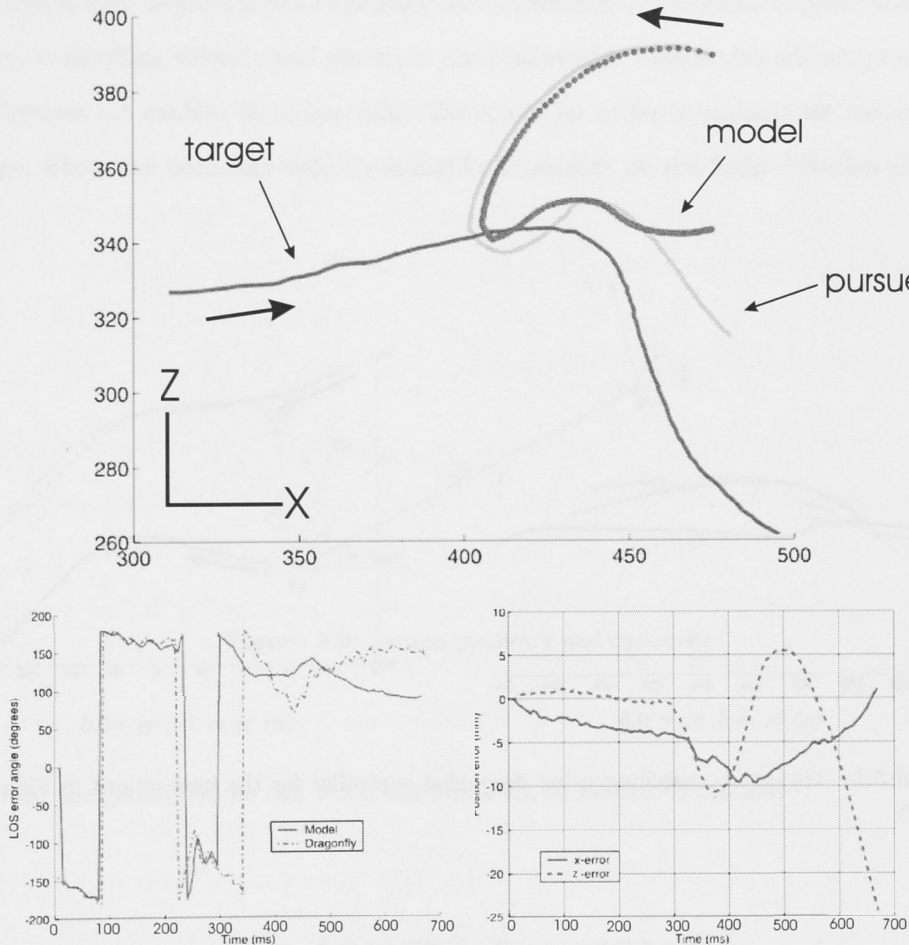


Figure 5.4: Top: Sample Trajectory matching for the interaction shown in Figure 5.2: $\gamma_1 = 2$, $\gamma_2 = 0.8$. The real pursuit path began with an offset angle $\theta_0 = -40^\circ$, which remained fairly constant for about 300ms, then changed to 160° . This change in offset, however, is not accounted for in the model and is the main reason for the divergence between real and model path in the latter part of the trajectory. Bottom left: the line of sight angle relative to the flight direction, for both model and dragonfly. Bottom right: position error along the x and z axes.

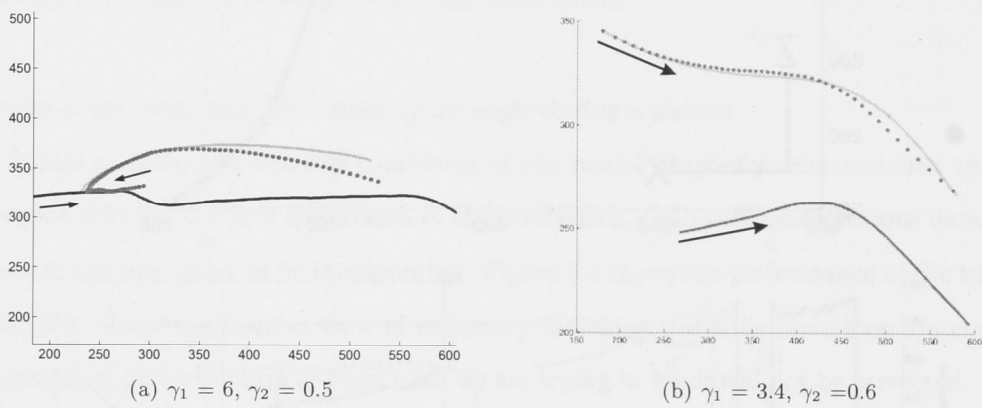


Figure 5.5: Trajectory matching using decoupled controller for the interactions in Figures 5.1 and 5.3

5.4 Acceleration-based Control and PN guidance

The kind of decoupled controller demonstrated above has been successful in modeling insect behaviors [AM03], [BKE03]. But for the guidance of artificial systems, and for analysis purposes, it may be more useful to present the controller as a non-linear acceleration-driven system, controlling velocity and direction simultaneously. This is also advantageous for a third reason - it enables us to specialize the controller into one suitable for motion camouflage, where the necessary velocity is highly dependent on the flight direction chosen.

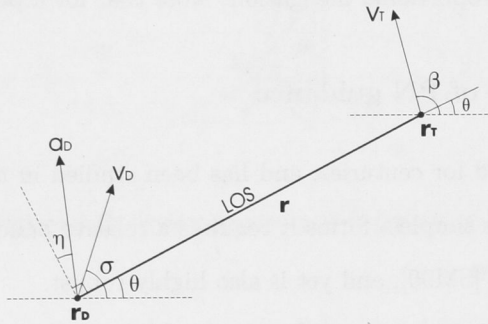


Figure 5.6: System geometry and dynamics

From the geometry, we can write the following equations of motion:

$$v_r = \dot{r} = v_T \cos(\beta - \theta) - v_D \cos(\sigma - \theta) \quad (5.3)$$

$$v_\theta = r\dot{\theta} = v_T \sin(\beta - \theta) - v_D \sin(\sigma - \theta) \quad (5.4)$$

$$\dot{\sigma} = \frac{a_D}{v_D} \cos(\sigma - \theta + \eta) \quad (5.5)$$

$$\dot{\beta} = \frac{a_T}{v_T} \cos(\sigma - \theta + \eta) \quad (5.6)$$

η is the offset angle between the acceleration vector and the line perpendicular to the LOS. β is the direction of flight of the target, σ and θ are, as before, the direction of flight of the pursuer and the line of sight angle between the pursuer and target. a_D is the pursuer acceleration, a_T is the target acceleration. Together with the initial conditions, these equations completely define the system. Using our two-dimensional controller, we

can then write the necessary acceleration command for a bio-mimicking system as

$$a_D = \gamma_1 \gamma_2 \frac{r\dot{\rho} + v_0}{\cos(\sigma - \theta + \eta)} \dot{\theta} \quad (5.7)$$

$$= cv^\epsilon \dot{\theta}. \quad (5.8)$$

Recall that $\dot{\theta}$ is the angular rate of the error angle, in other words the rate of change of the line of sight vector. v^ϵ is an estimate of the target speed, hence, by definition, this controller belongs to a class of control laws known as Proportional Navigation Guidance Laws. More specifically, it is a form of GTPN, or generalized true proportional navigation, where the acceleration is applied at some angle offset to LOS perpendicular. If $\eta = 0 \quad \forall t$, the law becomes true proportional navigation. Note that for a point mass, $\dot{\rho} = \dot{\theta}$.

5.4.1 Explanation of PN guidance

PN guidance has existed for centuries, and has been studied in the theoretical literature for some decades - in its simplest forms it requires a relative paucity of information input compared to other laws [SM90], and yet is also highly robust.

Many forms of proportional navigation exist, but most of them can be divided into two classes - true proportional navigation (TPN) and pure proportional navigation (PPN). Pure proportional navigation uses an acceleration command applied laterally to the guided body, perpendicular to the velocity vector. True proportional navigation conventionally applies the acceleration perpendicular to the line of sight direction (which is distinct from the velocity vector) [Gho94], however TPN may more accurately be referred to as a special case of a more general type of guidance law, ‘generalized true proportional navigation’, or GTPN [MS89]. Bodies using GTPN apply an acceleration at an angle to the line of sight, not necessarily perpendicularly.

Although PPN is generally regarded as the most ‘natural’ PN law [Tya03], it is not necessarily the one best suited to our purpose. LOS-referenced laws are not in common usage as they require forward acceleration and deceleration, and are not particularly efficient in terms of control effort. However when attempting to model real biologically-based scenarios, a forward acceleration capability becomes desirable, even necessary. And the inefficiency of the control action is offset by the greater flexibility of the controller when it comes to dealing with a maneuvering target [YY96]. In addition, the oft-used argument

that TPN is less robust with regards to capturability is not that relevant in this situation [Adl56], since capture may not be the primary objective in the interaction.

5.5 Extrapolation into Three Dimensions

Now consider the three-dimensional dynamics (Figures 5.7, 5.8).

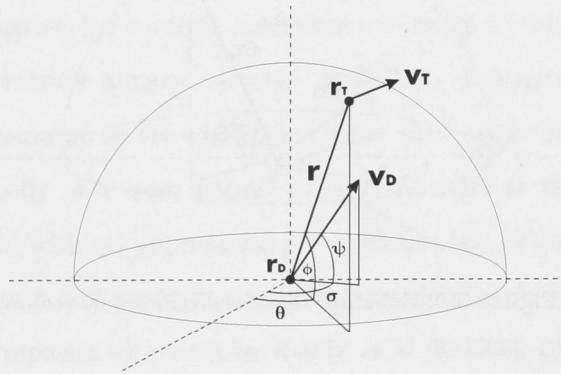


Figure 5.7: System geometry and dynamics: 3D

By a similar process to that used in the two dimensional case, we can derive equations for the magnitude of the total acceleration, and the acceleration in the x-y plane.

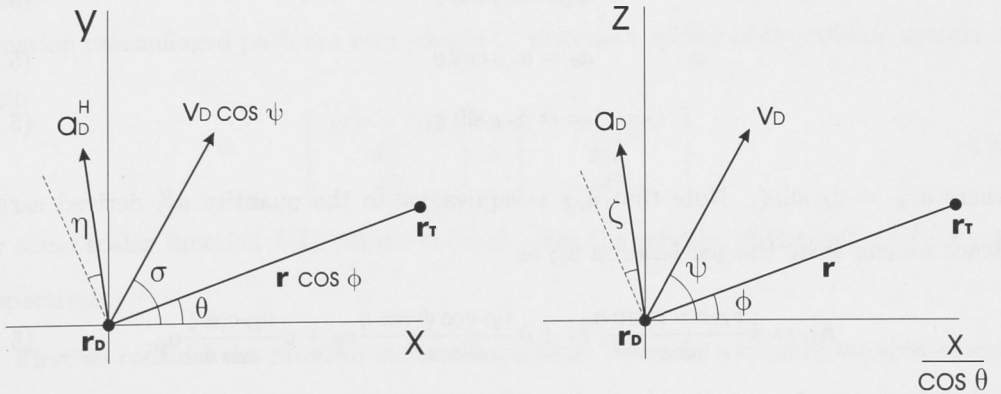


Figure 5.8: Dynamics in the horizontal and vertical plane

$$a_D^H = \dot{\sigma} \frac{v_D \cos \psi}{\cos \nu} \tag{5.9}$$

$$a_D = \dot{\psi} \frac{v_D}{\cos \delta} \tag{5.10}$$

where $\nu = \sigma - \theta + \eta$ and $\delta = \psi - \phi + \zeta$. To pose these equations of motion into a more tractable form, we convert to an orthogonal co-ordinate system $(\mathbf{e}_r, \mathbf{e}_\theta, \mathbf{e}_\phi)$ centred on the controlled body with the unit vector \mathbf{e}_r in the direction of the LOS (Figure 5.9).

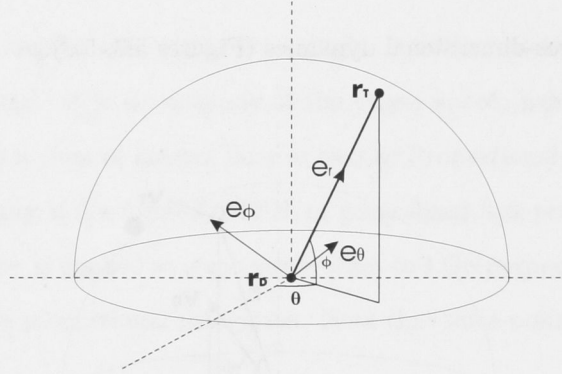


Figure 5.9: Spherical reference frame: unit vectors

It is a straightforward procedure to express the acceleration vector \mathbf{a}_D as

$$\mathbf{a}_D = a_r \mathbf{e}_r + a_\theta \mathbf{e}_\theta + a_\phi \mathbf{e}_\phi.$$

We find the following equations of motion:

$$a_\phi = a_D \cos \zeta \quad (5.11)$$

$$a_\theta = a_{r,\theta} \cos \eta \quad (5.12)$$

$$a_r = a_{r,\theta} \sin \eta \quad (5.13)$$

where $a_{r,\theta} = a_D \sin \zeta$. Note that $a_{r,\theta}$ is equivalent to the quantity a_D^H derived earlier.

Hence we can write the acceleration \mathbf{a}_D as

$$\mathbf{a}_D = \dot{\sigma} \frac{v_D \cos \psi \sin \eta}{\cos \nu} \mathbf{e}_r + \dot{\sigma} \frac{v_D \cos \psi \cos \eta}{\cos \nu} \mathbf{e}_\theta + \dot{\psi} \frac{v_D \cos \zeta}{\cos \delta} \mathbf{e}_\phi. \quad (5.14)$$

In three-dimensions, the decoupled control laws are

$$v_D = \gamma_1 (v_0 + r \dot{\rho}) \quad (5.15)$$

$$\dot{\sigma} = \gamma_2 \dot{\theta} \quad (5.16)$$

$$\dot{\psi} = \gamma_3 \dot{\phi}. \quad (5.17)$$

We can substitute these values into equation (5.14) to close the loop and obtain a

three-dimensional model of dragonfly pursuit.

5.6 PN Guidance and Motion Camouflage

5.6.1 Background

Motion camouflage is a natural candidate for a modified PN guidance law. In proportional navigation, the corrective (or control) acceleration is applied with a magnitude that is proportional to the relative angular velocity. In §2.2 we demonstrated that if we scale a camouflaged environment to the stationary frame with origin at P (focal point), the relative angular velocity of T with respect to D is the same as that of T with respect to P. In other words, with an appropriate PN guidance law in place, deviation from a motion camouflage path will result in a corrective acceleration being applied by the PN controller. This corresponds with work by Reddy, et al [RJK06], who showed that under suitable hypothesis, a version of PPN with range-dependent gain leads to eventual motion camouflage in finite time in a precise sense.

5.6.2 2D Problem Definition

Suppose we have a two-body motion camouflaged system. The governing kinematics for a motion camouflaged path are very simple to write in a spherical co-ordinate system, to wit:

$$\begin{bmatrix} (r_P - r_D) \\ \theta_P^D \\ \phi_P^D \end{bmatrix} = \begin{bmatrix} k(r_P - r_T) \\ \theta_P^T \\ \phi_P^T \end{bmatrix} \quad (5.18)$$

for some scalar function $k(t)$, where r_T, r_D, r_P are the lengths of the vectors $\mathbf{r}_T, \mathbf{r}_D, \mathbf{r}_P$ respectively.

First we consider the problem in two dimensions. We make a co-ordinate shift to scale the dynamics such that \mathbf{r}_P is at the origin. The physical positions of a camouflaged 2D engagement at a particular instant in time are shown in Figure 5.10. Clearly,

$$\theta_D = \theta_T = \theta_R \quad (5.19)$$

and we have shown in chapter 2 that

$$\dot{\theta}_D = \dot{\theta}_T. \quad (5.20)$$

Now, the dynamic description of the pursuer motion is

$$\dot{\sigma} = \frac{a_D \cos(\sigma - \theta + \eta)}{v_D} \quad (5.25)$$

and our M.C. dynamic constraint is

$$v_D \sin(\sigma - \theta) = r_D \dot{\theta}. \quad (5.26)$$

Differentiating and simplifying, we end up with

$$a_D \sin(\sigma - \theta + \eta) \sin(\sigma - \theta) = \dot{r}_D \dot{\theta} + r_D \ddot{\theta} - v_D (\dot{\sigma} - \dot{\theta}) \cos(\sigma - \theta) \quad (5.27)$$

$$= 2\dot{r}_D \dot{\theta} + r_D \ddot{\theta} - \dot{\sigma} \dot{r}_D. \quad (5.28)$$

Substitute (5.25) to find

$$a_D \cos \eta = 2\dot{r}_D \dot{\theta} + r_D \ddot{\theta} \quad (5.29)$$

Expressed in terms of one variable, this fundamental differential equation is:

$$\ddot{r}_D = (2\dot{r}_D \dot{\theta} + r_D \ddot{\theta}) \tan \eta. \quad (5.30)$$

From this equation, we can determine the requisite acceleration for any particular pursuer path r_D , as defined by $r_D = kr_T$. Moreover, if the target angular acceleration $\ddot{\theta} = 0$, then we can find a solution for the pursuer path $r_D(t)$ in terms of the constraining angular position of T, θ :

$$r_D(t) = c_1 + c_2 \int e^{2 \tan \eta \theta(t)} dt. \quad (5.31)$$

where c_1, c_2 are dependent on initial conditions. If $\ddot{\theta}$ is not zero, then the fundamental dynamic equation (5.30) is not generally solvable in closed form (at least analytically).

Some examples of the acceleration required to achieve particular camouflaged pursuit trajectories are now derived:

5.6.3 Required acceleration for a non-maneuvering target

Let \dot{r}_T be constant. Then $\dot{v}_T = 0$, hence

$$\ddot{r}_T = r_T \dot{\theta}^2 \quad (5.32a)$$

$$\ddot{\theta} = -2 \frac{\dot{r}_T}{r_T} \dot{\theta} \quad (5.32b)$$

therefore the required acceleration command is

$$a_c = 2\dot{\theta} \frac{\dot{r}_D - r_D \frac{\dot{r}_T}{r_T}}{\cos \eta}. \quad (5.33)$$

Since the engagement is camouflaged, we know $r_D = kr_T$, $\dot{r}_D = k\dot{r}_T + \dot{k}r_T$, and we can extrapolate the desired range and range-rate from these conditions.

Example: constant k

Let k be a constant. If $k(t) = k_0 \forall t$, and the target does not change speed or direction, then no acceleration is required for the pursuer to remain camouflaged. We can thus use this scenario as a test-case for the control equations. To proceed: $\dot{r}_D = k\dot{r}_T$, hence

$$\dot{r}_D = k\dot{r}_T. \quad (5.34)$$

Moreover,

$$v_D \cos(\sigma - \theta) = v_D^r = k\dot{r}_T \quad (5.35)$$

so together with (5.29) and (5.32b), we obtain

$$a_c = 2\dot{\theta} \frac{k\dot{r}_T - k\dot{r}_T}{\cos \eta} \quad (5.36)$$

$$= 0 \quad (5.37)$$

as required.

Example: extremal k , from Chapter 2

Since we have designated \mathbf{r}_P as the origin, we can write the length of the optimal energy path vector as

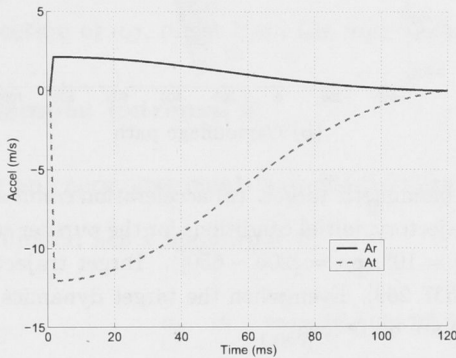
$$r_D(t) = c_1 t + c_2 \quad (5.38)$$

for some constants c_1 and c_2 dependent on initial conditions. From the previous calculations, the magnitude of the control acceleration is

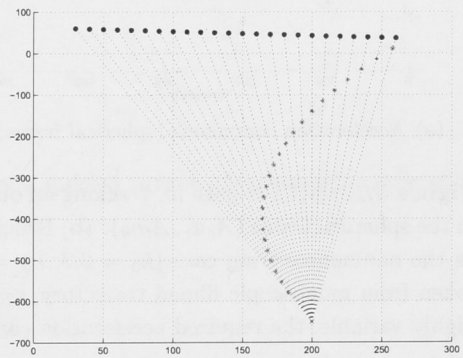
$$a_C = 2\dot{\theta} \frac{(k\dot{r}_T + r_T \dot{k}) - k\dot{r}_T}{\cos \eta}, \quad (5.39)$$

hence for an energy-extremal trajectory the acceleration required of the pursuer to remain camouflaged can be written

$$a_c = 2\dot{\theta} \frac{c_1 r_T - \dot{r}_T (c_1 t + c_2)}{r_T^2 \cos \eta}. \quad (5.40)$$



(a) Acceleration commands (spherical frame)



(b) Camouflage path

Figure 5.11: Motion Camouflage path for a non-maneuvering target using PN-derived acceleration commands. (a) acceleration commands in the spherical frame ($A_r \mathbf{e}_r, A_t \mathbf{e}_\theta$). (b) Resulting trajectory, given $\dot{k}_0 = 0.2$, $k_0 = 0.1$, $\eta = 10^\circ$. In cartesian co-ordinates, the initial conditions were: $\mathbf{r}_T(0) = [30, 60]$, $\dot{\mathbf{r}}_T = [200, -20]$, $\mathbf{r}_P = [200, -650]$.

Compare the acceleration required for an LQR solution for the same trajectory (Figure 5.12). Even without the sharp control spike at the beginning of the interaction, the command effort required to capture the target in the same time as the PN guided action-optimal form is considerably higher across the entire interaction.

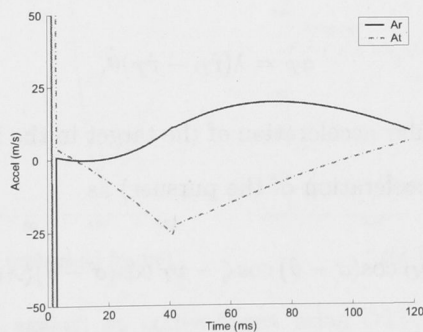


Figure 5.12: Control commands for a linear quadratic regulator solution to the same target trajectory as Figure 5.11(b).

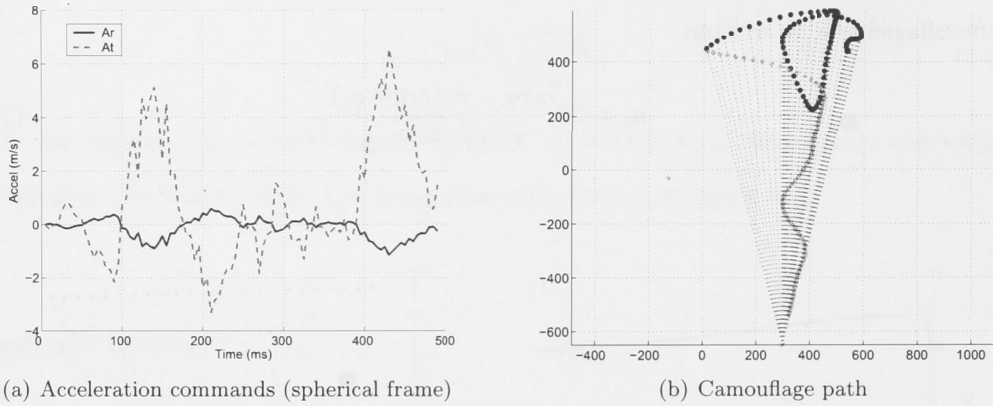


Figure 5.13: MCPN path for tracking an oblivious biomimetic target. (a) acceleration commands in the spherical frame ($A_r \mathbf{e}_r, A_t \mathbf{e}_\theta$). (b) Resulting trajectory, initial conditions for the pursuer same as the nonmaneuvering case ($\dot{k}_0 = 0.2, k_0 = 0.1, \eta = 10^\circ, \mathbf{r}_P = [200 - 650]$). Target trajectory taken from monoscopic filmed trajectory, $\mathbf{r}_T(0) = [537, 269]$. Even when the target dynamics are highly variable, the required acceleration commands are quite low.

5.6.4 Solution for a maneuvering target

If T is also governed by a PN equation of the form

$$a_T = \lambda \dot{r} \dot{\theta}$$

that is,

$$a_T = \lambda(\dot{r}_D - \dot{r}_T)\dot{\theta}, \quad (5.41)$$

then we can write the angular acceleration of the target in the inertial (P) reference frame (and hence the required acceleration of the pursuer) as

$$\ddot{\theta} = \frac{\dot{\theta}}{r_T} [\lambda v_D \cos(\sigma - \theta) \cos \zeta - v_T \cos(\sigma - \theta)(\lambda \cos \zeta + 2)]. \quad (5.42)$$

Hence the rate of change of direction of the velocity vector necessary to maintain camouflage is

$$a_C = \frac{\dot{\theta}}{\cos \eta} \left[2\dot{r}_D + \frac{r_D}{r_T} (\lambda \dot{r}_D \cos \zeta - \dot{r}_T (\lambda \cos \zeta + 2)) \right]. \quad (5.43)$$

Example: constant k

With constant k , $\dot{r}_D = k\dot{r}_T$, hence the magnitude of the control acceleration for a camouflaged path reduces to

$$a_C = k\lambda \frac{\cos \zeta}{\cos \eta} \dot{r} \dot{\theta}. \quad (5.44)$$

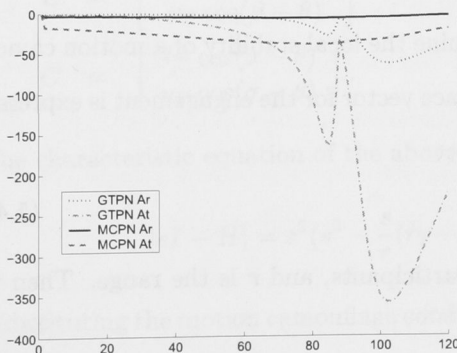
which is a straightforward GTPN law. \dot{r} is the range, $\dot{r}_T - \dot{r}_D$. Recall that η is the angular direction of a_C , offset from the unit vector \mathbf{e}_θ .

Example: extremal k

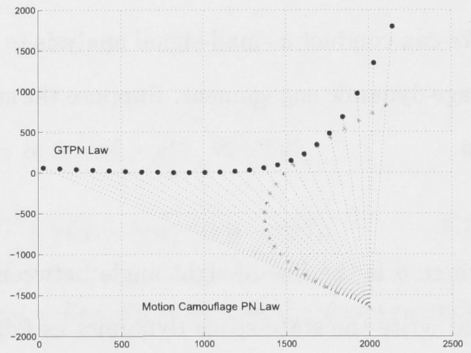
For an energy-extremal camouflaged path against a guided target, the desired acceleration command has a magnitude of

$$\begin{aligned} a_c &= \frac{\dot{\theta}}{\cos \eta} \left[k\lambda \cos \eta \dot{r} + 2r_T \dot{k} \right] \\ &= \frac{\dot{\theta}}{r_T \cos \eta} \left[(c_1 t + c_2) \lambda \cos \eta \dot{r} + 2(c_1 r_T - (c_1 t + c_2)) \right] \end{aligned} \quad (5.45)$$

where c_1 and c_2 are the energy constants which can be determined from initial conditions. Note that obtaining a path that is locally energy-minimal requires an estimate of the target's position relative to the static point of the engagement, which is not necessarily biologically plausible. However the trajectory may still be useful for an artificial system with range-finding capabilities.



(a) Acceleration commands (spherical frame)



(b) Camouflage path

Figure 5.14: MCPN path against an active target using GTPN guidance. (a) acceleration commands in the spherical frame for both pursuer and target ($A_r \mathbf{e}_r, A_t \mathbf{e}_\theta$). (b) Resulting trajectory: initial conditions for the pursuer are $[1803, -1479]$, ($\dot{k}_0 = 0.08$, $k_0 = 0.1$, $\eta = 10^\circ$, $\mathbf{r}_P = [2000 - 1650]$). Target initial conditions in the cartesian inertial frame are $\mathbf{r}_T(0) = [30, 60]$, $\dot{\mathbf{r}}_T(0) = [200, -20]$.

5.6.5 PN guidance for motion camouflage

To close the loop and produce a stable guidance law, we proceed as follows. Recall that a PN law takes the form

$$a_C = N v_D \dot{\theta}. \quad (5.46)$$

For $\ddot{\theta} = 0$, we find

$$N = 2 \frac{\cos(\sigma - \theta)}{\cos \eta}. \quad (5.47)$$

If σ is applied at a constant angle to the line-of-sight vector, then we simply obtain a GTPN law. However, this condition may not always be desirable. For a changing $(\sigma - \theta)$, N is a dynamic gain with known parameter variation. In both cases, we intuit that capturability is dependent on then angle the acceleration is applied at, η . It has been shown that a PN guidance law will produce a capture trajectory if $N \geq 3$ [Fri96]. Clearly, the larger value chosen for η (ie the greater the proportion of the acceleration applied in the direction of the line-of-sight vector), the higher N becomes, hence the higher the chance of capture, as might be expected.

For $\ddot{\theta} \neq 0$, we require an augmented law which takes the manoeuvres of the target into account. The derivation of such a law is of interest, but outside the scope of this chapter.

5.6.6 Stability

We can conduct a small-signal analysis to determine the local stability of a motion camouflage dynamic engagement. Suppose the state-space vector for the engagement is expressed as

$$\begin{bmatrix} \dot{\theta} \\ \dot{r} \end{bmatrix} \quad (5.48)$$

where θ is the line-of-sight angle between the participants, and r is the range. Then we can write the state-space dynamics as follows:

$$\dot{\theta} = \frac{1}{r} (v_T \sin(\beta - \theta) - v_D \sin(\sigma - \theta)) \quad (5.49)$$

$$\dot{r} = v_T \cos(\beta - \theta) - v_D \cos(\sigma - \theta) \quad (5.50)$$

$$\dot{\sigma} = \frac{a_D}{v_D} \cos(\sigma - \theta + \eta) \quad (5.51)$$

$$\dot{\beta} = \frac{a_T}{v_T} \cos(\sigma - \theta + \eta). \quad (5.52)$$

To conduct a small-signal analysis, we assume v_T and v_D are constant over a short time period, and examine the system response to small changes in the state-space variables, $\delta\theta$, δr , $\delta\sigma$, $\delta\beta$. It is worth noting at this point that if v_T and v_D are assumed constant, then a_D and a_T can be assumed negligible, which simplifies the problem considerably.

$$\begin{aligned}\delta\dot{\theta} &= \frac{\delta r}{r^2}(v_T \sin(\beta - \theta) - v_D \sin(\sigma - \theta)) + \\ &\quad \frac{1}{r}(-v_T(\delta\beta - \delta\theta) \cos(\beta - \theta) + v_D(\delta\sigma - \delta\theta) \cos(\sigma - \theta))\end{aligned}\quad (5.53)$$

$$\delta\dot{r} = v_T(\delta\beta - \delta\theta) \cos(\beta - \theta) - v_D(\delta\sigma - \delta\theta) \cos(\sigma - \theta) \quad (5.54)$$

$$\delta\dot{\sigma} = 0 \quad (5.55)$$

$$\delta\dot{\beta} = 0 \quad (5.56)$$

We can write this as

$$\begin{bmatrix} \delta\dot{\theta} \\ \delta\dot{r} \\ \delta\dot{\sigma} \\ \delta\dot{\beta} \end{bmatrix} = H \begin{bmatrix} \delta\theta \\ \delta r \\ \delta\sigma \\ \delta\beta \end{bmatrix} \quad (5.57)$$

such that

$$H = \left[\begin{array}{c|c|c} A & B & C \\ \hline 0_{2,4} & 0_{1,2} & 0_{1,2} \end{array} \right] \quad (5.58)$$

where

$$\begin{aligned}A &= \begin{bmatrix} \frac{1}{r}(v_T \cos(\beta - \theta) - v_D \cos(\sigma - \theta)) & \frac{1}{r}(v_T \sin(\beta - \theta) - v_D \sin(\sigma - \theta)) \\ v_D \cos(\sigma - \theta) - v_T \cos(\beta - \theta) & 0 \end{bmatrix} \\ B &= \begin{bmatrix} \frac{-v_T}{r} \cos(\beta - \theta) \\ v_T \cos(\beta - \theta) \end{bmatrix} \\ C &= \begin{bmatrix} \frac{v_D}{r} \cos(\sigma - \theta) \\ v_D \cos(\sigma - \theta) \end{bmatrix}.\end{aligned}$$

The characteristic equation of the above system is $\det(sI - H)$. We find

$$|sI - H| = s^2(s^2 - \frac{s}{r}(\dot{r}_T - \dot{r}_D) - \frac{1}{r}(r_T\dot{\theta}_T - r_D\dot{\theta}_D)(\dot{r}_D - \dot{r}_T)). \quad (5.59)$$

Substituting the motion camouflage conditions $r_D = kr_T$, $\theta_D = \theta_T$ into the above equation, we discover

$$|sI - A| = s^2(s^2 - s\frac{\dot{r}}{r} - \dot{r}\dot{\theta}). \quad (5.60)$$

The eigenvectors of the characteristic matrix are therefore real and negative if

$$\frac{\dot{r}}{r} < 0, \quad (5.61)$$

hence the system is stable if the following conditions apply:

$$\text{if } r_T > r_D \quad \text{then} \quad \dot{r}_T < \dot{r}_D \quad (5.62)$$

$$\text{if } r_T < r_D \quad \text{then} \quad \dot{r}_T > \dot{r}_D. \quad (5.63)$$

Note that if equation (5.63) holds, then D is not camouflaged with respect to T , but rather T is camouflaged with respect to D . We generally ignore this case as artificial pursuit scenarios rarely encompass role-swapping.

5.7 Discussion

5.7.1 Limitations of the biomimetic decoupled control

The proposed controller for a dragonfly is a decoupled first-order model which separately controls for flight speed and angular velocity using visual inputs. The forward speed is controlled by the apparent speed of the target scaled by the range between the participants, the angular velocity is modeled as having a linear relationship to the line-of-sight error angle velocity. The controller itself is by no means comprehensive, and other visual cues than those incorporated are likely responsible for characteristics of the interactive behaviour seen in dragonflies - elevation, predictive tracking and looming effects are but a few. In spite of this, in its current form the controller successfully mimics many test trajectories, with little tuning required.

Although simplicity is a virtue in control laws, it seems likely that the actual controller used by dragonflies is slightly more involved than that presented above. Not every interaction could be successfully mimicked in both flight speed or angular velocity using a constant gain. It is possible that the gains vary throughout the engagement, affected by headwind and other environmental influences. Hence if conditions change during the chase, the gain required to match the trajectory may also change, sometimes abruptly. Mizutani (unpublished) has had some success in modeling dragonfly encounters using an heuristic dynamic gain with PN guidance, however further investigation is required into whether these dynamic gain functions correspond to real dynamic features of the engagement which influence the flight paths.

Simplifications and approximations of the dynamic features were also made. The most obvious was the modeling of the simulated dragonfly as a point mass, with no wing

kinematics and, perhaps more importantly, no body axis information. The aerodynamics of flapping wing flight influence heavily the inertial forces and body torque acting on the insect, but were not included here except as a subset of the heuristic gain. The body axis information lost from the controller has possibly a more significant effect on the deviations of the model from the real trajectories, especially since we are considering the visual mechanisms underlying the flight control. Investigating a way of incorporating body axis angle into the current model would be of great value, especially since it does not appear to be a straightforward function of visual fixation. Noise was not included in the simulation, and the retinal size was modeled as a simple linear function of distance, when in reality there is likely to be error in the measurement, induced by (a) motion blur, (b) retinal location (since resolution differs across the eye), and (c) (perhaps most significant), viewing direction, since the target will appear largest when viewed perpendicularly, but quite small as seen from the head or directly behind. Forces due to translatory inertia and wind effects were not taken into account.

5.7.2 Proportional Navigation and biomimetic control

Minimizing the angular error between the actual and the desired retinal position of the target is a feature of both biological and artificial pursuit systems ([CL75], [RW69], [LC74] [Ros83]). Traditionally, in pursuit, the target is held steady in the frontal region of the visual field. However dragonflies, whether as a feature of some type of predictive tracking or a result of the responsive nature of the target, are apparently poor fixators when compared with other insects. What response there is to change in the line-of-sight position is most evident in the *course* angular velocity, ie the change in flight direction, rather than a change in orientation. When modeling the control system as a PN guided system, this distinction becomes moot since we assume a body axis orientation aligned with flight direction. In reality, this is not necessarily the case. As mentioned above, a method of incorporating the body axis orientation into the controller might give valuable insight into the behaviour of the insects.

It was demonstrated that the controller used could be represented by a generalized true proportional navigation controller. A GTPN law for achieving motion camouflage was then derived. This law does require knowledge about the position of the static point,

at least in terms of its position relative to the target, in order to determine the necessary angular movement. Range to the target is less vital, although may be required under certain conditions in order to ensure capture. In most cases, though, the pursuer may only need to have a good estimate of the velocity of the target, and know its own distance from the static point of the engagement, a task which is simplified if the initial position is chosen to be the fixed point of the interaction.

A comparison of the biomimetic law and that derived for motion camouflage shows that the dragonfly guidance model will naturally produce motion camouflage if the following conditions are met:

Firstly, we use the proportional navigation version of the biomimetic law, such that

$$\begin{aligned} a_D &= \gamma_1 \gamma_2 \frac{r \dot{\rho} + v_0}{\cos(\sigma - \theta + \eta)} \dot{\theta} \\ &= \Gamma \frac{v^\epsilon}{\cos(\sigma - \theta + \eta)} \dot{\theta} \end{aligned} \quad (5.64)$$

where $\Gamma = \gamma_1 \gamma_2$ and v^ϵ is an estimate of the target speed.

Secondly, if v^ϵ is reasonably accurate and the gain function γ is not untoward, then the forward speed of the pursuer will match that of the target as per the decoupled control law, and we can say that a motion camouflaged trajectory will be produced if we choose Γ such that

$$\Gamma = \frac{2 \cos(\sigma - \theta + \eta)}{\cos \eta} \left(1 - \frac{r_D}{r_T}\right). \quad (5.65)$$

This equation depends primarily on the relative distances of the insects from the static point, and the heading direction of the pursuer (σ). Assuming the insects concerned are capable of range measurement, it is possible that certain features of an interaction could conspire to bring about an approximation of this gain value, especially given that motion camouflage has been shown to be a more effective capture strategy than pure pursuit [Gle04]. An insect trying to track or capture prey, a conspecific, etc., may thus stumble upon a motion camouflaged trajectory while pursuing an entirely different objective.

Discussion

6.1 Thesis summary

The mechanics behind visually-guided pursuit are of enormous interest to investigators in the fields of animal behaviour as well as the control of autonomous aerial machines. Motion camouflage, a subset of pursuit, has recently received particular attention because of its elegant structure and potential for stealth applications. In addition, the observations of its use amongst insects imply there must exist methods of achieving camouflage which rely neither on extensive and precisely detailed knowledge of the environment, nor on intricate and complex computations.

In this study, I first approached motion camouflage from a purely analytical viewpoint. Using as a starting point Glendinning's [Gle04] research, I derived in Chapter 1 a dynamic law which was both a necessary and sufficient condition for camouflage to have occurred. Then by applying the theory of Lagrangian optimization, I established a 'natural' form of action-optimal motion camouflage - ie the paths a camouflaged trajectory would naturally take if these camouflage requirements were the only forces acting on the pursuing body.

Chapter 2 explored possible algorithms for implementing camouflage in artificial systems, and showed that applying linear dynamics is sufficient to generate camouflaged paths that are stable, robust, and unlikely to encounter unexpected singularities. Using a linear quadratic-cost based controller, first in two then three dimensions, I was able to successfully produce camouflaged trajectories. However the drawbacks of such a method were significant. Uncapped, the need to produce an accurately camouflaged path resulted occasionally in extreme control actions, to such a degree that most autopilots would not be able to respond to the required command in time. On the other hand, if a limitation was placed on the control action, or the cost of an excessive action was weighted more

heavily, the result was a decline in the system performance. If the path taken by the target was highly non-linear, this decrease could be quite marked. In addition, the nature of an optimal LQR controller is such that the system is traditionally first solved for its desired endpoint, then iterated backwards to arrive at the initial conditions. This method works well if the target is on a predictable path, but becomes unwieldy and loses efficacy if it is not, because the whole future trajectory must be re-solved each time the target moves, increasing the computations required many-fold.

In an attempt to eliminate the latter problem with the optimal LQR controller, I then designed a solution using a three-dimensional greedy controller. This solved the issue of backwards iteration by using an engagement horizon limited to the next discrete time interval, minimizing cost only over that short instance and removing the requirement for costly computations when confronted with a non-predictable target path.

However the greedy control formulation was still handicapped by the tradeoff between large control action and camouflage accuracy. Moreover, its finite-horizon meant that while it worked well for stealthy shadowing, it would not result in a capture path except under very restrictive and unnatural conditions. Greedy LQR camouflage may certainly have its uses in tracking applications, but without additional strictures placed upon it, will not result in target capture.

To find a solution for the performance tradeoff between control commands and camouflage accuracy, I designed an autopilot which could respond quickly to large control actions without becoming unstable. Instead of a rule-based, decoupled attitude control, I sought an holistic solution which could take advantage of the many possible attitudes which could potentially produce a given control acceleration vector.

Although highly non-linear, the resulting autopilot was successfully implemented on a linux-based F16 simulator, where its responsiveness was restricted solely by the physical limitations of the aircraft itself. Several analytic solutions to various controller inputs were presented at the end of Chapter 2, including a simulation using greedy LQR commands for motion camouflage.

Even with a flexible autopilot which could respond well to large control accelerations, the linear dynamic solutions to motion camouflage still suffered from their computational intensity and inaccuracies in the face of non-linearities, and required precise knowledge of

target position and dynamics to achieve a camouflaged path. When noise and measurement limitations were introduced to the controller, the performance suffered, although not to an excessive degree. However the linear quadratic cost translated poorly into a moving polar reference frame, where the idea of measuring cost as a linear deviation from an invisible ‘constraint line’ seemed contrived and artificial.

In Chapter 3, I returned to the analysis of insect motion camouflage in the hope of identifying relevant control laws. The starting point of my experimental work was an earlier behavioral study published by Mizutani, et al [MCS03], where male dragonflies in territorial disputes had been recorded apparently using camouflage. I analysed flights involving interactions between two or more males, in two and three dimensions, seeking information which could be used to build a phenomenological model of the dragonfly guidance system. The limitations of filming these interactions in natural settings are great, as discussed. Nevertheless, some overall characteristics of dragonfly and satellite fly responses to visual targets during instances of motion camouflage could be extracted from available video footage.

The speed of the target influenced the forward speed of the pursuer, such that the relative velocity between the insects was small compared to their forward speed. In addition, the apparent retinal motion of the target was closely related to the changes in flight direction of the pursuer. Camouflaged sequences were observed quite frequently in both dragonfly and satellite-fly/wasp interactions, although they were often of short duration, suggesting they occurred as a behavioral subset of an overall guidance strategy.

A comparison of the camouflaged sequences in these two distinct types of insect interaction revealed that the rate of the line of sight angle from pursuer to target was closely related to the rate of the change in flight direction in naturally occurring camouflaged flight.

In Chapter 4, I used the flight characteristics found in Chapter 3 to build an approximate model of the dragonfly guidance system. The forward speed of the model is governed by the apparent speed of the target and the range between the participants; the change in flight direction is proportional to the rate of the line of sight to the target insect. Both pursuer and target were simulated as point masses, so the effect of body axis direction on either pursuer velocity or target retinal size and position were not modeled. Processing

delay was incorporated simply as a measurement lag gleaned from experimental results, with no attempt made to accurately simulate neuronal processing time.

The model dragonfly, when compared to that of the 'real' pursuer in filmed two-body trajectories, performed fairly well in terms of matching gross flight characteristics, performing qualitatively similar turns and speed responses to those of the real dragonfly. To further refine and improve the controller, it is suggested it be tested on flights of dragonflies under more predictable and controlled conditions, for example artificial prey pursuit in a fully observable arena.

A change in flight direction proportional to the line of sight error rate is a key feature of a class of guidance laws known as proportional navigation (PN) guidance. I hence manipulated the controller equations and found they could be formulated as an acceleration-based control. Thus inspired by the biologically-based guidance model and the successful models developed by Justh, et al, [JK06], [RJK06], I developed a PN-based controller for static-point motion camouflage in two dimensions. The controller fits well into the biomimetic model for dragonfly guidance. As designed, even range estimation is not necessary to achieve camouflage, although some measurement of range is required for approach or capture. However inaccuracies in this measurement will not affect the accuracy of the camouflage, although the problems with overshoot outlined in Chapter 3 should still be taken into consideration.

6.2 Future Work

Models of insect control systems have largely been confined to highly controlled situations in which control parameters can be easily manipulated. Modeling free-flying insects without the benefits of repeatable experimentation is far more of a challenge. Much work remains to be done on accurately describing and modeling dragonfly guidance systems. The current model does not fully account for some of the more complex and unusual behaviour patterns observed in the insects. Nevertheless, it is unlikely that the flight system, once unraveled, will be revealed to be significantly more complex than that presented here. A way to more fully explore the nuances of interaction and gain a more complete picture of the significant visual cues used to navigate during a non-predatory chase might involve using a dummy target (as has been done by Land and Collett [Lan97], Boeddeker and

Egelhaaf [BKE03], etc). However my work suggests clear developmental directions for developing camouflage strategies in man-made systems. A three-dimensional version of the PN system described in Chapter 5 can be developed in a straightforward way. Using this model, or even one of the linear models described earlier, in conjunction with a force-based autopilot such as that developed in Chapter 2, implementing camouflage in a sufficiently capable unmanned craft should not be too arduous a task.

Lagrangian Optimization and Lagrange Multipliers

Lagrange, in his seminal work of 1765 *Mecanique Analytique*, first introduced the principle of virtual velocities, and from that context conceived of the analysis method now known as Lagrangian optimization and the constructs termed Lagrange Multipliers.

A.1 Virtual Velocity

To quote the man himself:

By virtual velocity, it has to be meant the one that a body in an equilibrium condition would receive if the equilibrium were interrupted, namely, the velocity that the body would really assume in the first instant of movement; the principle consists in this: the forces are in equilibrium if they are in the inverse proportion to their virtual velocities.

J. L. Lagrange, *Mecanique Analytique*, 1765, 17-18

The quantity of force times velocity has had a number of different appellations over the years, but here we refer to it as Lagrange did, as the ‘moment’, and hence the product of a force and its virtual velocity may be known as the ‘virtual moment’. Thus we arrive at the formal declaration of the principle of virtual velocity: A body will be in equilibrium iff the (algebraic) sum of the virtual moments is zero [Bus03].

For example, if there exists a point with two forces applied to it, P and Q , and if p and q are the respective directions of P and Q , then the body is in equilibrium if

$$P \frac{dp}{dt} + Q \frac{dq}{dt} = 0. \quad (\text{A.1})$$

Applying this principle to the study of a system of points at equilibrium, we can analyze the conditions of translational and rotational equilibrium. However such a analysis may be algebraically complex. By using the method of Lagrange Multipliers, the analysis can be conducted in a simpler, more general way, and we can look at the equilibrium of a system under constraints.

A.2 Multipliers and constrained systems

Firstly, a brief aside: We have explained the virtual moment in terms of the differential functions $\frac{dp}{dt}$, $\frac{dq}{dt}$, etc. In practise, Lagrange replaced these derivative terms in his analysis

with the quantities dp, dq , etc. His justification:

In order to express this principle by means of formulas, we suppose that the forces P, Q, R are directed along given lines and that they are in equilibrium; let p, q, r denote the lines that are the directions of the forces P, Q, R . We indicate the variations or differences (now called differentials) of these lines with dp, dq, dr and suppose they are caused by an arbitrary infinitesimal change in the position of the different bodies or points of the system. It is clear that these differences will express the spaces that are covered in the same instant by the actions of the forces P, Q, R . In order to simplify the treatment, it is possible to consider these differences instead of the velocities.

J. L. Lagrange, *Mecanique Analytique*, 1965, 24

Consider the equilibrium of a material point (or a system of material points) subjected to constraints. If the constraining equations are $\mathcal{L} = 0$, $\mathcal{M} = 0$, and if \mathcal{L} and \mathcal{M} are functions of several variables, it follows necessarily that $d\mathcal{L} = 0$, $d\mathcal{M} = 0$. Hence, let μ, λ be arbitrary real numbers, then $\lambda d\mathcal{L} = 0$, $\mu d\mathcal{M} = 0$, etc. By considering the sum of all the moments of the forces that must be in equilibrium, we can add the different differential functions that must be zero if the system is to satisfy the requisite constraints. To do this, we multiply each function by an indeterminate coefficient and set the whole sum equal to zero. We therefore have a differential equation which can be treated as an ordinary equation with maxima and minima, etc. Hence the general equation of equilibrium for a constrained system is

$$Pdp + Qdq + \dots + \lambda d\mathcal{L} + \mu d\mathcal{M} = 0. \quad (\text{A.2})$$

Considering the problem in an orthogonal reference frame, we can for each orthogonal variable develop a particular equation of equilibrium. For example, in the direction x ,

$$P \frac{dp}{dx} + Q \frac{dq}{dx} + \dots + \lambda \frac{d\mathcal{L}}{dx} + \mu \frac{d\mathcal{M}}{dx} = 0.$$

From a physical point of view, the reaction of the constraint is equated to an agent force. Hence λ, μ are equivalent to forces and the expressions $\lambda d\mathcal{L}$ and $\mu d\mathcal{M}$ represent the virtual moments realized by these forces. The principle advantage of this method is that it allows us to treat the problems with constraints in the same manner as free problems.

For example: If \exists two forces P, Q on a point, and a constraint represented by the equation $\mathcal{L} = 0$ is added, then in an orthogonal reference frame (x, y, z) we can write

$$P \frac{dp}{dx} + Q \frac{dq}{dx} + \lambda d\mathcal{L} dx = 0 \quad (\text{A.3})$$

$$P \frac{dp}{dy} + Q \frac{dq}{dy} + \lambda d\mathcal{L} dy = 0 \quad (\text{A.4})$$

$$P \frac{dp}{dz} + Q \frac{dq}{dz} + \lambda d\mathcal{L} dz = 0 \quad (\text{A.5})$$

$$\mathcal{L} = 0. \quad (\text{A.6})$$

If we interpret the multiplier as a new co-ordinate, then equation A.6 can be replaced by the equally valid equation

$$P \frac{dp}{d\lambda} + Q \frac{dq}{d\lambda} + \lambda d\mathcal{L} d\lambda = 0. \quad (\text{A.7})$$

Hence the solution of the problem of the equilibrium of a point (or a system of points) is analogous to the problem of determining the maximum or minimum of a function under constraints [Lei81].

Attitude Representation

The attitude of a rigid body is defined as the orientation of a set of axes fixed to the body with respect to a set of axes fixed to the earth. The attitude is represented by a rotation matrix R which maps the axes of the body to the axes of the earth. The body axes are denoted by \mathbf{e}_i and the earth axes by \mathbf{e}_i^e .

A.2.1 Rotation matrices

A rotation matrix is a matrix which rotates the axes of a rigid body without changing their length. The special orthogonal group of all rotation matrices is denoted by $SO(3)$. The elements of a rotation matrix R are represented as follows:

$$R = \begin{bmatrix} r_{11} & r_{12} & r_{13} \\ r_{21} & r_{22} & r_{23} \\ r_{31} & r_{32} & r_{33} \end{bmatrix} \quad (A.2.1)$$

$$= \begin{bmatrix} r_{11} & r_{12} & r_{13} \\ r_{21} & r_{22} & r_{23} \\ r_{31} & r_{32} & r_{33} \end{bmatrix} \quad (A.2.2)$$

There are two possible conventions for defining the axes of a rigid body. The matrix can be defined to map the axes of the body to the axes of the earth, or to map the axes of the earth to the axes of the body. Both are equally valid, but the two resulting matrices are inverses (and transposes) of each other.

A.2.1.1 Coordinate transformations

The rotation matrix for the rest of the world is $R = I$, where I is the identity matrix. If the axes of the body are rotated by an angle θ about the \mathbf{e}_3 axis, then the rotation matrix is given by

$$R = \begin{bmatrix} \cos \theta & -\sin \theta & 0 \\ \sin \theta & \cos \theta & 0 \\ 0 & 0 & 1 \end{bmatrix} \quad (A.2.3)$$

This expression applies to rotation about the \mathbf{e}_3 axis. If the axes of the body are rotated by an angle θ about the \mathbf{e}_1 axis, then the rotation matrix is given by

Attitude Representation

The attitude of a rigid body in space is traditionally represented in one of three ways: (1) by a rotation matrix, (2) by a Euler triple angle, (3) by unit quaternions.

When describing attitude, two co-ordinate systems must be considered. The first is the world, or inertial, frame, which is fixed in inertial space and is denoted by I . The second is the body co-ordinate system, which is rigidly attached to the object under consideration, and is denoted by B .

B.1 Rotation matrices

A rotation matrix is a matrix whose multiplication with a vector rotates the vector while preserving its length. The special orthogonal group of all 3x3 rotation matrices is denoted by $SO(3)$. The elements of a rotation matrix R are referenced as follows:

$$R = \begin{bmatrix} \mathbf{r}_1 & \mathbf{r}_2 & \mathbf{r}_3 \end{bmatrix} \quad (\text{B.1})$$

$$= \begin{bmatrix} r_{11} & r_{12} & r_{13} \\ r_{21} & r_{22} & r_{23} \\ r_{31} & r_{32} & r_{33} \end{bmatrix}. \quad (\text{B.2})$$

There are two possible conventions for defining the rotation matrix that encodes the attitude of a rigid body. The matrix can be written in such a way as to map body-fixed co-ordinates onto world co-ordinates, or to map world (inertial) co-ordinates onto body co-ordinates. Both are equally valid, and the two conversion matrices thus defined are inverses (and transposes) of each other.

B.1.1 Co-ordinate transformations

The rotation matrix for the rest of this appendix is defined as follows: if $\mathbf{x} \in \mathbb{R}^3$ is a vector in the world co-ordinates, and $\mathbf{x}' \in \mathbb{R}^3$ is the same vector expressed in the body co-ordinate system, then the rotation matrix for conversion between the two has the following properties:

$$\mathbf{z}' = R\mathbf{z} \quad (\text{B.3})$$

$$\mathbf{z} = R^T\mathbf{z}'. \quad (\text{B.4})$$

These expressions apply to vectors, which by definition are relative quantities lacking a position in space. To transform a point from one co-ordinate system to the other, we must subtract the offset to the origin of the target co-ordinate system before applying the rotation matrix. Let \mathbf{z}, \mathbf{z}' be as before, and let the origins of the two co-ordinate systems

be designated \mathbf{x}_I and \mathbf{x}_B respectively (note that $\mathbf{x}_I, \mathbf{x}_B$ are both in the inertial frame, so $\mathbf{x}_I = 0$ and $\mathbf{x}'_B = 0$ by definition, however \mathbf{x}'_I and \mathbf{x}_B may not). Then we may write:

$$\mathbf{z}' = R(\mathbf{z} - \mathbf{x}_B) = R\mathbf{z} + \mathbf{x}'_I \quad (\text{B.5})$$

$$\mathbf{z} = R^T(\mathbf{z}' - \mathbf{x}'_I) = R^T\mathbf{z}' + \mathbf{x}_B. \quad (\text{B.6})$$

Substituting $\mathbf{z} = 0$ into B.5 and $\mathbf{z}' = 0$ into B.6 yields

$$\mathbf{x}'_I = -R\mathbf{x}_B \quad (\text{B.7})$$

$$\mathbf{x}_B = -R^T\mathbf{x}'_I. \quad (\text{B.8})$$

When a rotation and translation are combined in this manner, we call the procedure a co-ordinate transformation, and can easily write the necessary equations in the form of a matrix termed a co-ordinate transformation matrix, as follows:

$$\begin{bmatrix} \mathbf{z}' \\ 1 \end{bmatrix} = \begin{bmatrix} R & \mathbf{z}'_I \\ \mathbf{0}^T & 1 \end{bmatrix} \begin{bmatrix} \mathbf{z} \\ 1 \end{bmatrix} \quad (\text{B.9})$$

$$\begin{bmatrix} \mathbf{z} \\ 1 \end{bmatrix} = \begin{bmatrix} R^T & \mathbf{z}_B \\ \mathbf{0}^T & 1 \end{bmatrix} \begin{bmatrix} \mathbf{z}' \\ 1 \end{bmatrix}. \quad (\text{B.10})$$

B.1.2 Co-ordinate rotations

A co-ordinate rotation is a rotation about a single co-ordinate axis. Let the co-ordinate rotation about the x-axis be designated 1, about the y-axis designated 2, and about the z-axis designated 3. Then the corresponding co-ordinate rotations $R_i : \mathbb{R} \rightarrow SO(3)$, for $i \in [1, 2, 3]$ are [Cra89]

$$R_1(\alpha) = \begin{bmatrix} 1 & 0 & 0 \\ 0 & \cos \alpha & \sin \alpha \\ 0 & -\sin \alpha & \cos \alpha \end{bmatrix} \quad (\text{B.11})$$

$$R_2(\alpha) = \begin{bmatrix} \cos \alpha & 0 & -\sin \alpha \\ 0 & 1 & 0 \\ \sin \alpha & 0 & \cos \alpha \end{bmatrix} \quad (\text{B.12})$$

$$R_3(\alpha) = \begin{bmatrix} \cos \alpha & \sin \alpha & 0 \\ -\sin \alpha & \cos \alpha & 0 \\ 0 & 0 & 1 \end{bmatrix}. \quad (\text{B.13})$$

B.1.3 Rotation matrix multiplication

The multiplication of two rotation matrices yields another rotation matrix whose application to a point effects the same rotation as the sequential application of the two original matrices [Cra89].

B.2 Euler Angles

Recall the definition of co-ordinate rotations from above. Three co-ordinate rotations in sequence can describe any rotation. Consider triple rotations in which the first rotation is an angle ψ about the k-axis, the second rotation is an angle θ about the j-axis, and the

third rotation is an angle ϕ about the i -axis (orthogonal co-ordinate system (i, j, k)). We can arrange these angles in a three dimensional vector, termed the Euler Angle Vector \mathbf{u} [Gre88]:

$$\mathbf{u} = [\phi, \theta, \psi]^T \quad (\text{B.14})$$

The function that maps an Euler angle vector to its corresponding rotation matrix, $R_{i,j,k} : \mathbb{R}^3 \rightarrow SO(3)$ is

$$R_{i,j,k}(\phi, \theta, \psi) = R_i(\phi)R_j(\theta)R_k(\psi). \quad (\text{B.15})$$

As in the general case, if $\mathbf{z} \in \mathbb{R}^3$ is a vector in the world co-ordinates and $\mathbf{z}' \in \mathbb{R}^3$ is the same vector expressed in the body co-ordinates, then the following relationships hold:

$$\mathbf{z}' = R_{i,j,k}(\mathbf{u})\mathbf{z} \quad (\text{B.16})$$

$$\mathbf{z} = R_{i,j,k}(\mathbf{u})^T\mathbf{z}'. \quad (\text{B.17})$$

B.2.1 Euler angle rates

The time-derivative of the Euler angle vector is the vector of *Euler angle rates*. The relationship between the Euler angle rates and the angular velocity of the body is encoded in the Euler angle rates matrix [Gre88]. Multiplying this matrix by the vector of Euler angle rates gives the angular velocity in the global co-ordinates. Let $\mathbf{e}_i, \mathbf{e}_j, \mathbf{e}_k$ be the unit vectors in the directions (i, j, k) . The function that maps an Euler angle vector to its corresponding Euler angle rates matrix, $E : \mathbb{R}^3 \rightarrow \mathbb{R}^{3 \times 3}$, is

$$E_{i,j,k}(\phi, \theta, \psi) = [R_k(\psi)^T R_j(\theta)^T \mathbf{e}_i, R_k(\psi)^T \mathbf{e}_j, \mathbf{e}_k]. \quad (\text{B.18})$$

Hence

$$\boldsymbol{\omega} = E_{i,j,k}(\mathbf{u})\dot{\mathbf{u}} \quad (\text{B.19})$$

$$\boldsymbol{\omega}' = E'_{i,j,k}(\mathbf{u})\dot{\mathbf{u}}. \quad (\text{B.20})$$

The angular velocity in the body co-ordinates is related to the angular velocity in the global co-ordinates by

$$\boldsymbol{\omega}' = R_{i,j,k}(\mathbf{u})\boldsymbol{\omega} \quad (\text{B.21})$$

$$\boldsymbol{\omega} = R_{i,j,k}(\mathbf{u})^T\boldsymbol{\omega}'. \quad (\text{B.22})$$

Hence we may eliminate $\boldsymbol{\omega}, \boldsymbol{\omega}'$ and $\dot{\mathbf{u}}$ to obtain

$$R_{i,j,k}(\mathbf{u}) = E'_{i,j,k}(\mathbf{u})[E_{i,j,k}(\mathbf{u})]^{-1} \quad (\text{B.23})$$

$$R_{i,j,k}(\mathbf{u})^T = E_{i,j,k}(\mathbf{u})[E'_{i,j,k}(\mathbf{u})]^{-1}. \quad (\text{B.24})$$

B.2.2 Valid rotation sequences

Only certain sequences of co-ordinate rotations are able to span the space of all three dimensional rotations. Of the 27 possible sequences of three integers in $\{1, 2, 3\}$, there are only 12 that satisfy the span constraint (that no two consecutive numbers in a valid sequence may be equal). These are

$$(i, j, k) = \{(1, 2, 1), (1, 2, 3), (1, 3, 1), (1, 3, 2), (2, 1, 2), (2, 1, 3) \quad (\text{B.25})$$

$$(2, 3, 1), (2, 3, 2), (3, 1, 2), (3, 1, 3), (3, 2, 1), (3, 2, 3)\} \quad (\text{B.26})$$

The three bolded sequences are the most common choices for order of rotation.

B.2.3 Singularities

The main problem with Euler angle representations of attitude is the pervading presence of singularities, such that no one rotation sequence can represent a full rotation space in all three dimensions without encountering one or more singularities in the process. These singularities are said to arise from *gimbal lock*, which may be understood in several different ways. Intuitively, it arises from the indistinguishability of changes in the first and third Euler angles when the second Euler angle is at some critical value. Take, for example, the (1,2,3) sequence. When the pitch angle is 90° , the vehicle is pointing straight up, and roll and yaw are indistinguishable. In the case of the (3,1,3) sequence, when the nutation angle is zero, changes in the spin angle are the same as changes in the precession angle.

The phenomenon may also be seen mathematically. Again, consider the (1,2,3) sequence. In this case, when $\cos\theta = 0$, then $r_{23} = r_{33} = r_{12} = r_{11} = 0$, and the expressions for $\phi_{123}(R)$ and $\psi_{123}(R)$ are undefined ($\phi_{123}(R)$, $\psi_{123}(R)$ are the Euler angles ϕ, ψ expressed as a function of rotation matrix elements).

A common strategy for dealing with this problem is to change representations whenever an object nears a singularity. Even more popular is the use of unit quaternions to represent an object's attitude. Using unit quaternions to represent the attitude of an object completely avoids the problem of gimbal lock.

B.3 Quaternions

Quaternions were first devised by Hamilton in the 19th century [Ham63]. The term is used to denote a certain quadrimonial expression, of which one term was called (by analogy to the language of ordinary algebra) the real part, while the three other terms made up together a trinomial, which (by the same analogy) was called the imaginary part of the quaternion [Ham63]. Quaternions have many useful applications, but here we are primarily interested in their use as a representation of the attitude of an object.

Generally speaking, a quaternion $\mathbf{q} \in \mathcal{H}$ may be represented as a vector

$$\mathbf{q} = [q_0, q_1, q_2, q_3]^T = \begin{bmatrix} q_0 \\ \mathbf{q}_{123} \end{bmatrix}. \quad (\text{B.27})$$

Quaternions are additive but not commutative, and it is often found to be more convenient to write a quaternion multiplication as a matrix-vector product of the second quaternion pre-multiplied by a matrix-valued function of the first.

The attitude of a rigid body is usually most conveniently represented as a unit quaternion, where

$$\|\mathbf{q}\| = (q_0^2 + q_1^2 + q_2^2 + q_3^2)^{\frac{1}{2}} = 1. \quad (\text{B.28})$$

Consider a vector $\mathbf{z} \in \mathfrak{R}^3$, in the inertial co-ordinate system. If $\mathbf{z}' \in \mathfrak{R}^3$ is the same vector in the body co-ordinate system, then the following relations hold:

$$\begin{bmatrix} 0 \\ \mathbf{z}' \end{bmatrix} = \mathbf{q} \begin{bmatrix} 0 \\ \mathbf{z} \end{bmatrix} \cdot \mathbf{q}^{-1} \quad (\text{B.29})$$

$$= \begin{bmatrix} 1 & \mathbf{0}^T \\ \mathbf{0}^T & R_q(\mathbf{q}) \end{bmatrix} \begin{bmatrix} 0 \\ \mathbf{z} \end{bmatrix} \quad (\text{B.30})$$

where

$$R_q(\mathbf{q}) = \begin{bmatrix} q_0^2 + q_1^2 + q_2^2 + q_3^2 & 2(q_1q_2 + q_0q_3) & 2(q_1q_3 - q_0q_2) \\ 2(q_1q_2 - q_0q_3) & q_0^2 - q_1^2 + q_2^2 - q_3^2 & 2(q_2q_3 + q_0q_1) \\ 2(q_1q_3 + q_0q_2) & 2(q_2q_3 - q_0q_1) & q_0^2 - q_1^2 - q_2^2 + q_3^2 \end{bmatrix}. \quad (\text{B.31})$$

In other words,

$$\mathbf{z}' = R_q(\mathbf{q})\mathbf{z} \quad (\text{B.32})$$

$$\mathbf{z} = R_q(\mathbf{q})^T \mathbf{z}'. \quad (\text{B.33})$$

R_q is thus the rotation matrix for the body under consideration, and just as with rotation matrices based on Euler angles, sequences of rotations can be represented by products of quaternions. That is, for unit quaternions \mathbf{p} and \mathbf{q} it holds that

$$R_q(\mathbf{p} \cdot \mathbf{q}) = R_q(\mathbf{q})R_q(\mathbf{p}). \quad (\text{B.34})$$

B.3.1 Conversions

Converting between quaternions and Euler angles is straightforward:

$$\phi = \tan^{-1} \frac{2(q_0q_2 + q_1q_3)}{1 - 2(q_1^2 + q_2^2)} \quad (\text{B.35})$$

$$\theta = \sin^{-1}(2(q_0q_2 - q_1q_3)) \quad (\text{B.36})$$

$$\psi = \tan^{-1} \frac{2(q_0q_3 + q_1q_2)}{1 - 2(q_2^2 + q_3^2)}. \quad (\text{B.37})$$

For the reverse case, moving from a set of Euler angles (ϕ, θ, ψ) to the corresponding quaternion:

$$\mathbf{q} = \begin{bmatrix} \cos \frac{\phi}{2} \cos \frac{\theta}{2} \cos \frac{\psi}{2} + \sin \frac{\phi}{2} \sin \frac{\theta}{2} \sin \frac{\psi}{2} \\ \sin \frac{\phi}{2} \cos \frac{\theta}{2} \cos \frac{\psi}{2} - \cos \frac{\phi}{2} \sin \frac{\theta}{2} \sin \frac{\psi}{2} \\ \cos \frac{\phi}{2} \sin \frac{\theta}{2} \cos \frac{\psi}{2} + \sin \frac{\phi}{2} \cos \frac{\theta}{2} \sin \frac{\psi}{2} \\ \cos \frac{\phi}{2} \cos \frac{\theta}{2} \sin \frac{\psi}{2} - \sin \frac{\phi}{2} \sin \frac{\theta}{2} \cos \frac{\psi}{2} \end{bmatrix}. \quad (\text{B.38})$$

We have shown above that a quaternion rotation matrix is qualitatively equivalent to an Euler-angle rotation matrix. We can if necessary convert the elements of an Euler-angle rotation matrix directly to a quaternion, which results in four different mappings, of which

some will be complex.

$$q_0^0 = (1 + r_{11} + r_{22} + r_{33})^{\frac{1}{2}} \quad (\text{B.39})$$

$$\mathbf{q}_R^0 = \frac{1}{2} \begin{bmatrix} (1 + r_{11} + r_{22} + r_{33})^{\frac{1}{2}} \\ (r_{23} - r_{32})/q_0^0 \\ (r_{31} - r_{13})/q_0^0 \\ (r_{12} - r_{21})/q_0^0 \end{bmatrix} \quad (\text{B.40})$$

$$(\text{B.41})$$

$$q_0^1 = (1 + r_{11} - r_{22} - r_{33})^{\frac{1}{2}} \quad (\text{B.42})$$

$$\mathbf{q}_R^1 = \frac{1}{2} \begin{bmatrix} (r_{23} - r_{32})/q_0^1 \\ (1 + r_{11} - r_{22} - r_{33})^{\frac{1}{2}} \\ (r_{12} + r_{21})/q_0^1 \\ (r_{31} + r_{13})/q_0^1 \end{bmatrix} \quad (\text{B.43})$$

$$(\text{B.44})$$

$$q_0^2 = (1 - r_{11} + r_{22} - r_{33})^{\frac{1}{2}} \quad (\text{B.45})$$

$$\mathbf{q}_R^2 = \frac{1}{2} \begin{bmatrix} (r_{31} - r_{13})/q_0^2 \\ (r_{12} + r_{21})/q_0^2 \\ (1 - r_{11} + r_{22} - r_{33})^{\frac{1}{2}} \\ (r_{23} + r_{32})/q_0^2 \end{bmatrix} \quad (\text{B.46})$$

$$(\text{B.47})$$

$$q_0^3 = (1 - r_{11} - r_{22} + r_{33})^{\frac{1}{2}} \quad (\text{B.48})$$

$$\mathbf{q}_R^3 = \frac{1}{2} \begin{bmatrix} (r_{12} - r_{21})/q_0^3 \\ (r_{31} + r_{13})/q_0^3 \\ (r_{23} + r_{32})/q_0^3 \\ (1 - r_{11} - r_{22} + r_{33})^{\frac{1}{2}} \end{bmatrix} \quad (\text{B.49})$$

$$(\text{B.49})$$

There exists a composite function which allows us to choose between the four possible solutions, depending on the parameters of the rotation matrix [Sch65]. This function, $\mathbf{q}_R : SO(3) \rightarrow \mathbb{H}$, is

$$\mathbf{q}_R(R) = \left\{ \begin{array}{l} \mathbf{q}_R^0(R) \text{ if } r_{22} > -r_{33}, r_{11} > -r_{22}, r_{11} > -r_{33} \\ \mathbf{q}_R^1(R) \text{ if } r_{22} < -r_{33}, r_{11} > -r_{22}, r_{11} > r_{33} \\ \mathbf{q}_R^2(R) \text{ if } r_{22} > r_{33}, r_{11} < r_{22}, r_{11} < -r_{33} \\ \mathbf{q}_R^3(R) \text{ if } r_{22} < r_{33}, r_{11} < -r_{22}, r_{11} < r_{33} \end{array} \right\}. \quad (\text{B.50})$$

Bibliography

- [Adl56] F.P. Adler. Missile guidance by three-dimensional proportional navigation. *Journal of Applied Physics*, 27(5):500–507, 1956.
- [AM03] A.J. Anderson and P.W. McOwan. Model of a predatory stealth behaviour camouflaging motion. *Proc. R. Soc. Lond. B*, 270:489–495, 2003.
- [BAY98] J.X. Ben-Asher and I. Yaech. *Advances in Missile Guidance Theory, Progress in Astronautics and Aeronautics*, volume 180. AIAA Virginia, 1998.
- [BCS03] G.L. Barrows, J.S. Chahl, and M.V. Srinivasan. Biomimetic visual sensing and flight control. *The Aeronautical Journal*, 107:159–168, 2003.
- [BDD04] J. M. Birch, W.B. Dickson, and M.H. Dickinson. Force production and flow structure of the leading edge vortex on flapping wings at high and low reynolds numbers. *J. Experimental Biology*, 207:1063–72, 2004.
- [BE05] N. Boeddeker and M. Egelhaaf. A single control system for smooth and saccade-like pursuit in blowflies. *J. Experimental Biology*, 208:1563–72, 2005.
- [Ber95] D.P. Bertsekas. *Dynamic Programming and Optimal Control, Vol 1, 2nd Ed.* Athena, Massachusetts, 1995.
- [Ber96] D.P. Bertsekas. *Constrained optimization and lagrange multiplier methods.* Athena, Massachusetts, 1996.
- [Bis75] R.L. Bishop. There is more than one way to frame a curve. *American Mathematical Monthly*, pages 246–251, 1975.
- [BKE03] N. Boeddeker, R. Kern, and M. Egelhaaf. Chasing a dummy target: smooth pursuit and velocity control in male blowflies. *Proc. R. Soc. B: Biological Sciences*, 270:1971 – 78, 2003.
- [Bro98] E. Brookner. *Tracking and Kalman filtering made easy.* New York: Wiley, 1998.
- [BSO+06] R. Berry, G. Stange, R. Olberg, , and Josh van Kleef. The mapping of visual space by identified large second-order neurons in the dragonfly median ocellus. *J. Comp. Physiol A*, 192:1105–1123, 2006.
- [BSR92] A. Baader, M. Schäfer, and C.H.F. Rowell. The perception of the visual flow field by flying locusts: a behavioural and neuronal analysis. *J. Exp. Biol.*, 165:137–60, 1992.
- [Bus03] P. Bussotti. On the genesis of the lagrange multipliers. *J. Optimization Theory and Applications*, 117:453–59, 2003.

-
- [CFC04] N.E. Carey, J.J. Ford, and J.S. Chahl. Biologically inspired guidance for motion camouflage. In *Proc. 5th Asian Control Conference*, pages 1793–1799, 2004.
- [Chi97] A. Chikrii. *Conflict Controlled Processes*. Kluwer Academic Publishers, 1997.
- [CK98] M.C. Campi and P.R. Kumar. Adaptive linear quadratic gaussian control: the cost-biased approach revisited. *Siam J. Control Optim.*, 36(6):1890–1907, 1998.
- [CL75] T.S. Collett and M.F. Land. Visual control of flight behaviour in the hoverfly *syritta pipiens* l. *J. Comp. Physiol. A*, 99:1–66, 1975.
- [CL78] T.S. Collett and M.F. Land. How hoverflies compute interception courses. *J. Comp. Physiol*, 125:191–204, 1978.
- [Col80a] T.S. Collett. Angular tracking and the optomotor response: an analysis of visual reflex interaction in a hoverfly. *J. Comp. Physiol. A*, 140:145–158, 1980.
- [Col80b] T.S. Collett. Some operating rules for the optomotor system of a hoverfly during voluntary flight. *J. Comp. Physiol.*, 138:271–82, 1980.
- [Col96] T.S. Collett. Insect navigation en route to the goal: multiple strategies for the use of landmarks. *J. Exp. Biol.*, 199:227–35, 1996.
- [Cra89] J.J. Craig. *Introduction to Robotics, Mechanics and Control*. Addison-Wesley, 1989.
- [CT84] H. Collewijn and E.P. Tamminga. Human smooth and saccadic eye movements during voluntary pursuit of different target motions on different backgrounds. *J. Physiol.*, 351:217–50, 1984.
- [Dav62] H.T. Davis. *Introduction to Nonlinear Differential and Integral Equations*. Dover, 1962.
- [Dav82] C.T. David. Compensation for height in the control of groundspeed by *drosophila* in a new "barber's pole" wind stunnel. *J Comp Physiol*, 147:485–93, 1982.
- [dB01] C. de Boor. *Applied Mathematical Science*, chapter A Practical Guide to Splines. Springer, 2001.
- [DOL01] R.O. Dror, D.C. O'Carroll, and S.B. Laughlin. Accuracy of velocity estimation by reichardt correlators. *J. Opt. Soc. Am. A*, 18:241–52, 2001.
- [ES04] P.K. Eason and P.V. Switzer. The costs of neighbors for a territorial dragonfly, *perithemis tenera*. *Ethology*, 110(1):3747, 2004.
- [Eva70] H.E. Evans. Ecological-behavioral studies of the wasp of jackson hole, wyoming. *Bull. Mus. Comp. Zool.*, 140:451–511, 1970.
- [EZ01] M.P. Eckert and J. Zeil. *Motion Vision - Computational, Neural, and Ecological Constraints*, chapter Towards an Ecology of Motion Vision, pages 333–69. Springer Verlag, 2001.
- [FO95] M.A. Frye and R.M. Olberg. Visual field properties of feature detecting neurons in the dragonfly. *J Comp Physiol A*, 177:569–576, 1995.

-
- [Fri96] B. Friedland. *Advanced Control System Design*. Prentice Hall, 1996.
- [FW02] S.N. Fry and R. Wehner. Honeybees store landmarks in an egocentric reference frame. *J. Comp Phys. A*, 187:1009–16, 2002.
- [Gho94] D. Ghose. On the generalization of true proportional navigation. *IEEE Transactions on Aerospace and Electronic Systems*, 30(2):545–555, 1994.
- [Gle04] P. Glendinning. The mathematics of motion camouflage. *Proc. R. Soc. Lond. B*, 271:277–481, 2004.
- [Gor95] S.N. Gorb. The dragonfly head-arrestor: a sensory organ connected to flight reflexes. *Proc 23rd Neurobiology Conference, Gottingen*, 2:193, 1995.
- [Gor99] S.N. Gorb. Evolution of the dragonfly head-arresting system. *Proc. R. Soc. Lond. B*, 266:525–535s, 1999.
- [Gre88] D.T. Greenwood. *Principles of Dynamics, 2nd Ed.* Prentice Hall NJ, 1988.
- [GS91] C. Gilbert and N.J. Strausfeld. The functional organization of male-specific visual neurons in flies. *J. Comp. Physiol A*, 169:395–411, 1991.
- [Ham63] Sir W.R. Hamilton. *Elements of Quaternions, 3rd Ed.* Chelsea Publishing Co., New York, 1963.
- [HE89] K. Hausen and M. Egelhaaf. *Facets of Vision*, chapter Neural mechanisms of visual course control in insects, pages 391–424. Berlin/Heidelberg: Springer-Verlag, 1989.
- [Hen93] R. Hengstenberg. *Visual Motion and its Role in the Stabilization of Gaze*, chapter Multisensory control in insect oculomotor systems, pages 285–596. Elsevier Science Publishers, 1993.
- [HJZB03] M. Hrnčir, S. Jarau, R. Zucchi, and F.G. Barth. A stingless bee *melipona seminigra* uses optic flow to estimate flight distances. *J. Comp. Phys. A*, 189:761–768, 2003.
- [Hom04] U. Homburg. In search of the sky compass in the insect brain. *Naturwissenschaften*, 91:199–208, 2004.
- [Hor86] G.A. Horridge. A theory of insect vision: Velocity parallax. *Proc R. Soc. Lond. B*, 229:13–27, 1986.
- [Ibb01] M. R. Ibbotson. Evidence for velocity-tuned motion-sensitive descending neurons in the honeybee. *Proc. R. Soc. Lond. B*, 230:279–92, 2001.
- [JC91] J.W. Jackson and P.E. Crouch. Curved path approaches and dynamic interpolation. *IEEE Aerospace and Electronic Systems Magazine*, 6:8–13, 1991.
- [JK05] E.W. Justh and P.S. Krishnaprasad. Natural frames and interacting particles in three dimensions. *Proc. 44th IEEE Conf. Decision and Control*, pages 2842–2846, 2005.
- [JK06] E.W. Justh and P.S. Krishnaprasad. Steering laws for motion camouflage. *Proc R Soc Lond A*, 462:3629–3643, 2006.

-
- [Kra00] H.G. Krapp. Neuronal matched filters for optic flow processing in flying insects. *Int Rev Neurobiol.*, 44:93–120, 2000.
- [Lan89] M.F. Land. *Facets of Vision*, chapter Variations in the structure and design of compound eyes, pages 90–111. Springer, 1989.
- [Lan97] M.F. Land. Visual acuity in insects. *Annual Review of Entomology*, 42:147–177, 1997.
- [Lav00] E. Lavretsky. Greedy optimal control. *Proc. American Control Conference*, 6:3888–3892, 2000.
- [LC74] M.F. Land and T.S. Collett. Chasing behaviour of houseflies *fannia canicularis*. *J. Comp. Physiol.*, 89:331–57, 1974.
- [Leh97] M. Lehrer. *Orientation and communication in arthropods*, chapter Honeybees' visual spatial orientation at the feeding site, pages 115–144. Basel: Birkhaeuser Verlag, 1997.
- [Lei81] G. Leitmann. *Calculus of Variations and Optimal Control: an Introduction*. Plenum Press New York, 1981.
- [LM02] T. Labhart and E.P. Meyer. Neural mechanisms in insect navigation: polarization compass and odometer. *Current Opinion in Neurobiology*, 12:707714, 2002.
- [MC06] I. Matychyn and A. Chikrii. Motion camouflage in differential games of pursuit. In *Proc. 12th International Symposium on dynamic games and applications*. INRIA, 2006.
- [MCS03] A. Mizutani, J.S. Chahl, and M.V. Srinivasan. Motion camouflage in dragonflies. *Nature*, 423:604, 2003.
- [M.F92] M.F.Land. Visual tracking and pursuit : humans and arthropods compared. *J. Insect Physiol.*, 38:939–951, 1992.
- [MO98] A.A. Milyutin and N.P. Osmolovskii. *Calculus of variations and optimal control*. American Mathematical Society, 1998.
- [MS89] P.R. Mahapatra and U. S. Shukra. Accurate solution of proportional navigation for maneuvering targets. *IEEE Transactions on Aerospace and Electronic Systems*, 31(1):81–89, 1989.
- [NB02] T.R. Neumann and H.H. Bülthoff. Behavior-oriented vision for biomimetic flight control. *Proc. EPSRC/BBSRC International Workshop on Biologically Inspired Robotics*, pages 627–36, 2002.
- [NO96] K. Nordström and D.C. O'Carroll. Small object detection neurons in female hoverflies. *Proc. Royal Soc. B*, 273:1211–16, 1996.
- [OWV00] R.M. Olberg, A.H. Worthington, and K.R. Venator. Prey pursuit and interception in dragonflies. *J. Comp. Physiol A*, 186:155–162, 2000.

-
- [PK87] H.J. Poethke and H. Kaiser. The territoriality threshold: a model for mutual avoidance in dragonfly mating systems. *Behavioral Ecology and Sociobiology*, 20(1):11–19, 1987.
- [PR81] T. Poggio and W. Reichardt. Visual fixation and tracking by flies: Mathematical properties of simple control system. *Biological Cybernetics*, 40:101–112, 1981.
- [R89] G. Ruppell. Kinematic analysis of symmetrical flight manoeuvres of odonata. *J. Exp. Biol.*, 144:13–42, 1989.
- [Rei69] W. Reichardt. *Processing of Optical Data by Organisms and By Machines*, chapter Movement perception in insects, pages 465–93. New York: Academic, 1969.
- [RJK06] P. V. Reddy, E. W. Justh, and P. S. Krishnaprasad. Motion camouflage in three dimensions. *Prof 45th IEEE Conf. Decision and Control*, pages 3327–3332, 2006.
- [Ros80] S. Rossel. Foveal fixation and tracking in the praying mantis. *Journal of Comparative Physiology A*, 139:307–31, 1980.
- [Ros83] S. Rossel. Binocular stereopsis in an insect. *Nature*, 302:821 – 822, 1983.
- [Ros97] R.M. Rosenberg. *Analytical Dynamics of Discrete Systems*. Plenum Press NY, 1997.
- [RW69] W. Reichardt and H. Wenking. Optical detection and fixation of objects by fixed flying flies. *Naturwissenschaften*, 56(8):424, 1969.
- [Sch65] A.L. Schwab. *Quaternions, finite rotation and euler parameters, 4th Ed.* Albert Blanchard, France, 1965.
- [SD95] M.V. Srinivasan and M. Davey. Strategies for active camouflage of motion. *J. Experimental Biology*, 199:129–140, 1995.
- [SH79] G. Stange and J. Howard. An ocellar dorsal light response in a dragonfly. *J. Exp. Biol.*, 83:351–55, 1979.
- [SL92] B.L. Stevens and F.L. Lewis. *Aircraft Control and Simulation*. Wiley, NY, 1992.
- [SLKZ91] M. V. Srinivasan, M. Lehrer, W. Kirchner, and S.W. Zhang. Range perception through apparent image speed in freely-flying honeybees. *Vis. Neurosci.*, 6:519–35, 1991.
- [SM90] U.S. Shukla and P.R. Mahapatra. The proportional navigation dilemma - pure or true? *IEEE Transactions on Aerospace and Electronic Systems*, 26(2):382–392, 1990.
- [SPK99] M.V. Srinivasan, M. Poteserb, and K. Kral. Motion detection in insect orientation and navigation. *Vision Research*, 39:2749–2766, 1999.
- [Sri93] M.V. Srinivasan. *How insects infer range from visual motion*. Miles and Wallman, 1993.

-
- [Sta81] G. Stange. The ocellar component of flight equilibrium control in dragonflies. *J. Experimental Biology*, 141:335–347, 1981.
- [Str80] N.J. Strausfeld. Male and female visual neurones in dipterous insects. *Nature*, 283:381–83, 1980.
- [STS06] M. Srinivasan, S. Thurrowgood, and D. Soccol. An optical system for guidance of terrain following in uavs. *IEEE International Conference on Video and Signal Based Surveillance (AVSS'06)*, page 51, 2006.
- [SvH99] C. Schilstra and J.H. van Hateren. Blowfly flight and optic flow: I thorax kinematics and flight dynamics. *J. Exp Biol.*, 202:1481–90, 1999.
- [SZ04] M.V. Srinivasan and S.W. Zhang. Visual motor computation in insects. *Annual Rev. Neuroscience*, 27:679–96, 2004.
- [SZB97] M. V. Srinivasan, S.W. Zhang, and N. Bidwell. Visually mediated odometry in honeybees. *J. Exp. Biol.*, 200:2513–22, 1997.
- [SZC⁺00] M.V. Srinivasan, S.W. Zhang, J.S. Chahl, E. Barth, and S. Venkatesh. How honeybees make grazing landings on flat surfaces. *Biol. Cybernetics*, 83:171–83, 2000.
- [SZLC96] M.V. Srinivasan, S.W. Zhang, M. Lehrer, and T.S. Collett. Honeybee navigation en route to the goal: visual flight control and odometry. *J. Exp. Biol.*, 199:237–44, 1996.
- [TD02] L.F. Tammero and M.W. Dickinson. The influence of visual landscape on the free flight behavior of the fruit fly *drosophila melanogaster*. *J. Exp. Biol.*, 205:327–343, 2002.
- [TW97] D.H. Titterton and J.L. Weston. *Strapdown inertial navigation technology*. Peter Peregrinus, Ltd., IEEE, Stevenage UK, 1997.
- [Tya03] F. Tyan. 3d unified approach to missile guidance laws. *Proc. 4th International Conference on Control and Automation ICCA*, pages 335– 339, 2003.
- [TZS⁺04] J. Tautz, S.W. Zhang, J. Spaethe, A. Brockmann, A. Si, and M. Srinivasan. Honeybee odometry: Performance in varying natural terrain. *PLoS Biol.*, 2:e211, 2004.
- [Ugo87] A. Ugolini. Visual information acquired during displacement and initial orientation in polistes gallicus. *Animal Behaviour*, 35:590–95, 1987.
- [VR76] R.P. Virsik and W. Reichardt. Detection and tracking of moving objects by the fly musca domestica. *Biol. Cybernetics*, 23:83–98, 1976.
- [Wag82] H. Wagner. Flow-field variables trigger landing in flies. *Nature*, 297:147–48, 1982.
- [Wag86] H. Wagner. Flight performance and visual control of flight of the free-flying housefly *musca domestica* l i. organisation of the flight motor. *R. Soc. Lond. B*, 312:527–551, 1986.

-
- [Wci84] W.T. Wcislo. Gregarious nesting of a digger wasp as a selfish herd response to a parasitic fly *hymenoptera: sphecidae; diptera: sacrophagidae*. *Behavioral Ecology and Sociobiology*, 15:157–160, 1984.
- [WE97] J.M. Wakeling and C.P. Ellington. Dragonfly flight. ii. velocities, accelerations and kinematics of flapping flight. *J. Experimental Biology*, 200:557–582,, 1997.
- [Wil78] M. Wilson. The functional organization of locust ocelli. *J Comp Physiol.*, 124:297–316, 1978.
- [YY96] C.D. Yang and C.C. Yang. Analytical solution of 3d true proportional navigation. *IEEE Transactions on Aerospace and Electronic Systems*, 32(4):1509–1522, 1996.
- [Zar02] P. Zarchan. *Tactical and Strategic Missile Guidance, 4th Ed., Progress in Astronautics and Aeronautics*, volume 199. AIAA Virginia, 2002.
- [Zei86] J. Zeil. The territorial flight of male houseflies (*fannia canicularis*). *Behav. Ecol. Sociobiol.*, 19:213–19, 1986.
- [ZKV96] J. Zeil, A. Kelber, and R. Voss. Structure and function of learning flights in ground-nesting bees and wasps. *J. Exp. Biol.*, 199:245–52, 1996.